Lazaroid Formulations for Brain Delivery:

Development of Nano-structured Lipid Carriers, Optimization, and Pharmacokinetic Evaluation

A Dissertation Presented to the

Faculty of the Department of Pharmacological and Pharmaceutical Sciences

College of Pharmacy, University of Houston

In Partial Fulfillment of

the Requirements for the Degree of

Doctor of Philosophy

By

Prajakta S. Gadgil

May, 2016

Acknowledgement

I would like to take this opportunity to acknowledge the people for their support and encouragement without which this doctoral dissertation would have not been possible.

Firstly, I owe my deepest gratitude to my advisor Dr. Diana S-L. Chow for providing me the opportunity to be a graduate student in her lab. Dr. Chow gave me freedom to explore my work, supported me during difficult times and provided timely guidance on both professional and personal front. Dr. Chow is truly an inspiration and I hope one day I can emulate her.

I would like to thank my committee members, Drs. Shah, Alkadhi, Ghose, New and Li for providing me valuable suggestions and inputs for my dissertation. This dissertation has been enriched by their expert comments and review.

I would like to acknowledge Dr. Karoline Muller for her help in the XRD analysis and Ms. Debra Townley for her assistance in TEM imaging. Ms. Tristan Mathis has been of constant help in scheduling various appointments and providing administrative support.

I would like to recognize all my past and current lab-mates especially Tanay, Stanley, Lei, Daping, Mahua, Nashid, Yu Jin and my friends at University of Houston Sumit, Pankajini, Guncha, Sonal, Ankita, Suchi for helping and supporting me throughout my graduate pursuit.

I am obliged to my parents, in-laws and grandparents for being my pillar of strength, and for their unconditional love during my graduate journey. This dissertation would not have

been possible without the constant support, love, patience, motivation and sacrifice of my husband Manas. I am thankful to God for giving me such a lovely family who has been instrumental in making me the person I am today.

Abstract

Purpose and Specific Aims: There are several limitations associated with the current gliobalstoma therapy, namely radiation induced lipid peroxidation and resistance to chemotherapy, resulting in recurrence of glioblastoma. In order to overcome these problems, alternative agents such as lazaroid U74389-G (LAZ) need to be explored. LAZ, a 21-aminosteroid, is a known lipid peroxidation inhibitor *in vivo* and has also demonstrated anti-proliferative activity *in vitro*. However, LAZ a potential substrate of P-glycoprotein (P-gp) efflux transporter, is extensively metabolized by Phase I enzymes and has shown high hepatic clearance on intravenous administration leading to poor brain penetration and restricting its potential in treating glioblastoma. One approach to overcome the limitations associated with LAZ is to design drug-loaded nano-carriers engineered to have surface properties and sub-micron size conducive for delivery across the blood brain barrier (BBB) while escaping the clearance by liver. The goal of this study was to investigate the utility of LAZ loaded nano-carriers such as nanostructured lipid carriers (NLCs), increasing the brain exposure while decreasing the liver exposure of LAZ.

Three specific aims were proposed in order to achieve our goal; 1) Development, optimization and *in-vitro* characterization of lazaroid loaded NLCs, 2) development and validation of UPLC-MS/MS for quantification of lazaroid in bio-matrices and 3) evaluation of pharmacokinetics and bio-distribution of lazaroid formulations in Sprague-Dawley rat model.

Method: A 2-factor, 5-level Central Composite Design (CCD) along with response surface plots were used to determine the effect of independent variables (amount of DSPE-PEG 2k and % liquid lipid) on dependent variables (particle size, zeta potential and encapsulation efficiency), and providing numerical optimization for LAZ-NLC composition. The optimal LAZ-NLCs were characterized for their physico-chemical properties such as particle size and morphology, surface charge, encapsulation efficiency, crystallinity, hemolytic potential and storage stability using various analytical techniques. A sensitive UPLC/MS-MS analytical method was developed and validated for the analytical quantification of LAZ in rat plasma and brain, liver and lung tissue samples. Male Spargue-Dawley rat groups were dosed intravenously with optimal LAZ-NLC (15 mg/kg) and comparative LAZ citrate (5 mg/kg) and LAZ co-solvent (15 mg/kg) solutions and the plasma pharmacokinetics and brain, liver and lung bio-distribution profiles were evaluated for up to 8 hours. Additionally, male Spargue-Dawley rats were dosed intravenously with increasing dose of the optimal LAZ-NLC from 15 to 60 mg/kg. The brain levels of LAZ 20 minutes post-dose were evaluated in each dose group and were evaluated using ANOVA and power model for assessing dose linearity.

Results: The DSPE-PEG 2k had an inverse effect on particle size and zeta potential and a synergistic effect on encapsulation efficiency of LAZ-NLCs. The liquid lipid Labrasol had an inverse effect on particle size and a slight synergistic effect on zeta potential without having any effect on encapsulation efficiency of LAZ-NLC. The optimal LAZ-NLCs measured 172.3 ± 3.54 nm in diameter with surface charge of -4.54 ± 0.87 mV and

encapsulation efficiency of 85.01 ± 2.60 %. The optimal LAZ-NLCs were spherical in shape as per transmission electron microscopy and *in vitro* hemolytic potential was within acceptable limits (<15%) for formulation to blood ratio up to 1. LAZ was solubilized in the lipid matrix of the NLC in an amorphous state as highlighted by differential scanning calorimetry and x-ray diffraction analysis. The optimal LAZ-NLC was stable on storage at 4°C for up to 3 months with slight increase (1.2 times) in particle size and slight decrease (3 times) in zeta potential and insignificant changes in encapsulation efficiency. Although the optimal LAZ-NLC had similar plasma pharmacokinetic profile compared to LAZ citrate solution and LAZ co-solvent groups, different inter-compartmental clearance between groups resulted in differential organ bio-distribution profiles. The LAZ exposure in brain was enhanced by two times with NLC and co-solvent compared to citrate group while a decrease in liver exposure by half was observed for NLC compared to citrate and co-solvent group. The optimal surface properties of optimal LAZ-NLC and presence of DSPE-PEG 2k and Polysorbate 80 were instrumental in increasing the LAZ brain permeability while decreasing its hepatic exposure. A combination of transport mechanisms such as passive diffusion, active endocytic uptake and/or inhibition of efflux transport were proposed for passage of free unbound LAZ as well as intact LAZ-NLC across the BBB. The optimal LAZ-NLC was retained twice longer than citrate group in the lungs. A dose-linearity study indicated non-proportional (11.6 times) increase in brain levels of LAZ at 20 minutes post-dose with linear (4 times) increase in dose of optimal LAZ-NLC from 15 to 60 mg/kg.

Conclusion and Significance: We demonstrated the utility of NLCs designed using logical methodology with favorable properties in enhancing LAZ exposure to the brain.

We established 1) a CCD matrix for determining the effect of NLC composition on particle size, zeta potential and encapsulation efficiency, 2) a selection criteria for formulation composition in enhancing brain delivery using CCD matrix with the resulting optimal LAZ-NLCs measuring < 200 nm, with a neutral surface charge and high drug payload, 3) the physico-chemical properties of optimal LAZ-NLCs viz. spherical in shape, retention of lipid crystallinity and conversion of LAZ to amorphous state, low hematotoxic potential, and stable on storage, 4) the optimal LAZ-NLC had similar plasma pharmacokinetics as LAZ citrate and co-solvent groups, but a disparity in the bio-distribution pattern was seen with two times increase in brain levels of LAZ for both NLC and co-solvent compared to citrate group with reduction in LAZ liver levels by half for LAZ-NLC compared to citrate and co-solvent group, and 5) a non-linear increase in amount of LAZ in brain on linearly increasing the dose of optimal LAZ-NLC.

Our study is significant since it laid the foundation for the pre-clinical efficacy testing of LAZ-NLC in treatment of glioblastoma and its potential translation to clinical setting.

List of Tables

List of Figures

List of Equations

List of Abbreviations

AUC – Area Under the Curve

BBB – Blood Brain Barrier

CCD – Central Composite Design

% CV – Percentage Coefficient of Variation

DIA – Daidzein

DLS – Dynamic Light Scattering

DOE – Design of Experiments

DSPE-PEG 2k – mPEG-DSPE, MW: 2000

DSC – Differential Scanning Calorimetry

EE – Encapsulation Efficiency

GBM – Glioblastoma Multiforme

GB – Glyceryl Behenate

GRAS – Generally Regarded as Safe

HPLC – High Performance Liquid Chromatography

LAZ – Lazaroid U74389G

LDL – Low-density Lipoporotein

LLOQ – Lower Limit of Quantification

MTS – Methyl Testosterone

MGMT – O^6-meG DNA methyltransferase

MMR – Mismatch Repair

NLC – Nanostructured Lipid Carriers

P-gp – P-glycoprotein

PK – Pharmacokinetic

PS – Particle Size

PUFA – Polyunsaturated Fatty Acid

QbD – Quality by Design

QC – Quality Control

RES – Reticuloendothelial System

ROS – Reactive Oxygen Species

SLN – Solid Lipid Nanoparticle

TEM – Transmission Electron Microscopy

TMZ – Temozolomide

TM – Trimyristin

TS – Tristearin

$t_{1/2}$ – Half-life

UPLC/MS-MS – Ultra performance Liquid Chromatography Mass Spectrometry

WHO – World Health Organization

XRD – X-ray Diffraction Analysis

λz – Terminal elimination rate constant

ZP – Zeta Potential

Table of Contents

Chapter 1: Literature Survey

1.1. Glioblastoma

Gliomas are tumors arising from glial or precursor cells and account for almost 80 % of malignant brain tumors [1]. The cellular origins of gliomas can be traced to various cell types such as neural stem cells, oligodendrocyte progenitor cells, polydendrocytes and reactive astrocytes [2, 3].

Gliomas can be classified as 'diffused' or 'circumscribed', depending on the degree of its infiltration in the normal brain tissues [4]. The World Health Organization (WHO) has classified gliomas into four grades from I to IV (**Table 1**) based on histological analysis, malignancy potential and its effects on the clinical outcome. Glioblastoma multiforme (GBM) is defined as cytologically malignant, mitotically active, necrosis-prone grade IV diffused glioma [5].

Grade	Histology	Proportion (%)	5-year survival (%)
I	Pilocytic astrocytoma	5.2%	>10
II	Diffuse astrocytoma	1.8%	>4
III	Anaplastic astrocytoma	13.8%	1.5-6.6
IV	**Glioblastoma multiforme (GBM)**	**53.9%**	**5**

Table 1: WHO classification of gliomas [5]

GBM accounts for 15.4% of all primary brain tumors, 46.1 % of primary malignant brain tumors and for the majority of gliomas (55.1%). GBM has the highest number of cases of all malignant tumors, with 11,890 cases predicted in 2015 and 12,120 in 2016 [1]. The current standard treatment involves maximal surgical removal of the tumor followed by concurrent radiation therapy and chemotherapy with temozolomide. With this therapy, the median survival of the patients is approximately 14 months with very low 5-year survival rate post-diagnosis of 5.1% [1, 6].

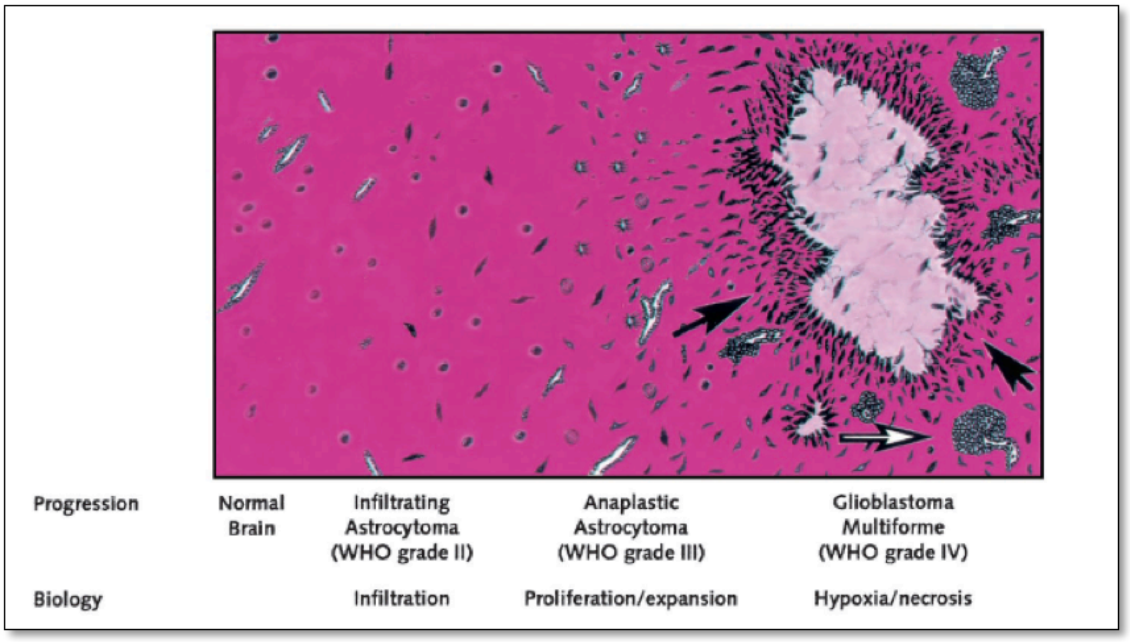

Figure 1: Histological progression of normal brain to GBM [7]

The progression of normal brain tissue to GBM is represented in **Figure 1**.The tumor cells penetrate through the normal brain parenchyma resulting in infiltrating astrocytoma with retention of normal cellular and vascular structures. The infiltrating astrocytoma

progresses into anaplastic astrocytoma where an increase in tumor cell proliferation rates with physical changes in vascular structures such as lumen dilation or thickened walls are observed. Anaplastic astrocytoma further transitions into GBM, which is characterized by necrosis **(black arrow Figure 1)** with tumor cells arranged in pseudopalisading structure and microvascular hyperplasia in the form of glomeruloid shaped vascular proliferation **(white arrow Figure 1)** [7].

1.2. Limitations of glioblastoma therapy

In spite of standard optimal treatment with radiation and chemotherapy, glioblastoma can relapse with median time of about 7 months. This recurrence is mainly due to histologically heterogeneous and invasive nature of GBM limiting the therapeutic efficacy of the current therapy [8]. The refractoriness and aggressiveness of GBM restricts the benefits of surgery and radiotherapy resulting in tumors located in inaccessible anatomic locations such as cortex, basal ganglia, or brain stem. Additionally, the efficacy of radiotherapy is also limited due to its low therapeutic index for normal brain and tumor tissues. The physico-chemical properties of chemotherapeutic agents coupled with the presence of blood-brain and blood-tumor barrier fortified with efflux transporters, limit the permeability and therapeutic efficacy of these agents [9-11].

1.2.1. Radiation-induced brain injury

The benefits of radiotherapy could be limited because of the exposure of healthy brain cells to radiation. Tofilon et. al., proposed a model for radiation-induced brain injury which constitutes a series of simultaneous multi-faceted processes starting with acute cell

injury/death, activation of bio-chemical cascade generating secondary reactive responses like oxidative stress and competing induction for coding of protective cytokines [12]. Of particular interest in radiation-induced brain injury, is lipid peroxidation, a symbol of oxidative stress resulting in formation of reactive oxygen species (ROS) and eventually leading to cell injury and death. The healthy brain is susceptible to radiation-induced lipid peroxidation mainly due to high oxygen consumption rate, high proportion of poly-unsaturated fatty acids (PUFA) and catecholamines, high iron content, and low level of anti-oxidant enzymes [13]. Lipid peroxidation is a chain of chemical reactions involving attack of ROS on PUFA, resulting in formation of several reactive products which interact with proteins, phospholipids and nucleic acids to form toxic adducts and complexes. There are three steps in lipid peroxidation; *initiation, propagation and termination* **(Figure 2, a and b).** The energy from ionizing particles in radiation is transferred to water leading to ionization of water molecules to yield ROS. In the *initiation* step [Step 1], ROS interacts with the reactive hydrogen atom in the methylene group next to the double bond of PUFA, resulting in formation of lipid radical (L·). In the propagation phase [Step 2], the lipid radical reacts with molecular oxygen to generate an unstable lipid peroxyl radical (LOO·) and lipid hydroperoxide (LOOH). Additionally, redox metal catalysts like iron or copper can also interact with the lipid hydroperoxide resulting in formation of ROS (alkoxy radical). The newly generated lipid peroxyl and alkoxy radicals will in turn interact with another PUFA, continuing the cyclic cascade of peroxidation reactions [Step 3].

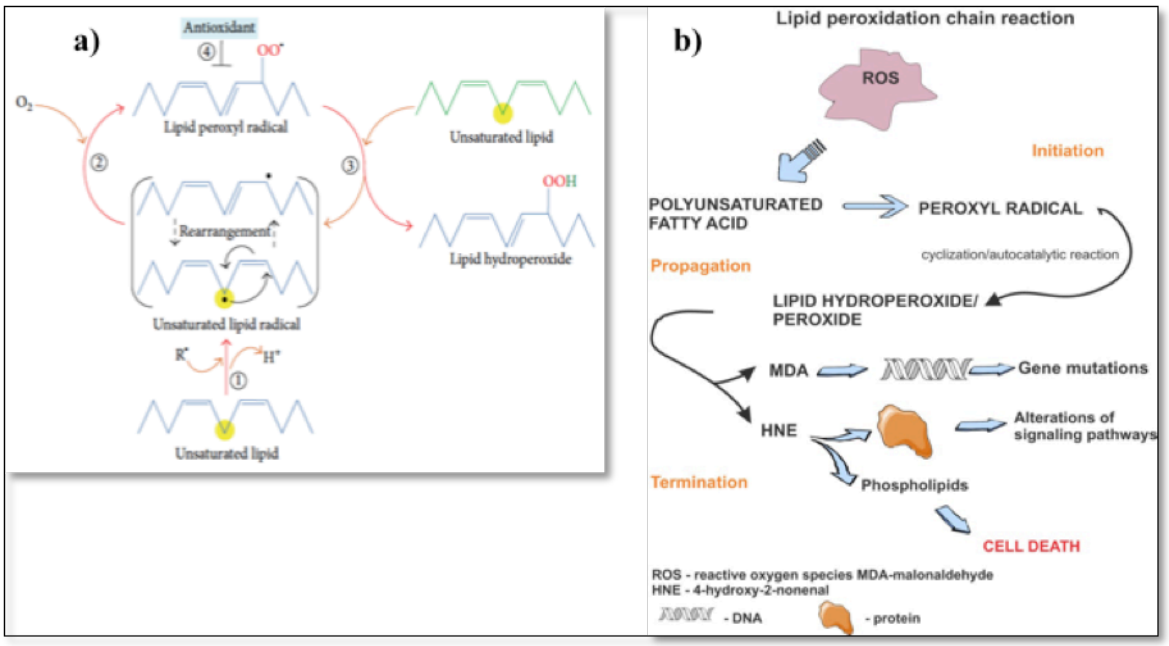

Figure 2: Steps in lipid peroxidation **a)** chemical reaction [14] and **b)** schematic representation [15]

The *termination* of the reaction [Step 4] involves, scavenging of the lipid peroxyl radical by anti-oxidants like α-tocopherol and thus inhibiting the chain reaction. The lipid hydroperoxide formed would degrade into end products such as malondialdehyde, 4-hydroxy-2-nonenal, acrolein and isoprostanes which cross link with DNA and proteins altering their functions and activities [14, 16, 17].

The radiation-induced brain injuries are classified as *pseudoprogression* and *radiation necrosis* [18]. Pseudoprogression occurs within 2-5 months whereas radiation necrosis could occur from 3 months to more than year after initiation of radiation therapy. The time-line of side effects due to radiation-induced brain injury is highlighted in **Figure 3.**

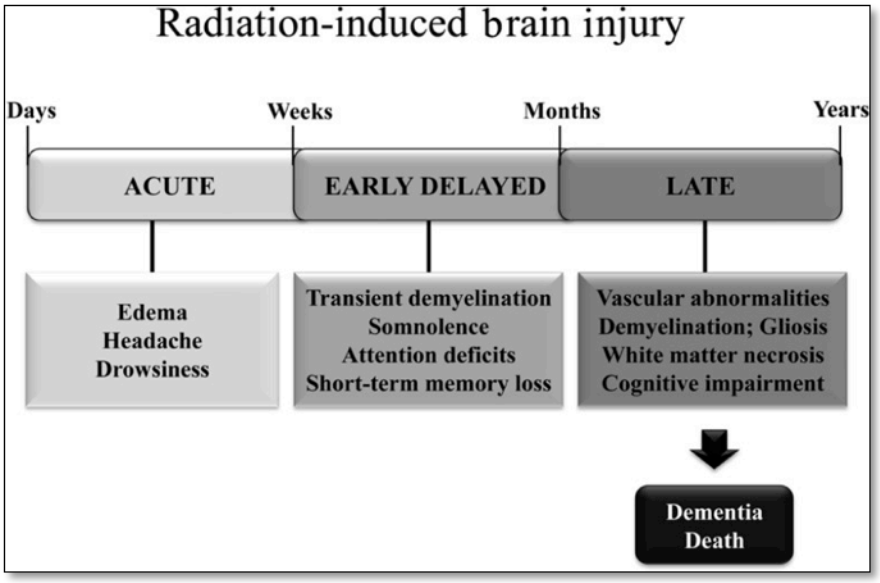

Figure 3: Time-line of effects of radiation-induced brain injury [19]

Pseudoprogression could result in range of acute side effects such as edema, headache to early delayed effects like transient demyelineation, which are reversible and can be resolved. Radiation necrosis causes series of late delayed effects such as vascular abnormalities, demyleniation, and white matter necrosis. With the advent of modern radiation therapy techniques, the manifestations of adverse, early delayed and most of the late delayed effects can be negated. However, in case of patients surviving beyond a year

after radiotherapy the dynamic interactions of various brain cells with radiation results in development of cognitive impairment affecting their quality of life [19].

1.2.2. Resistance to temozolomide (TMZ)

Temozolomide, an oral alkylating agent, is used as a gold standard in treatment of GBM. However resistance mechanisms such as methylation status of O^6-meG DNA methyltransferase (MGMT) and loss of mismatch repair (MMR) can affect the effectiveness of TMZ in treating GBM.

TMZ produces toxic lesions by methylation of the guanine residues in tumor cells forming O^6-methylguanine (O^6-meG) leading to tumor cell death. MGMT is a repair enzyme that removes the O^6-alkylguanine resulting in restoration of guanine residue in tumor cells and thus promoting their survival. In normal cells, the wild form of metabolic enzyme isocitrate dehydrogenase (IDH1) prevents the methylation of MGMT leading to cell survival **(Figure 4).** However, in GBM there can be a loss or mutation of IDH1 resulting in methylation of MGMT and causing a loss of its repair function resulting in cell death. Furthermore, it has been established clinically that patients expressing non-methylated promoter gene encoding MGMT have shown to have lower long-term progression-free survival compared to methylated promoter gene when treated with TMZ [4, 20, 21].

In normal cells, the genes encoding for mismatch repair (MMR) recognizes the mismatching of O^6-meG lesions with thymine base and activates cascade of reactions resulting in tumor cell death. However, mutation or loss of gene encoding for MMR in tumor cells results in DNA replication and cell survival [22].

Thus, MGMT and MMR pathways play an important role in deciding the sensitivity of TMZ to GBM. The determination of MGMT methylation status serves as clinically relevant biomarker in accessing the inclusion of TMZ in the treatment of GBM. Even if the patients show methylated MGMT promoter gene or absence of MGMT, the mutations in MMR gene would then play a crucial role in determining the success of TMZ therapy.

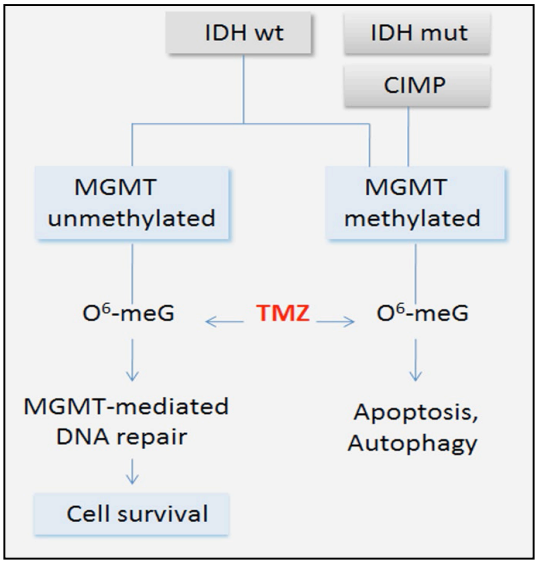

Figure 4: Resistance mechanism of TMZ [4]

1.3. Lazaroids

1.3.1. History

Methyl prednisolone was tested both pre-clinically and clinically in brain and spinal cord injury as a neuro-protective agent at high dose of 30 mg/kg. It was seen that the neuro-protective action was mediated via anti-oxidant effect inhibiting lipid peroxidation. Additionally the anti-lipid peroxidation effect was independent of the glucocorticoid receptor mechanism. Use of synthetic chemistry tools led to development of group of non-glucocorticoid steroids called as 21-aminosteroids, which were potent and effective inhibitors of lipid peroxidation [23]. The earliest 21-aminostroids developed was U-72099E having equivalent lipid peroxidation inhibition compared to methyl prednisolone and lacking glucocorticoid activity.

Additional efforts were directed to synthesize 21-aminosteroids such as U-74006F, U-74389G and U-74500A having more potent properties than U-72099E. Of all the 21-aminosteroids, U-74006F or tirilzad mesylate was selected to undergo phase III clinical trials in humans for brain and spinal injury, subarachnoid hemorrhage, and stroke [23]. Lazaroid U-74389G (LAZ) is a close structural analog of tirilazad mesylate, characterized by the absence of the methyl group in the 16-position of the steroid ring system (**Figure 5**) and has demonstrated similar pharmacokinetics and pharmacological properties as tirilzad mesylate [24].

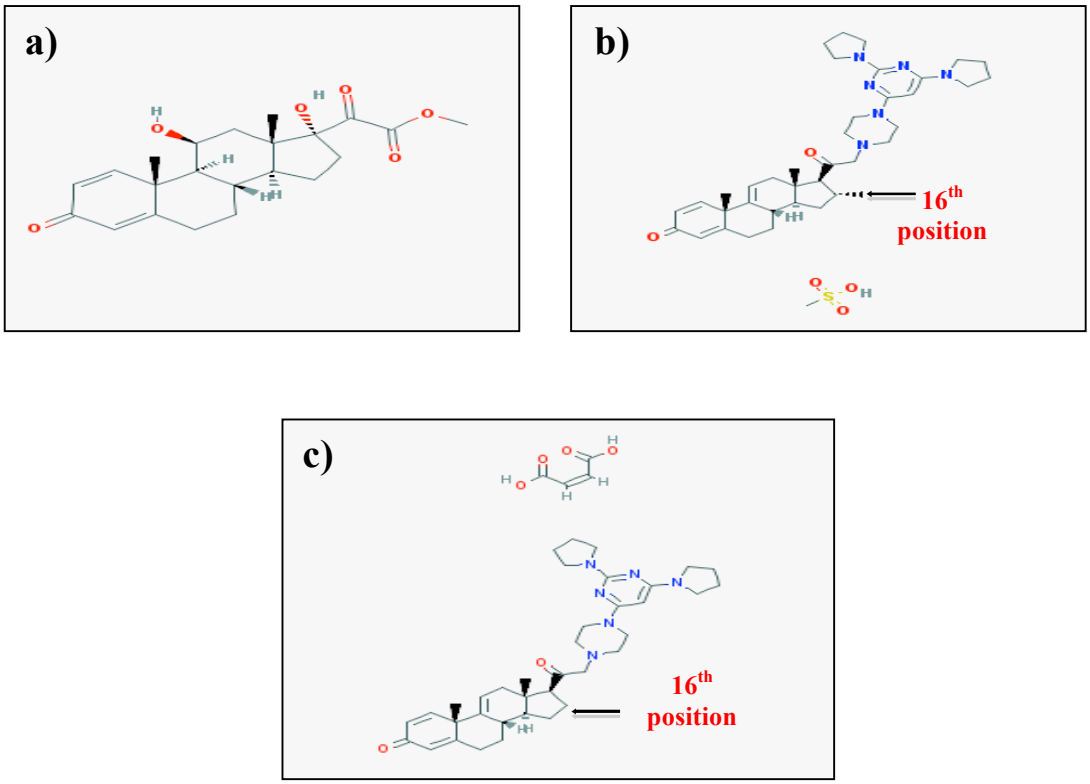

Figure 5: Chemical structures of **a)** methyl prednisolone, **b)** tirilazad mesylate (U-74006F) and **c)** U-74389G

1.3.2. Therapeutic uses

Lazaroids have demonstrated lipid peroxidation inhibitory activities (*in vitro* IC_{50} values: 2 to 60 μM) comparable to commonly used anti-oxidants, such as α–tocopherol and butylated hydroxytoluene (BHT) [25]. Additionally, lazaroids have shown effectiveness in various *in vivo* preclinical and clinical trials of head and spinal cord injury, chronic cerebral vasospasm, ischemia, subarachnoid hemorrhage [26-33]. Apart from the aforementioned conditions, LAZ could also potentially be used as a therapeutic adjuvant in the current glioblastoma therapy because of the following reasons:

1. LAZ has been tested as an *in vivo* radio-protectant in stereotactic radiosurgery induced radiation injury in healthy cats and rats, as well as in malignant glioma model in rat [34-36].
2. LAZ has also demonstrated anti-proliferative activities *in vitro* in primary cultures of glioma and human astrocytoma cell lines [37, 38].
3. LAZ distributes at level of vascular endothelium, selectively protecting normal tissues over tumor tissues [34].
4. The anti-oxidant, anti-inflammatory and cyto-protective activities of LAZ have been demonstrated in ischemia and reperfusion injury in rat liver [39], pig intestine [40] and pancreas [41], and in pig model of intracerebral haemorrhage [42]. Lazaroids have shown to exert cyto-protective effects by inhibiting arachidonic acid release, stabilizing cell membranes, suppressing Kupffer cell activation, suppressing the cytokine production by inhibiting nuclear factor kappa B activation [43].

1.3.3. Mechanism of action

The lazaroids inhibit lipid peroxidation via two pathways: free radical scavenging and membrane stabilization. The lazaroids exert a chemical anti-oxidant effect similar to Vitamin E by scavenging lipid peroxyl radicals and are also capable of scavenging and decreasing the production of hydroxyl radicals. The lazaroids have been established as inhibitors of both iron-dependent and iron-independent lipid peroxidation reactions [44]. The lazaroids have demonstrated high affinity for lipid bilayer in cell membrane resulting

in physcio-chemical interactions. At physiologic pH the piperazine nitrogen is positively charged resulting in ionic interaction with the negatively charged phosphate group of phospholipid in the lipid bilayer (**Figure 6**). Additionally, the pyrimidine amine group of lazaroids compresses the phospholipid head group. The bulky steroid moiety orients itself and localizes in the hydrophobic tail group of lipid bilayer. The interaction with free radicals lead to disordering and destabilization of the lipid bilayer whereas, the lazaroids incorporated in the lipid bilayer in defined positions and orientations help to decrease the membrane fluidity resulting in stabilization. The membrane stabilizing and anti-oxidant effects of lazaroids cumulatively aid in preventing the lipid peroxidation chain reaction by restricting the movement of free radicals thus preventing their interaction with membrane lipids [45]

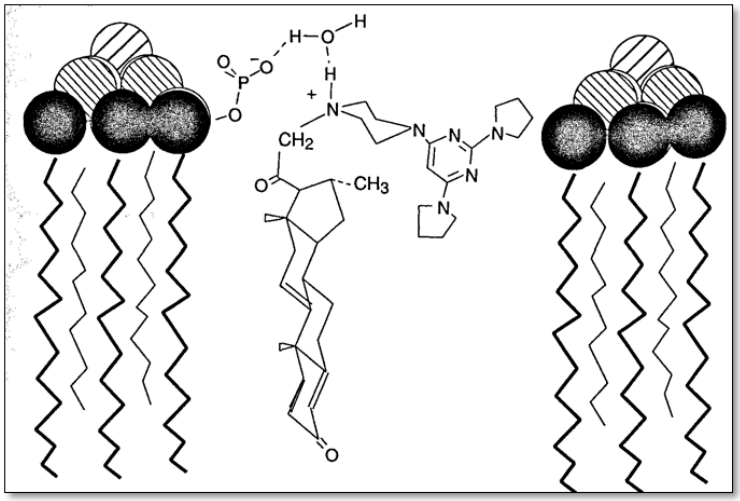

Figure 6: Physico-chemical interactions of lazaroid with cell membrane lipid bilayer [45]

1.3.4. Pharmacokinetics

Two phase-III clinical trials were conducted to test the efficacy of tirilazad mesylate on patients with acute stroke. Treatment with trilazad mesylate did not show improvement in overall patient survival compared to control group and since then further research on lazaroids was discontinued [46, 47]. The possible reasons for the failure of the clinical trials could be attributed to high hepatic clearance of lazaroids on intravenous administration [48]. Additionally, lazaroids are metabolized via both oxidative (cytochrome P450) and reductive (5α-reductase) pathways [49] and are potential substrates of P-glycoprotein (P-gp) efflux transporter [50]. This could have decreased the systemic exposure of lazaroids limiting their transport across blood brain barrier (BBB), leading to sub-therapeutic drug concentrations in the brain.

1.4. Delivery to the brain

1.4.1. Blood brain barrier (BBB)

The blood brain barrier (BBB) is an anatomic and physiological barricade essential in maintaining the normal brain function and homeostasis. The BBB is composed of brain blood capillary endothelial cells, astrocytes, basement membrane, pericytes, neurons and microglia and are called as the 'neurovascular unit' (**Figure 7**) [51]. The neurovascular unit has unique features that help to nourish the brain with nutrients and to protect it from invasion of harmful systemic toxic substances. The unique features of neurovascular unit are summarized as follows: [52, 53]

- The presence of intercellular tight junctions between the brain endothelial cells, the absence of fenestrations and very few pinocytic vesicles resulting in lower paracellular diffusion. The tight junctions form complex interactions between the transmembrane proteins (occludins, claudins) and cytoplasmic proteins (zonula occludens-1 and 2) and are strengthened by interactions with glial cells, astrocytes, pericyetes and neurons.
- High mitochondrial expression resulting in increased metabolic activity coupled with expression of specific influx (amino acid, insulin) and efflux (Pgp) transporters and receptors help to control the entry and exit of substances in and out of the brain.
- In addition to the brain endothelial cells, the glial cells and astrocytes maintain the integrity of BBB by releasing neuro-protective factors such as neurotrophic factor, angiopoietin-1, etc. The pericytes and neurons are in close contact with the brain blood vessels regulating their vascular structure and functions.
- The BBB limits the entry of immune cells like lymphocytes and lacks lymphatic clearance system. Additionally, the brain endothelial cells forms a network with perivascular macrophages, mast cells ad microglia forming an immune barrier.

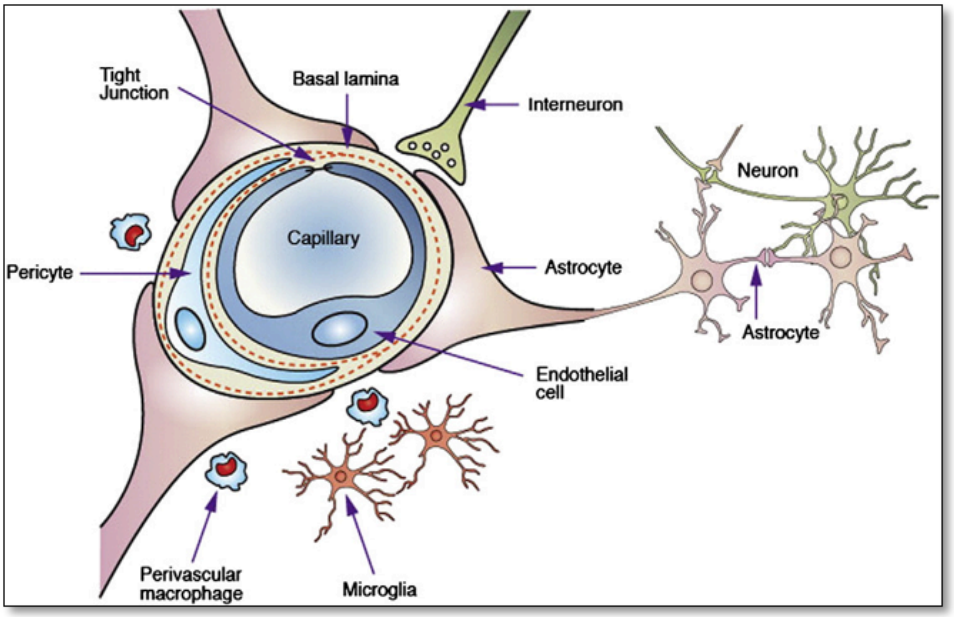

Figure 7: The neurovascular unit of blood brain barrier [52]

The brain uptake of drugs depends not only on its transport properties across the BBB but also on the drug concentration in the blood. This is known as the pharmacokinetic rule and could be described by **Equation 1**:

Equation 1

$$\%ID/g = PS \times AUC$$

- **%ID/g** is the percent of administered dose taken up by per gram of the brain,
- **PS** is the permeability-surface area of BBB,
- **AUC** is the area under the curve of drug plasma concentration

The PS is dependent on the transport properties of drug across BBB and the AUC is governed by the clearance of drug from systemic circulation by organs of reticuloendothelial system (RES) such as liver, spleen, etc. Based on the this rule, an

enhanced brain uptake of drugs is seen on increasing the systemic exposure of the drug (AUC) and drug modifications to increase passive and/or active transport across the BBB (PS). However, the increase in PS by chemically modifying drug structure to make it more lipophilic simultaneously increases the peripheral distribution of the drug resulting in more clearance and less systemic exposure. Thus, a fine balance has to be met, wherein an increased drug circulation time is achieved along with increased brain permeability [54]. Moreover, the distribution of drugs to the brain is further dictated by various factors such as plasma/tissue protein binding, rate of systemic and brain metabolism, BBB influx and efflux rates, cerebral blood flow, pathological conditions, etc [55].

The ideal physico-chemical properties of drug for passive as well as active transport across BBB are summarized in **Table 2** [56].

The different transport mechanisms for passage of drug molecules across BBB are depicted in **Figure 8**. The paracellular transport across the tight junctions is negligible due to lack of fenestrations and presence of pinocytic processes. The paracellular transport (a) is only restricted to small water-soluble agents.

Physico-chemical properties	Limits
Molecular weight	< 450 Da
Lipophilicity	cLogP < 5
Number of H-bond donor	< 3
Number of H-bond acceptor	< 7
Number of rotatable bonds	< 8
H-bonds	< 8
pKa	Neutral or basic with pK_a 7.5–10.5
Metabolic stability with	>80% remaining after 1 h
P450 enzyme CYP inhibition	< 50% at 30 uM
No significant CYP2D6 metabolism, not a potent CYP3A4 inducer, Not an efficient P-glycoprotein substrate (*in vivo*)	

Table 2: Physico-chemical properties of drug to cross BBB [56]

The transcellular transport consists of passive diffusion and active transport. Lipid soluble agents like oxygen, carbon di-oxide, alcohol, and steroid hormones can easily transported across the lipid bilayer via passive diffusion (b). Carrier-mediated transport (c) can use ATP (active transport) or not use ATP (facilitated diffusion) for moving small molecules across the BBB. The carrier-mediated transport involves movement of molecules from either blood to brain (influx) or from brain to blood (efflux) and the transporters can be saturated or inhibited. The influx transporters such as amino acid

transporters are used to deliver essential nutrients like basic amino acids to the brain while efflux transporters such as P-gp, multidrug resistance-associated protein (MRP) expel the drug molecules like cyclosporine from the brain. The receptor-mediated transcytosis (d) is an energy dependent process involving endocytosis of receptor-ligand complex and its transport across the cell membrane for exocytosis. Large molecules like transferrin, insulin are transported via receptor-mediated transcytosis. Adsorptive transcytosis involve ionic interaction of negatively charged cell membrane with positively charged molecules such as albumin for transport across the BBB [57, 58].

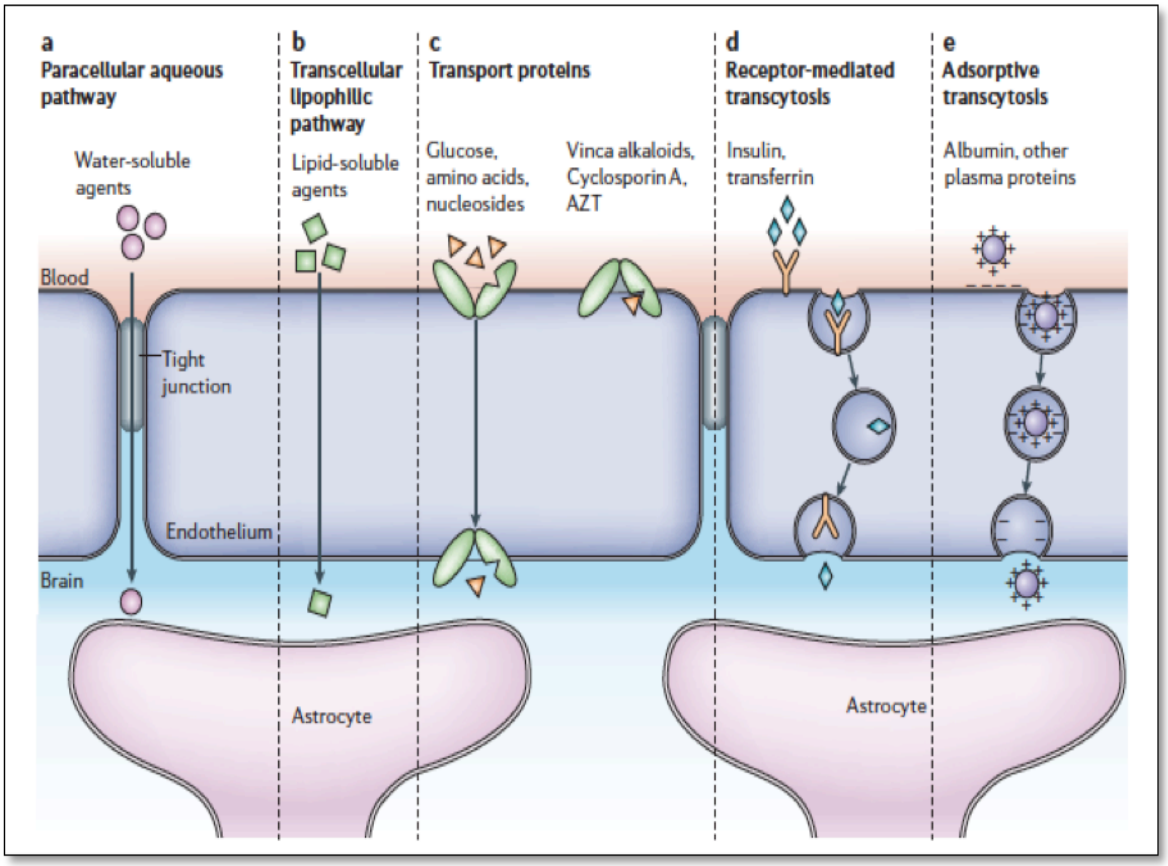

Figure 8: Transport routes across the blood brain barrier **(a-e)** [58]

The various strategies employed, to bypass the BBB to deliver drugs at therapeutic concentrations to the brain have been extensively studied and are summarized as follows:[57, 59-61]

1. Chemical modification of drugs for targeted delivery, use of prodrugs and lipophilic drug analogs
2. Biological transport using carrier and/or receptor mediated delivery
3. Convection enhanced delivery
4. Temporary osmotic, biochemical or ultrasound mediated disruption of BBB,
5. Circumventing BBB using alternative routes such as intra-nasal delivery, intra-cerebroventricular and intrathecal injections as well as intracerebral delivery using interstitial injections

We will be focusing in more detail on the use of nano-carrier systems as drug delivery vehicles to evade the BBB for delivering drugs to the brain.

The ideal nano-carrier should possess the following characteristics:[59, 62]

1. Particle size < 100 nm and hydrophilic surface coating to prevent clearance by reticuloendothelial system (RES) resulting in prolonged systemic circulation.
2. Made from biocompatible, biodegradable and non-toxic materials; resulting in increased systemic stability in blood/plasma and reduction in immunogenicity and inflammatory responses due to lower tendency of platelet aggregation, activation of neutrophils, etc.
3. Ability to engineer the surface by attaching targeting ligands for carrier or

receptor mediated transport.

4. To control/sustain drug release and protect the drugs from enzymatic or atmospheric degradation ensuring its stability.
5. Scale-up and manufacturing should be cost effective and commercially viable.

Nano-carriers due to their sub-micron size and surface modifications can escape the RES uptake resulting in prolonged systemic drug circulation and enabling better exposure to the brain via passive delivery and/or active targeting. Surface modifications of drug-loaded nanoparticle with selective ligands can result in shipping of the nano-carriers via carrier-mediated, receptor mediated and/or adsorptive mediated transport resulting in a 'Trojan-horse' effect [55]. The various approaches for active targeting of nanoparticles conjugated with ligands for delivery of drugs across BBB are listed as follows [63, 64]:

- Use of endogenous molecules such as Glucose, transferrin, folates, apolipoproteins for targeting glucose (GLUT), transferrin (Tfr) and folate (FR), low-density lipoprotein (LDL) receptors respectively.
- Use of monoclonal antibodies such as OX26 for targeting Tfr receptors.
- Use of cell penetrating peptides such as transactivator of transcription (TAT).

Polymeric nanoparticles, liposomes, nano/micro emulsions, lipid nanoparticles are the various nano-carrier systems used for delivering drugs to the brain. Of all the nano-carrier systems, lipid nanoparticles mainly solid lipid nanoparticles (SLN) and nano-structured lipid carriers (NLC) are currently gathering wide importance. This is mainly because they combine the advantages of conventional nano-carriers like polymeric nanoparticles and

liposomes, namely sustained drug release, protection of drug from degradation, ease of surface modifications and an ability to form particles in nanometer range. At the same time these lipid nanoparticles do not face limitations like toxicity issues related to polymer degradation, difficulties in scale-up and drug leakage associated with liposomes, etc [65].

1.4.2. Solid lipid nanoparticles (SLN)

Solid lipid nanoparticles (SLNs) are produced by replacing the entire liquid lipid (oil) in an emulsion with a solid lipid or a blend of solid lipids. The lipid matrix of SLNs is solid at body temperature. SLNs are composed of 0.1-30 % (w/w) solid lipid dispersed in an aqueous medium [66].

The loading capacity of the drugs in the lipid matrix of SLNs is dependent on drug solubility and/or miscibility in lipid melt, physico-chemical properties of lipids and polymorphic state of lipids [67]. The aforementioned factors influence the incorporation of drugs in the lipid matrix and, the SLNs can be divided into three types as depicted in **Figure 9**:

1. **Solid solution model:** The solid solution type SLN consists of drug homogeneously distributed in the lipid matrix without any use of surfactants or solubilizers mainly due to strong interaction between the drug and the lipid. This type of SLN is mainly obtained using cold homogenization technique.
2. **Drug enriched core model:** The drug enriched core type SLN is formed when the concentration of drug is close to its the saturation solubility in lipid during

processing at high temperatures. On cooling after processing at high temperature, there is super-saturation of drug in the lipid melt resulting in drug crystallization before lipid crystallization. On further cooling, there is recrystallization of melted lipid that surrounds the already crystalized drug core. Thus, a drug enriched core surrounded by lipid membrane is formed

3. **Drug enriched shell model:** The drug enriched shell type SLN is formed when the concentration of drug is below its saturation solubility in the lipid matrix. This results in partitioning of drug in the water phase during processing at high temperature and repartitioning back in the lipid phase as the temperature decreases. On cooling after processing at high temperature, the lipid melt first begins to recrystallize while the drug is still present in the water phase. As the temperature further drops, the drug begins to repartition in the already recrystallized lipid matrix shell and deposits on the outer surface of the lipid shell.

The drug incorporation models influence the drug release profiles from SLN. The solid solution model demonstrates a prolonged drug release over a period of several weeks, since the movement of molecularly dispersed drug is limited. In the drug enriched core model, the drug release is dependent on the diffusional distance between drug core and lipid shell and is thus governed by Fick's law of diffusion resulting in sustained drug release. For the drug shell enriched model, the localization of drug in outer shell results in initial fast burst release profile while the later part of release profile will be governed by factors such as particle size and surface area, diffusion coefficient of drug, matrix

viscosity and diffusion distance of drug from core to shell [68, 69].

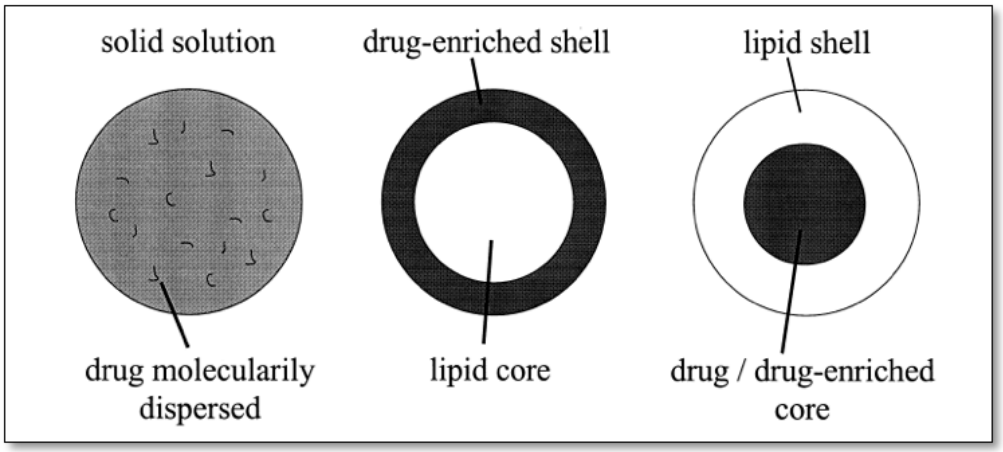

Figure 9: Drug incorporation models in SLN [67]

Drug loaded SLNs are widely used for enhancing brain exposure using the following approaches:

1. Protecting the drug from biological degradation and increasing systemic drug bioavailability especially for drugs which easily permeate across BBB and,
2. Increasing permeability across the BBB for drugs, which inherently have moderate to poor permeation properties.

Few studies using SLNs for enhancing drug delivery across BBB especially via intravenous route are summarized in **Table 3** [70-75].

Although the SLNs offer wide variety of advantages over the conventional nano-carrier delivery systems, the SLNs have some inherent shortcomings, which limits its utility. The low drug loading capacity and polymorphic lipid transitions leading to poor storage

stability are the prominent disadvantages of SLNs [76]. The SLNs are predominantly prepared from a single solid lipid or blend of chemically identical solid lipids **Table 5.**

Drug	**Solid Lipid**	**Method of preparation**	**NLC properties** **PS** (nm), **ZP** (mV), **EE** (%)
Camptothecin	Stearic acid	Ultrasonication	196.8 nm, -45.2 mV, 99.6 %
Noscapine	Stearic acid	Microemulsion	Non-stealth: 61.3, -35.1 mV, 80.4% Stealth: 80.5 nm, -42.4 mV, 83.6 %
Clozapine	Trimyristin, tripalmitin, tristearin	Ultrasonication	96.7 to163.3 nm, 21.3 to 33.2 mV, 96.5 to 98.8%
Quercetin	Compritol	Ultrasonication	159 nm, 21.05 mV, 85.7 %
Doxorubicin	Stearic acid	Microemulsion	Non-stealth: 80 nm, -11 mV Stealth: 90 nm, -33 mV
Riluzole	Compritol 888 ATO	Microemulsion	88 nm, -45.8 mV

Table 3: List of drug loaded SLNs intended for intravenous delivery for brain targeting [70-75]

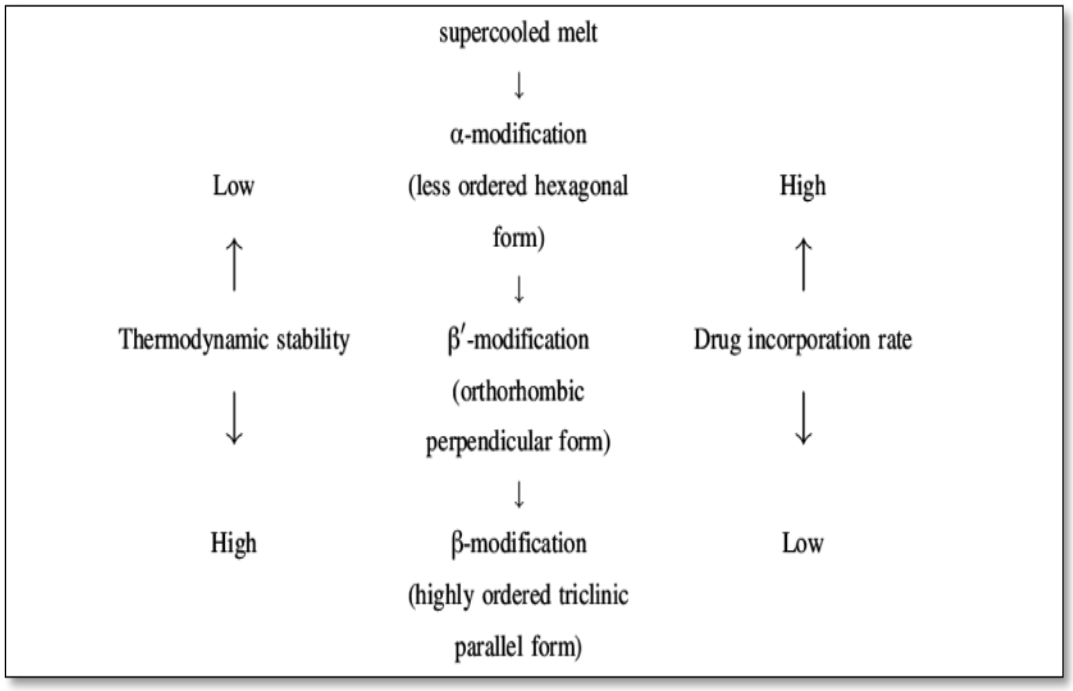

Figure 10: Relationship between thermodynamic stability, drug loading and crystal structure [77]

During production of SLNs the lipid melt needs to be cooled rapidly under controlled conditions to form solidified lipid matrix that aids in sustaining the release of the drug *in vivo*. However, the lipid matrix solidifies in a specific crystalline form and undergoes polymorphic transition during storage [78]. The crystal structure of lipid matrix and its consequent polymorphic transitions are strongly correlated to the thermodynamic stability and drug incorporation efficiency (**Figure 10)**. The crystallinity and polymorphic transitions are affected by method of SLN preparation, type and amount of lipid, drug and surfactant used, particle size of SLNs, etc [77]. The melted lipids on

cooling assume specific configurations resulting in formation of α, β′, and β crystals with hexagonal, orthorhombic, and triclinic unit structures, respectively. The thermodynamic stability and the degree of order for crystal lattice structures is α<β′<β. On cooling, the SLNs assume either a α or β′ configuration wherein the drug loading is high but thermodynamic stability is low. On storage a more thermodynamically stable polymorphic form β is achieved and the highly ordered crystal lattice assumes a 'brick-walled' structure failing to accommodate the drug species resulting in the expulsion of drug from the SLN matrix on storage **(Figure 11)**. The particle shape of the SLN also changes from spherical (α state) to needle like structures (β state) having high surface area, which the surfactant cannot stabilize resulting in flocculation of SLN dispersion [79].

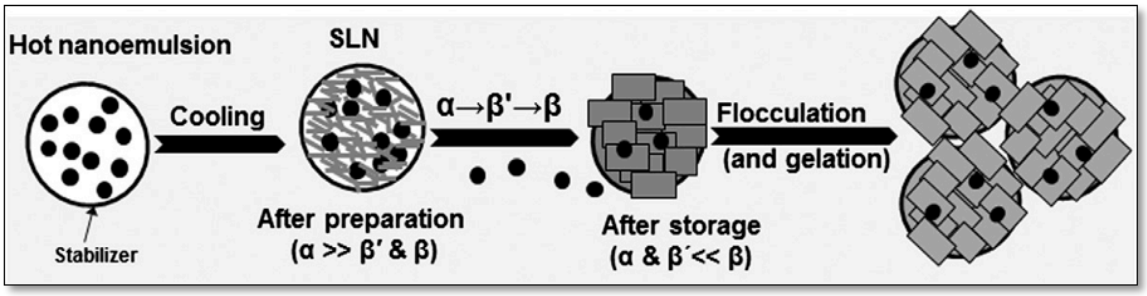

Figure 11: Schematic representation of lipid polymorphic changes in SLN [80]

1.4.3. Nano-structured lipid carriers (NLC)

Nanostructured lipid carriers (NLCs) are second generation of lipid nanoparticles introduced to overcome the limitations of SLNs with regards to low drug payload and short storage stability. Bunje et al previously observed the SLNs prepared from binary

solid lipid blends had less ordered crystal structures and demonstrated slower polymorphic transitions after cooling compared to SLNs prepared from single solid lipid [78]. Thus in order to create lipid nanoparticles with slow polymorphic transitions spatially dissimilar lipids with suitable miscibility properties are needed. NLCs are produced by blending of solid lipids with liquid lipids (oils). Although a melting point depression is observed on mixing solid and liquid lipids, the lipid blends are still maintained in a solid state at body temperature by preferably mixing solid and liquid lipid in ratios ranging from 70:30 to 99.9:0.1. NLCs possess a high capacity to accommodate solid lipids (~ 95 %) dispersed in aqueous medium [66]. The 3 different structural types of NLCs are depicted in **Figure 12:** [81, 82]

1. **The imperfect type:** It is observed that larger distances between fatty acid chains in lipids results in bigger the holes or spaces in the lipid crystal lattice for achieving higher drug loading capacity. Thus, instead of using solid lipids with longer carbon chain lengths or blends of saturated and unsaturated solid lipids; spatially different liquid lipids can be mixed with solid lipids to form imperfections in the crystal structure in order to accommodate a higher drug payload.
2. **The amorphous type:** Polymorphic transitions of solid lipid form amorphous to crystalline state leads to expulsion of drug from SLN during storage. Thus, mixing of solid lipids with liquid lipids such as hydroxyoctacosanylhydroxystearate, isopropyl myristate or medium chain

triglycerides, will result in formation of lipid matrix solidifying on cooling into amorphous state. The lipid matrix possesses less mobility and does not revert back into crystalline state.

3. **The multiple type:** This type of NLC is similar to a multiple emulsion system consisting of oil droplets-in-lipid matrix-in-aqueous dispersion. The liquid lipid is selected so as to have higher drug solubility compared to solid lipid. A high amount of liquid lipid is used to super-saturate the solid lipid. On cooling, the liquid lipid precipitates as tiny oil droplets resulting in oily nano-compartments dispersed in solid lipid matrix. Thus, the incorporation of different blends of solid and liquid lipids results in formation of specific crystal lattice structures capable of increasing drug encapsulation and preventing drug expulsion during storage

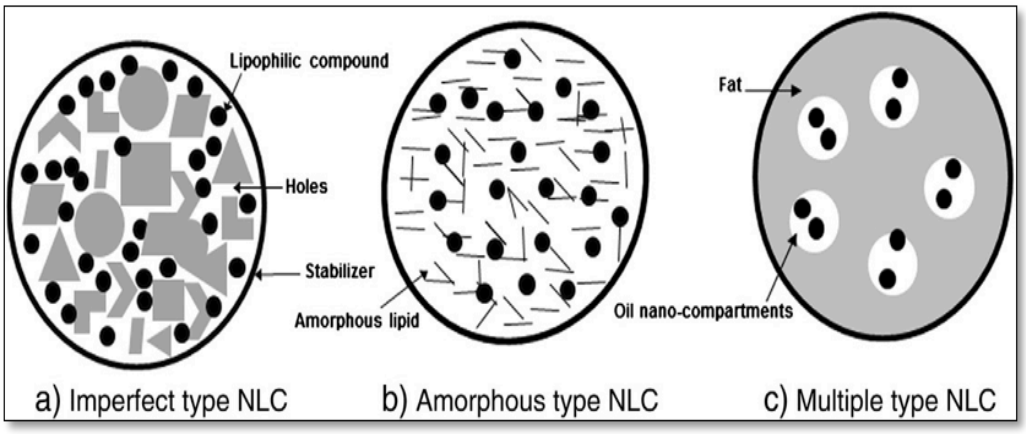

Figure 12: Structural types of NLC [80]

The NLCs have ability of incorporating higher lipid content (up to 98 %) compared to SLN (up to 30 %). Even with lower lipid content, the SLNs have lower storage stability than NLCs with higher lipid content. The low concentrated lipid particles in SLNs possess high diffusional energy resulting in collision and formation of aggregates during storage as well *in vivo*. Contrarily, the high concentrated lipid particles in NLCs are arranged in pearl like network resulting in low diffusion energy and collision thus preventing formation of aggregates and high storage stability **(Figure 13)**. After *in vivo* administration, this network can easily breakdown resulting in formation of non-aggregated particles [82].

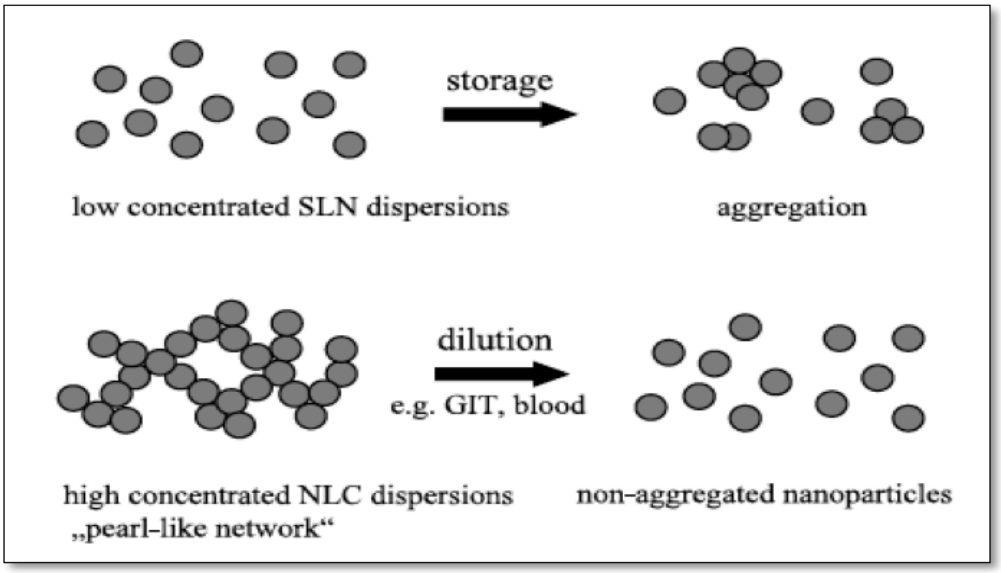

Figure 13: Stability of SLN and NLC on storage [82]

Unlike SLNs, there have been limited studies **(Table 4)** reported for exploring the brain exposure of drug loaded NLCs via intravenous route [83-87].

Drug	Lipids	Method of preparation	NLC properties **PS** (nm), **ZP** (mV), **EE** (%)
Bufadienolides	**Solid:** Glyceryl monostearate **Liquid:** Medium-chain triglyceride and oleic acid	Melt-emulsification and ultrasonication	104.1 nm, −15 to −20 mV, 87.4-95.6 %
Baicalein	**Solid:** Tripalmitin **Liquid:** Gelucire	High speed homogenization and ultrasonication	100 nm, -50 mV, N/A
Itraconazole	**Solid:** Glyceryl distearate **Liquid:** Diethyl glycol monoethyl ether	Hot high-pressure homogenization	313.7 nm, -18.7 mV, 70.5 %
Tamibarotene	**Solid:** Cetyl palmitate **Liquid:** Squalene	Microemulsion	201.6 nm, −20.1 mV, 94.3%
Apomorphine	**Solid:** Cetyl palmitate **Liquid:** Squalene	Not Available	370–430 nm, 42–50 mV, 60 %

Table 4: List of drug loaded NLCs intended for intravenous delivery for brain targeting [83-87]

1.4.4. Production methods and components of SLN and NLC

There are different approaches used in production of SLN and NLC such as high-pressure homogenization, microemulsion technique, solvent emulsification-evaporation, solvent diffusion and high-speed homogenization with ultrasonication and each of these technique is described as follows:[69, 88]

- **High-pressure homogenization**

The high-pressure homogenization can be processed at high (hot) or low (cold) temperatures depending on thermo-labiality and hydrophilicity of the drug. In hot high-pressure homogenization, the drug is firstly solubilized or dispersed in lipid heated at temperatures (5-10°C) above its melting point to which hot aqueous surfactant solution is added and mixed using high speed to form pre-emulsion. This hot pre-emulsion is fed to high-pressure homogenizer maintained at same temperature for defined number of cycles and at optimized pressure. In case of cold high-pressure homogenization, the dug is firstly solubilized or dispersed in lipid heated at temperatures (5-10°C) above its melting point and is cooled rapidly and milled to form microparticles. The resulting microparticles are suspended in cold aqueous surfactant solution and fed to high-pressure homogenizer maintained at the same cold temperature for defined number of cycles and at optimized pressure.

- **Microemulsion**

The drug is firstly solubilized or dispersed in lipid heated at temperatures (5-10°C) above its melting point and then an aqueous solution of surfactant and co-surfactant maintained

at same temperature is added to the drug lipid melt to spontaneously form microemulsion. This microemulsion is added to cold water using temperature controlled syringe and mild agitation resulting in breakdown of oil droplets to form nano-emulsion followed by immediate solidification of lipids to yield lipid nanoparticles.

- **Solvent emulsification-evaporation or diffusion**

In this technique, the drug is dissolved in water immiscible organic solvent. An aqueous surfactant mixture at room temperature is added to the organic phase resulting in formation of nano-emulsion. The removal of the organic solvents using low pressure or vacuum results in controlled precipitation of lipid nanoparticles.

- **Solvent diffusion**

Solvent diffusion is combination of microemulsion and solvent emulsification-evaporation technique and involves use of partially water miscible organic solvents. Both the organic solvents and water are saturated with each other to reach thermodynamic equilibrium. The lipids are dissolved in water saturated organic solvents and then the organic solvent saturated water surfactant solution is added to lipid solution to form microemulsion. This microemulsion is then added to excess of water resulting in formation of lipid nanoparticles due to partition of lipids from organic droplets to continuous aqueous phase.

- **High-speed homogenization with ultrasonication**

The drug is first solubilized or dispersed in lipid heated at temperatures (5-10°C) above its melting point to which hot aqueous surfactant solution is added and mixed using high

speed to form pre-emulsion. The hot pre-emulsion is then ultrasonicated using a probe sonicator at optimum time and amplitude to obtain hot nano-emulsion. The hot nano-emulsion is then cooled at or below room temperature to obtain lipid nanoparticles.

The different types of solid lipids, liquid lipids and surfactants used in production of SLN and NLC are summarized in **Table 5** [76, 80, 89, 90]. These ingredients are recognized as GRAS (Generally Recognized As Safe) by the USA FDA. In addition to the aforementioned ingredients, coating of SLNs and NLCs with hydrophilic agents helps prevent the systemic clearance of the nanoparticles by RES. The hydrophobic surface properties of the lipid nanoparticles could result in adsorption of plasma proteins or opsonins on their surface resulting in uptake and clearance by RES. The coating of SLNs and NLCs by hydrophilic agents like polyethylene glycol (PEG) polymers of different molecular weights, form a sterically stabilized shell around the surface of nanoparticles preventing its detection and subsequent clearance by the RES [55, 68].

Solid Lipids	• Glyceryl palmitostearate, Glyceryl monostearate, Glyceryl dibehenate, Glyceryl monocaprate, Propylene glycol monostearate, Witeposol bases • Cetyl palmitate, Beeswax, Carnauba wax • Stearic acid, Palmitic acid, Decanoic acid, Behenic acid • Tripalmitin, Tricaprin, Trilaurin, Trimyristin, Tristearin, Hydrogenated coco-glycerides
Liquid Lipids	• Soybean oil • Medium chain triglycerides (MCT)/caprylic- and • capric-triglycerides • Oleic acid • α-tocopherol/vitamin E • Corn oil • Squalene • Lauroyl Polyoxylglycerides • Monoacylglycerols

Table 5: List of solid lipids, liquid lipids, surfactants and co-surfactants used in SLN and NLC [76, 80, 89, 90]

Surfactants/ Co-surfactants	• Polysorbates • Poloxamers • Sodium cholate, Sodium glycocholate • Taurocholic acid and Taurodeoxycholic acid sodium salt • Butanol, Butyric acid • Lecithin • Macrogol-15-hydroxystearate • Polyoxiethylene stearate • Polyoxyl castor oil • Sodium dodecyl sulfate, Sodium deoxycholate

Table 5 (contd.): List of solid lipids, liquid lipids, surfactants and co-surfactants used in SLN and NLC [76, 80, 89, 90]

1.5. Design of experiments (DoE)

Since 2008, ICH has stressed on the paradigm of 'building in quality by design, rather than testing it' by introducing a systematic Quality by Design (QbD) approach in pharmaceutical product development. QbD approach is based on sound science utilizing prior knowledge, experimentation and risk assessment to help determine the effects of formulation and process parameters on critical product quality attributes creating a design space. The design space is an integrated multidimensional region comprising of vital formulation and process variables along with their interactions that have demonstrated to

provide assurance of product quality. A design space is commonly established using a design of experiment approach (DoE), which is a structured, organized method for determining the relationship between factors affecting a process and the output of that process [91]. Building an experimental design involves the use of statistical modeling to provide maximum information with minimal number of experiments and provide simultaneous multivariate analysis along with its interactions [92]. Response surface methodology (RSM) is a type of experimental design involving use of statistical and mathematical techniques for developing, improving, and optimizing processes [93]. RSM is used to determine the optimal conditions that are derived from response surfaces build using results from the design matrix for the most important factors. Central composite design (CCD) commonly involves the use of RSM. CCDs are factorial or fractional factorial designs with center points and supplemented by a group of axial points (star points) for estimating response surface curvature **(Figure 14)**.

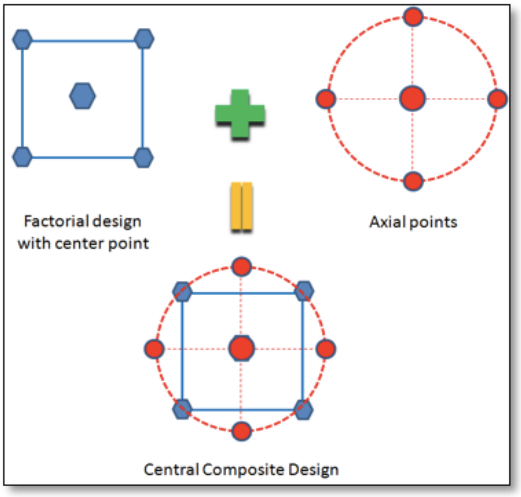

Figure 14: Graphical representation of central composite design

1.6. Scope of research

Firstly, the solubility of LAZ is limited by pH with maximum solubility of 2 mg/mL at pH 3.0 using buffered citrate solution. The intravenous use of LAZ citrate solution results in pain and irritability at site of injection and also limits the potential of high dose bolus administration [94]. **Secondly,** in clinical trials, lazaroid (tirilazad mesylate) dissolved in citrate buffer solution was administered as intravenous infusion to patients. These clinical trials were unsuccessful resulting in insignificant improvement in patient survival compared to control [33]. The failure of the clinical trials could be attributed to high hepatic clearance, susceptibility to metabolism and efflux transporters of lazaroid resulting in its poor brain exposure. **Finally,** Ciuffi et.al., had advocated the importance of using lazaroid as a retard formulation (solution in 1% PEG 4000) instead of a buffered solution, helping lower lazaroid systemic clearance and increasing its brain levels for achieving therapeutic lipid peroxidation inhibition [95].

Thus taking lessons from previously reported observations, formulating LAZ into nano-carriers especially NLC would help to provide protection for LAZ from hepatic exposure, enabling prolonged systemic circulation and higher exposure of LAZ in the brain. The NLCs is the ideal choice of nano-carrier not only because of properties such as sustained and targeted drug release, nano-size, ease of surface modifications and better *in vivo* safety profile; but mainly due to their superior physiological and storage stability as well as higher drug loading compared to polymeric nanoparticles, liposomes, emulsions and SLNs. NLCs are predominantly used for topical and oral administration and are not

extensively explored for intravenous administration especially for delivery to the brain **(Table 4)**. Also, during the development of NLCs using DoE approach factors such as surfactant, drug to lipid ratio and process parameters like ultrasonication or homogenization cycles are commonly investigated [96-98]. The effect of surface modifiers like PEG on formulation properties like particle size, zeta potential ad encapsulation efficiency have not been widely studied. The development of PEGylated LAZ-NLCs is reported for the first time for intravenous delivery in enhancing LAZ delivery to the brain and reducing its hepatic exposure for potential application in treatment in glioblastoma.

Chapter 2: Objectives and Specific Aims

2.1. Hypotheses

Our first hypothesis is '*lazaroid U74389-G loaded NLCs developed using design of experiments approach will increase the brain exposure and reduce the liver uptake of lazaroid U74389-G.*'

Our second hypothesis is '*the developed lazaroid U74389-G loaded NLCs will show a non-linear increase in brain levels of lazaroid U74389-G with increase in dose.*'

2.2. Objective

The objective of our research was to evaluate the utility of lazaroid loaded NLCs optimized using a systematic and rational approach for enhanced brain exposure as well as estimate the dose-proportionality of optimal lazaroid loaded NLCs in the brain. The rationale behind our approach was based on methodical use of minimal experimental runs to engineer NLCs with optimal surface properties capable of altering the bio-distribution of lazaroid for preferential accumulation in the brain.

2.3. Specific aims

In order to achieve our objective, we proposed three specific aims as follows:

2.3.1. Specific aim 1

Development, optimization and *in-vitro* characterization of lazaroid loaded NLCs

a. To develop and optimize the composition of lazaroid NLCs using 2-factor 5-level central composite design.

b. To characterize *in vitro* physcio-chemical properties of optimal lazaroid loaded NLCs such as morphology (TEM), physical state and crystallinity (DSC and XRD), *in vitro* hemolytic potential and storage stability.

2.3.2. Specific aim 2

Development and validation of UPLC-MS/MS for quantification of lazaroid in bio-matrices

a. To develop a sensitive method for analytical quantification of lazaroid in plasma, brain, liver and lungs using UPLC-MS/MS.
b. To validate the developed UPLC-MS/MS using US-FDA guidelines for bio-analytical validation.

2.3.3.Specific aim 3

Evaluation of pharmacokinetics and bio-distribution of lazaroid formulations in Sprague-Dawley rat model

a. To characterize the plasma pharmacokinetics of lazaroid citrate solution, lazaroid co-solvent and optimal lazaroid loaded NLCs in Sprague-Dawley rats.
b. To characterize the brain, liver and lung bio-distribution of lazaroid citrate solution, lazaroid co-solvent and optimal lazaroid loaded NLCs in Sprague-Dawley rats.
c. To characterize the dose linearity of optimal lazaroid loaded NLCs in brain of Sprague-Dawley rats.

Chapter 3: Materials and Methods

3.1. Materials

3.1.1. Chemicals and Reagents

- Lazaroid U74389G (LAZ) was purchased from Enzo Life Sciences Inc (Farmingdale, NY, USA).
- Daidzein, used as internal standard (IS) in LC/MS was purchased from LC Laboratories (Woburn, MA, USA).
- 17-α-methyl testosterone used as internal standard in HPLC was purchased from Sigma Aldrich (St. Louis, MO, USA).
- Glyceryl behenate (Compritol 888 ATO), PEG-8 caprylic/capric glyceride (Labrasol), medium chain triglyceride (Labrafac^{TM} Lipophile WL 1349) and glyceryl mono-oleate (Pecol) were purchased from Gattefosse (Saint-Priest Cedex, France).
- Trimyrsitin (Dynasan 114) and tristearin (Dynasan 118) were purchased from Cremer Oleo Division (Witten, Germany).
- Safflower and flaxseed oil were purchased from Jedwards International, Inc. (Braintree, MA, USA).
- Oleic acid was purchased from Sigma Aldrich (St. Louis, MO, USA).
- Soybean oil and polysorbate 80 were purchased from PCCA (Houston, TX, USA).
- mPEG-DSPE, MW: 2000 (DSPE-PEG 2k) was purchased from Nanocs (Boston, MA, USA).
- Tetra-ethyl ammonium acetate was purchased from Acros Organics (NJ, USA).

- Propylene glycol was purchased from J. T. Baker Chemical Co. (Phillipsburg, NJ, USA) for LAZ co-solvent.
- Amicon Ultra-4 centrifugal filters MWCO: 10,000 were purchased from Merck Milipore (Cork, Ireland) for determining encapsulation efficiency.
- Male Sprague Dawley rats (250–300 g) with jugular vein cannula were purchased from Harlan (Indianapolis, IN, USA).
- Pooled male Sprague-Dawley rat and human plasma were purchased from Equitech-Bio, Inc. (Kerrville, TX, USA)
- Fresh heparinized blood and individual rat plasma from male Sprague-Dawley rats were purchased from BioChemMed Services (Winchester, VA, USA)
- Methanol, acetonitrile and water were purchased from EMD Millipore (Billerica, MA, USA) and were LC/MS grade.
- Formic acid (~ 98% for mass spectroscopy) was purchased from Fluka Analytical (St. Louis, MO, USA).
- Heparin sodium salt from porcine intestinal mucosa from EMD Millipore (Billerica, MA, USA) for heparinizing centrifuge tubes used in pharmacokinetic study.
- Citrate buffer (pH 3.0): 42 mg citric acid monohydrate (Sigma Aldrich, St. Louis, MO, USA), 9.4 mg sodium citrate dihydrate (EMD Millipore, Billerica, MA, USA), 90 mg NaCl (Acros Organics, Waltham, MA, USA) dissolved in 10 mL distilled water as a vehicle for dissolving LAZ.

- Phosphate-buffered saline (pH 7.4): 0.8gm sodium chloride, 0.02 gm KCl (Sigma Aldrich, St. Louis, MO, USA), 0.144 gm Na2HPO4 (MCB Reagents, Cincinnati, OH, USA), 0.024 gm KH2PO4 (BDH chemicals, Radnor, PA, USA) dissolved in 100 mL distilled water as release medium for *in vitro* release study.
- Glacial Acetic acid purchased from EMD Millipore (Billerica, MA, USA).

3.1.2. Supplies

- Centrifuge tubes, 1.7 mL Ultraclear microtubes, RNase, DNase and pyrogen free from Phenix Research Products (Candler, NC, USA).
- 5cc and 1cc syringes from BD Medical (Franklin Lakes, NJ, USA) for pharmacokinetic study.
- 10, 200 and 1000 pipette tips purchased from VWR (Radnor, PA, USA).
- Spectra/Por Dialysis membrane MWCO: 6000-8000 purchased from Spectrum Labs (Rancho Dominguez, CA, USA) for *in vitro* release study.
- Polystyrene cuvettes purchased from Sarstedt, Germany for particle size and zeta potential measurement.

3.1.3. Equipments, Apparatus and Software

- HPLC apparatus consisted of Waters Model 515 pump, Waters Model 717 plus auto-sampler and Waters Model 2996 photodiode array detector (Waters, Milford, MA, USA).
- QTRAP 5500 System (AB SCIEX, Framingham, MA, USA) coupled with Waters ACQUITY UPLC H-Class system (Waters, Milford, MA, USA).

- XTerra C18 column, 4.6 x 150 mm i.d., 5 μm (Waters, Milford, MA, USA)
- ACQUITY UPLC BEH C18 column, 2.1 × 50 mm, 300A, 1.7 μm (Waters, Milford, MA, USA)
- Buchi R200 rotary evaporator (Flawil, Switzerland)
- ZetaPALS for particle size and zeta potential analysis (Brokhaven Instrument Corporation, Holltsville, NY, USA)
- Design-Expert software Version 9.0 (Minneapolis, MN, USA)
- Transmission electron microscope H7500 (Hitachi, Japan)
- DSC 60A Plus (Shimadzu Corporation, Japan)
- Rigaku Smartlab X-ray Diffractometer (The Woodlands, TX, USA)
- Plasma pharmacokinetic parameters were derived using Phoenix NLME software (Princeton, NJ, USA).
- Power model for dose linearity was derived from Phoenix WinNonlin WNL5 Classic Linear Modeling (Princeton, NJ, USA).
- GraphPad Prism Version 6.0 (La Jolla, CA, USA).
- SAS 9.3 software (Cary, NC, USA)

3.2. Methods

3.2.1. HPLC Assay for LAZ

3.2.1.1. Chromatographic Conditions

The HPLC apparatus consisted of Waters Model 515 pump, Waters Model 717 plus auto-sampler and Waters Model 2996 photodiode array detector. The chromatographic separation of LAZ and internal standard methyl testosterone (MTS) was achieved using C18 column (XTerra®, 5 μm, 150 x 4.6 mm i.d.) at room temperature. The mobile phase consisted of acetonitrile: 22mM tetraethyl ammonium acetate 70:30 (% v/v) at pH adjusted to 6.8 using glacial acetic aicd. The flow rate was 1.0 ml/min with injection volume of 10 μL and LAZ detection was measured at 254 nm. The HPLC assay for LAZ was used in the *in vitro* characterization of LAZ loaded NLCs (LAZ-NLCs).

3.2.1.2. Preparation of Aqueous Calibration Curve and Quality Control Standards

The linear range of calibration curve was established at 1-100 μg/mL. Standard stock solution of LAZ was prepared in acetonitrile at the concentration of 1 mg/mL. Standard stock solution of MTS was prepared in methanol at the concentration of 1 mg/mL. The calibration curve was prepared by diluting different volumes of the standard stock solution of LAZ with acetonitrile to yield final concentrations of 100, 50, 10, 5, 2.5, 1 μg/mL. The standard stock solution of MTS was diluted 10 times with acetonitrile to yield working stock solution of 100 μg/mL. Each calibration curve standards were spiked with 10 μL of 100 μg/mL MTS solution. Three levels of aqueous quality control (QC) samples low, medium and high (4, 40 and 80 μg/mL) were prepared in a manner similar

to the calibration standard. Linearity, selectivity, accuracy and precision were used to validate the HPLC method. Selectivity of the analytical method was tested at the lowest limit of quantification (LLOQ) of 1 μg/mL where LAZ signal to noise ratio was ≥10 when compared with blank acetonitrile solution. The accuracy and precision of the analytical method were tested at the three sets of the QC samples (low, medium and high). Accuracy was expressed as percentage (**Equation 2**) while precision was expressed as percent coefficient of variation (% CV) (**Equation 3**)

Equation 2

$$Accuracy\ (\%) = \frac{observed\ concentartion}{theoretical\ concentartion} \times 100$$

Equation 3

$$Precision\ (\%\ CV) = \frac{standard\ deviation}{mean} \times 100$$

Accuracy and precision were performed using three replicates of three sets of QC standards each on the same day for intra-day validation and on two consecutive days for inter-day validation.

3.2.2. Selection of Lipids

3.2.2.1. Selection of Liquid Lipid (Oil)

The oil component of NLC was selected by evaluating the saturation solubility of LAZ in different oils. An excess amount of LAZ was added to 0.5 mL of the oil and was shaken in a temperature controlled water bath (37°C) at 50 rpm for 40 hours. LAZ was found to be stable (> 90 %) at this experimental condition. The oil and LAZ mixtures were centrifuged at 17,968 x *g* for 20 minutes. The supernatant was diluted with 50:50 (% v/v)

mixtures of methanol and chloroform, and analyzed using validated HPLC method described in **Section 3.2.1.**

3.2.2.2 Selection of Solid Lipid

There is no direct method to determine the solubility of LAZ in solid lipids. The main role of solid lipid component of NLC is to ensure the maximum drug solubilization followed by sustained drug release over a period of time. The solubility of LAZ in various solid lipids trimyrsitin (TM), tristearin (TS) and glyceryl behenate (GB) was estimated semi-quantitatively by assessing the melting point transition of LAZ mixed with solid lipids in ratio of 1:5 (% w/w), using differential scanning calorimetric (DSC) analysis [99]. The conditions for DSC analysis are described in **Section 3.2.5.4.** Furthermore, LAZ loaded SLNs (LAZ-SLNs) were prepared using the three aforementioned lipids in a similar manner as in **Section 3.2.3.** The *in vitro* release profiles of the LAZ loaded SLN incubated in plasma were measured (N=3: Mean ± SD). The procedure for *in vitro* release study is described in **Appendix 1.1**. The solid lipid was selected based on the results of DSC analysis, and the percent cumulative LAZ release from the prepared SLNs.

3.2.3. Preparation of LAZ-NLC and LAZ-SLN

LAZ-NLCs and LAZ-SLNs were prepared using a simple stirring and ultra-sonication method as previously described [100] with some modifications **(Figure 15)**. In case of SLNs the lipid phase consisting of LAZ (20 mg), lecithin (100 mg) and solid lipids (200 mg) and for NLCs the lipid phase consisting of LAZ (20 mg), lecithin (100 mg), and as

per the CCD varying amounts of liquid lipid, solid lipid and DSPE-PEG 2k (200 mg). The lipid matrix was dissolved in 2 mL mixture of methanol and chloroform 50:50 (% v/v). The organic solvents were removed completely under reduced pressure using Buchi R200 rotary evaporator (Flawil, Switzerland).

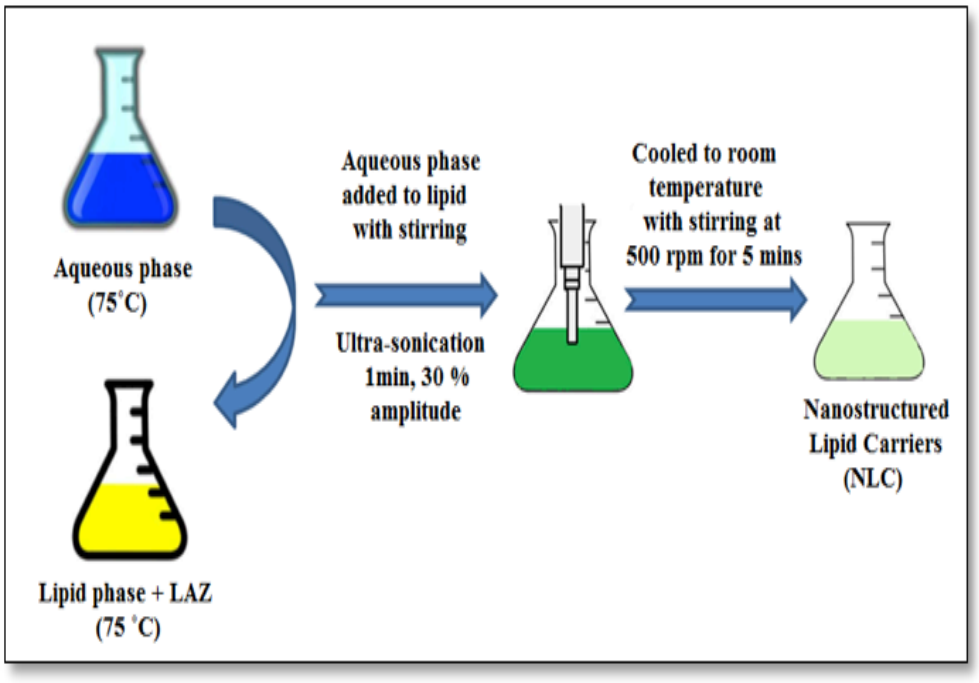

Figure 15: Schematic outline for preparation of SLNs and NLCs using ultrasonication

The LAZ containing lipid matrix was heated at 75°C. The aqueous phase containing Polysorbate 80 (100 mg) dissolved in 10 mL double distilled water was also heated at 75°C and added drop-wise with stirring to the drug loaded lipid melt. The resulting coarse oil in water emulsion was ultra-sonicated using ultra-sonic processor Q500 (Qsonica, Newton, CT, USA) for 1 minute at 30% amplitude to obtain hot nano-

emulsion. The SLNs or NLCs were obtained by cooling the hot nano-emulsion in a water bath (25°C) with stirring at 500 rpm for 5 minutes. The non-encapsulated LAZ was separated from SLNs or NLCs using ultra-filtration technique discussed in **Section 3.2.5.2.**

3.2.4. Central Composite Design

A full factorial central composite design was used to determine the influence of NLC composition on its physico-chemical properties. Design-Expert software Version 9.0 (Stat-Ease, Inc., Minneapolis, MN) was used to generate the CCD matrix and the response surfaces plots and also provide statistical analyses. After preliminary experiments, the amount of DSPE-PEG 2k and % liquid lipid were chosen as the two independent factors whose effects were tested at five levels coded as -α, -1, 0, +1, +α. The value of α (distance between center and axial points) 1.414 and was chosen to ensure that the model is orthogonally blocked and is rotatable. Orthogonal blocks helps to independently estimate the model terms and block effects independently minimizing variation, whereas rotatibility helps to provide constant prediction variance at all points from the center. The physico-chemical properties of LAZ-NLC such as particle size, zeta potential and encapsulation efficiency were tested as three dependent response variables. The design consisted of two-level (-1 and +1) four factorial points, six center points augmented with two-level (-α and +α) four axial points resulting in merely 14 experimental runs to construct the CCD matrix.

3.2.5. Physico-chemical Characterization

3.2.5.1. Particle Size and Zeta Potential Analysis

The mean particle size with polydispersity index and zeta potential of the LAZ-NLCs were measured using dynamic light scattering (DLS) and phase analysis light scattering, respectively (ZetaPALS, Brokhaven Instrument Corporation, Holltsville, NY). The NLC formulations were diluted 100-fold with distilled water before the measurements. The measurements for particle size, polydispersity index and zeta potential for each sample was carried in triplicates and reported as mean values.

3.2.5.2. Entrapment Efficiency

The entrapment efficiency (EE) was measured using ultra-filtration technique where the non-encapsulated free LAZ in the NLC was measured. The LAZ-NLCs (1 mL) were placed in the Amicon Ultra-4 filtration unit with molecular weight cut-off of 10,000 Da and centrifuged for 30 minutes at 3500 rpm at 4°C. The LAZ entrapped in the NLCs were collected in the filtration unit and the filtrate containing free LAZ was collected at the bottom of the filtration unit. The filtrate was analyzed by HPLC method described in **Section 3.2.1.** The EE was calculated using the following equation:

Equation 4

$$EE\ (\%) = \frac{Amont\ of\ LAZ\ added\ in\ NLC\ -\ Amont\ of\ free\ LAZ}{Amount\ of\ LAZ\ added\ in\ NLC} \times 100$$

In order to determine the concentration of LAZ-NLCs collected in filtration unit separated from the non-encapsulated LAZ, acetonitrile was used to precipitate the lipid matrix and extract LAZ. The mixture was centrifuged for 20 minutes at 17,968 x *g* and

the concentration of the supernatant was analyzed using the HPLC method to quantify the entrapped LAZ and also confirm the mass balance.

3.2.5.3. Morphological Assessment

Transmission electron microscope H7500 (Hitachi, Japan) was used to determine the surface morphology of the optimal LAZ-NLC. The optimal LAZ-NLCs were diluted with deionized water and a drop was placed on carbon grid. Staining was carried out using 2 % uranyl acetate followed by the fixation with 1 % osmium tetroxide.

3.2.5.4. Differential Scanning Calorimetry

Differential scanning calorimetry (DSC) analysis was performed to study the physical state and thermal properties of individual components such as LAZ, GB, and DSPE-PEG 2k, as well as of optimal LAZ-NLC. Furthermore, DSC analysis was used to qualitatively estimate the solubility of LAZ in different solid lipids. The thermal analysis was performed using DSC 60A Plus (Shimadzu Corporation, Japan). Samples were sealed in standard aluminum pans with lids and heated from 25 to 200°C under nitrogen purge (50 mL/min) with the heating rate of 10°C/min.

3.2.5.5. X-ray Diffraction Analysis

The X-ray diffraction (XRD) analysis was used to determine the degree of crystallinity of LAZ in the optimal NLC. The XRD patterns for LAZ, GB and optimal LAZ-NLC were obtained using Rigaku Smartlab X-ray Diffractometer (The Woodlands, TX, USA). The samples were scanned using CuKα radiation, over 2θ range from 5-50° with the operating voltage of 40 kV and current of 44 mA.

3.2.5.6. Hemolytic Potential of Optimal LAZ-NLC

The hemolytic potential of the optimal LAZ-NLC was determined using fresh heparinized blood from male Sprague-Dawley rats (BioChemMed Services, Winchester, VA) using a previously established protocol in our lab [101]. The water to blood ratio causing complete hemolysis and resulting in insignificant absorbance at 540 nm was selected as 1:9 (Solution A). A series of standard solutions (1 mL) were prepared by mixing varying proportions of solution A with fresh heparinized rat blood to yield healthy cells in range of 0 to 100 %. The mixture of solution A and blood were vortexed for 10 seconds, incubated for 2 minutes and centrifuged at 1,000 x g for 5 minutes. The supernatant was discarded and 5 mL normal saline was added to the intact cells pellet to stop the hemolysis. The healthy cells in the pellet were lysed by the addition of 1 mL distilled water. The resulting mixture was centrifuged at 1,000 x g for 5 minutes and the supernatant was diluted 1:9 with distilled water and absorbance was measured at 540 nm. The hemolytic potential of the optimal LAZ-NLC was evaluated by mixing fresh heparinized rat blood with the formulations at ratios of 0.0375, 0.3, 0.5, 1, 2 and 3. Formulation and blood mixture was processed in the aforementioned manner, followed by measuring the absorbance at 540 nm. The hemolytic potential was determined by plotting percent healthy cells versus formulation to blood ratio.

3.2.5.7. Stability Evaluations

The optimal LAZ-NLC was stored at 4°C and the storage stability was evaluated by measuring the changes in particle size, zeta potential and encapsulation efficiency at different time points over a period of 3 months.

3.2.6. UPLC-MS/MS Assay of LAZ in Bio-matrices

3.2.6.1. Chromatographic and Spectrometric Conditions

Chromatographic separation of LAZ and IS was achieved by using ACQUITY UPLC BEH C18 column (2.1 mm × 50 mm, 300˚A, 1.7 µm, Waters, Milford, MA, USA) on Waters ACQUITY UPLC H-Class system. The mobile phase comprised of 0.1 % v/v formic acid in water (A) and 0.1 % v/v formic acid in acetonitrile (B) and a gradient elution was employed with 95 % A (0-0.5 mins), 95-80 % A (0.5-2 mins), 80-10 % A (2-3 mins), 10-5 % A (3-3.5 mins), 5-95 % A (3.5-4 mins) and 95 % A (4-4.5 mins) at a flow rate of 0.45 mL/min. The column temperature was maintained at 45°C. The total run time for a single injection was 4.5 minutes. The injection volume was 10 µl. LAZ and internal standard daidzein (DIA) were detected by electrospray ionization (ESI) using multiple reaction monitoring (MRM) in a positive mode on QTRAP 5500 System (AB SCIEX, Framingham, MA, USA). The optimal MRM transitions for precursor ion to specific product ion $[M+H]^+$ for LAZ (m/z 612 → 260) and DIA (m/z 255 → 199) were selected. The compound dependent parameters for LAZ and DIA were optimized with declustering potential (DP) at 61 V and 76 V, entrance potential (EP) at 10 V, collision energy (CE) at 79 V and 39 V and collision cell exit potential (CXP) at 18 V and 16 V, respectively. The instrument dependent parameters such as curtain gas, collision gas,

ionspray voltage, temperature and ion source gas 1 were optimized to 20 psig, medium, 5500 V, 500 °C and 20 psig, respectively. Analyst®1.5.2 software was used to acquire, analyze and process the data.

3.2.6.2. Preparation of Calibration and Quality Control (QC) Samples

Standard stock solution of LAZ was prepared in acetonitrile at the concentration of 1 mg/mL. Standard stock solution of DIA was prepared in a mixture of DMSO and methanol (1:4 v/v) at the concentration of 2.54 mg/mL. The working solutions for calibration curve were prepared in acetonitrile by a serial dilution. The plasma or tissue homogenate samples for the calibration curve were prepared by spiking 10 µL of working solution in 100 µL of blank rat plasma or blank rat tissue homogenates to yield final concentrations of 250, 125, 62.5, 31.25, 15.63, 7.81, 3.91, and 1.95 ng/mL, respectively. The tissue homogenates were prepared by homogenizing tissues in normal saline to form a homogenous tissue suspension. The brain tissue and lung tissue samples were entirely homogenized in 2.5 mL and 5 mL of normal saline respectively. In case of the liver tissue samples, 1.5 gm of the tissue was homogenized in 5 mL normal saline. The tissue homogenates were stored at -80°C until further analysis. Three levels of plasma QC samples low, medium and high (5, 50 and 200 ng/mL) and two levels of tissue homogenate QC samples low and high (5, and 200 ng/mL) were prepared in a similar manner as previously described. The calibration curve and QC samples were prepared from separate stock solutions prepared freshly at the time of experiment.

3.2.6.3. Sample Preparation

Acetonitrile was used to precipitate plasma proteins and extract LAZ from the rat plasma or tissue homogenates. Standard stock solution of DIA (2.54 mg/mL) was diluted in acetonitrile to obtain a final concentration of 1.27 µg/mL. Five hundred µL of acetonitrile spiked with DIA was added to plasma or tissue homogenate standards and quality control samples. The resulting mixtures were vortexed for 30 seconds, sonicated for 5 minutes and centrifuged at 17,968 x g at 4°C for 20 minutes. Five hundred µL of organic supernatant was air-dried and the residue was reconstituted with 100 µL of mixture of 0.1 % formic acid in water and acetonitrile 50:50 (% v/v), then centrifuged at 17,968 x *g* at 4°C for 10 minutes. The aliquot of 10 µL of reconstituted sample was injected in UPLC-MS/MS for LAZ quantification.

3.2.6.4. Full Method Validation of LAZ in Plasma

The method validation was performed in compliance with US Food and Drug Administration Guidance for Industry: Bio-analytical Method Validation [102].

3.2.6.4.1. Linearity, Sensitivity and Selectivity

The calibration curve in blank rat plasma was obtained by plotting the peak area ratios of LAZ and IS against concentrations. The slope, intercept and correlation coefficient for the calibration curve were determined using weighted linear regression analysis. Sensitivity of the analytical method was tested at the lowest limit of quantification (LLOQ) where LAZ signal to noise ratio was ≥ 10 when compared with plasma blank. Selectivity of the analytical method for any endogenous substances was tested at LLOQ

using six individual non-pooled, analyte free, blank rat plasma samples. Selectivity of the analytical method for any endogenous substances was tested at LLOQ using pooled, analyte free, blank rat brain, liver and lung homogenates.

3.2.6.4.2. Accuracy and Precision

The accuracy and precision of the analytical method were tested at LLOQ with three sets of the QC samples (low, medium and high). It was anticipated that the samples from initial time points in the pharmacokinetic study would yield LAZ concentration above the upper linear range of calibration curve. Thus, very high concentration QC sample (1000 ng/mL) was prepared which was diluted to yield concentration within the linear range of calibration curve and was also tested for the accuracy and precision. Accuracy and precision were calculated using **Equations 2 and 3.** Accuracy and precision for rat plasma samples were performed using six replicates of LLOQ, the three sets of QC standards and very high concentration QC sample each on same day for intra-day variation and on three consecutive days for inter-day variation. Accuracy and precision for rat brain, liver and lung tissue homogenate samples were performed using three replicates of two sets of QC standards (low and high) each on same day for intra-day variation and on two consecutive days for inter-day variation.

3.2.6.4.3. Recovery and Matrix Effect

The extraction recovery and matrix effect of LAZ in blank rat plasma were tested at the three QC levels. The percentage extraction recovery was calculated by comparing peak area ratio of LAZ and DIA spiked in blank rat plasma before and after extraction. The

matrix effect was quantitatively determined in terms of percent matrix factor, which was calculated by comparing peak area ratio of LAZ and DIA spiked in blank plasma extract to that in mixture of 0.1% v/v formic acid in water and acetonitrile 50:50 (% v/v). A percent matrix factor with value of 100 % indicates no matrix effect and is often desirable but not achievable in a bio-analytical assay. The matrix effect is acceptable when the variability in percent matrix factor is within ±15% [103].

3.2.6.4.4. Stability

The stability of LAZ in plasma under different storage and handling conditions was evaluated at two QC levels (low and high). The stability of LAZ in plasma was evaluated for short-term bench-top stability (1 hour and 3 hours at 25°C), long-term storage stability (-80°C for 1 month), one and three freeze-thaw cycles, and processed sample stability in auto-sampler (24 hours at 10°C).

3.2.6.5. Partial Method Validation of LAZ in Brain, Liver and Lung Bio-matrices

As per the US-FDA guidelines for bio-analytical validation, partial validation is employed in case of already established and validated method. Partial validation is used in case of change in matrix between the same species (eg. human plasma to human urine) or in case of rare matrices [102]. Partial validation of UPLC/MS-MS assay for quantification of LAZ in brain, liver and lung bio-matrices was performed, owing to the limited supply of blank organs. The linearity, sensitivity, intra-day and inter-day accuracy and precision were performed as a part of partial validation for each of the tissue homogenates.

3.2.7. *In vivo* Studies

3.2.7.1. Pharmacokinetics and Bio-distribution Studies

The pharmacokinetic and bio-distribution study in rats was performed using the protocol approved by University of Houston Institutional Animal Care and Use Committee. The male Sprague-Dawley rats (250-300 gm) were randomized into three groups (3-6 animals in each group), namely LAZ citrate solution, LAZ co-solvent and LAZ-NLC groups. The rats were dosed via bolus intravenous injection through the jugular vein cannula at doses of 5 mg/kg for LAZ citrate solution and 15 mg/kg for LAZ co-solvent and LAZ-NLC groups. The LAZ citrate solution group consisted of LAZ dissolved in citrate buffer (pH: 3.0) at concentration of 2 mg/mL. The LAZ co-solvent group comprised of LAZ dissolved in co-solvent solution consisting of propylene glycol and citrate buffer pH: 3.0 (40:60 % v/v) at a concentration of 8.5 mg/mL. The LAZ-NLC group consisted of optimal LAZ-NLC obtained using CCD at a concentration of 5 mg/mL. At pre-determined time points post dose (0.33, 0.66, 1, 2, 3, 4, 6, and 8 h), blood samples of 200 µL were withdrawn from each rat and plasma was collected after the centrifugation at 4°C at 9,168 x *g* for 10 minutes. The plasma samples were stored at −80°C until analysis by the validated UPLC–MS/MS assay. The plasma profile of LAZ was constructed and pharmacokinetic parameters were derived using Phoenix NLME software. Additionally, at 4, 6 and 8 hour post-dose of the pharmacokinetic study, rats were sacrificed by carbon dioxide asphyxiation. The brain, liver and lung tissues were harvested following whole body perfusion with normal saline to remove residual blood in the tissues. The organ

tissue homogenization, storage conditions and sample preparation are mentioned in **Sections 3.2.6.2 and 3.2.6.3.** Since a truncated bio-distribution profile of LAZ in the brain, liver and lung was obtained, the pharmacokinetic parameters for each of the tissue were estimated using **Equations 5-7** [104]. The plots of log normal-transformed LAZ amounts in the respective tissues versus time (4, 6 and 8 hours) were used to estimate the terminal elimination rate constant (λ_z) using linear regression analysis. In case of LAZ citrate solution, the brain levels of LAZ were quantifiable only at 4 hours. The levels of LAZ in brain tissue at 6 and 8 hours were below the LLOQ, but were still detectable and were used to estimate the half-life and AUC.

The terminal elimination half-life ($t_{1/2}$) of was calculated from λ_z using **Equation 5.**

Equation 5

$$\lambda z = \frac{0.693}{t1/2}$$

The truncated area under the curve from 4 to 8 hours ($AUC_{4\text{-}8hrs}$) for plasma and tissues was calculated using the log-linear trapezoidal rule as stated in **Equation 6** where C1 and C2 are the concentrations at time t1 and t2.

Equation 6

$$AUCt1 - t2 = \frac{C1 - C2}{\ln(C1) - \ln(C2)} \times t2 - t1$$

The tissue to plasma ratio was calculated using **Equation 7.**

Equation 7

$$Tissue/Plasma = \frac{(AUCt1 - t2)tissue}{(AUCt1 - t2)plasma}$$

3.2.7.2. Dose Linearity Studies

The male Sprague-Dawley rats (250-300 gm) were randomly divided in three groups (3 animals in each group) and were dosed at three different doses, 15, 30 and 60 mg/kg. The optimal LAZ-NLC was given via intravenous infusion to rats through the jugular vein cannula at rate of 0.75 mL/min at the three different doses. At 20 minutes post dose, the rats were sacrificed by carbon dioxide asphyxiation. The brain tissues were harvested following whole body perfusion with normal saline to remove residual blood in the tissues. The brain tissue homogenization storage conditions and sample preparation are mentioned in **Sections 3.2.6.2 and 3.2.6.3.** The dose linearity was assessed using two different approaches namely, analysis of variance (ANOVA) model and power model. In both the models, pharmacokinetic (PK) parameters like area under the curve (AUC) and maximum concentration (C_{max}) are correlated with the administered dose [105, 106]. In this study, a correlation between amounts of LAZ in brain at 20 minutes ($C_{20min,\ brain}$) (PK parameter) with increase in optimal LAZ-NLC dose from 15 to 60 mg/kg was studied.

In the ANOVA model, statistical tests such as analysis of variance was performed on natural log-transformed dose normalized amounts of LAZ in the brain at 20 minutes to test the differences in the PK parameter at doses of 15, 30 and 60 mg/kg. Statistical significance was indicated by $p< 0.05$.

In the power model, the relationship between PK parameter and dose is given as follows:

Equation 8

$$PK = \beta_0 \times Dose^{\beta 1}$$

On logarithmic transformation, the PK parameter and dose were linearly correlated as given by **Equation 9**.

Equation 9

$$\ln(PK) = \beta_0 + \beta_1 \times \ln(Dose)$$

Dose proportionality is obtained when β_1 (slope) is 1 and its 90 % confidence interval lies within user-defined critical region ($1+\frac{\ln(\theta_l)}{\ln(r)}$, $1+\frac{\ln(\theta_h)}{\ln(r)}$). The values for θ_l and θ_h are 0.8 and 1.25, derived from the US-FDA guidance for bioequivalence, while 'r' indicates the ratio of the highest tested dose to the lowest tested dose.

A plot of natural log-transformed amount of LAZ in brain at 20 minutes versus the natural-log transformed dose was analyzed using weighted linear regression analysis (Phoenix WinNonlin WNL5 Classic Linear Modeling) in order to determine the slope β_1 and 90% confidence interval.

3.2.8. Statistical Analyses

Statistical analyses were carried using one-way ANOVA with Tukey's post-hoc analysis with significance at $p<0.05$ using GraphPad Prism Version 6.0.

Chapter 4: Results

4.1. HPLC Assay for LAZ

The linear range of calibration curve was established at 1–100 µg/mL. The mean coefficient of correlation (r) for inter-day calibration curve (n = 3) was 0.9996 with % CV of 0.03. The mean value for slope of inter-day calibration curve (n = 3) was 0.526 with % CV of 3.54. Selectivity was tested by comparing blank acetonitrile and LAZ spiked samples at LLOQ (1 µg/mL) in blank acetonitrile solution. The signal to noise ratio was ≥10. The retention time for LAZ and methyl testosterone (IS) was 2.6 and 6.8 minutes respectively **(Figures 16, a and b)**. The intra-day and inter-day accuracy and precision values for the QC samples were between 90.61 – 105.86 % and < 11 %, respectively, within the acceptance range of ± 15% **(Table 6)**.

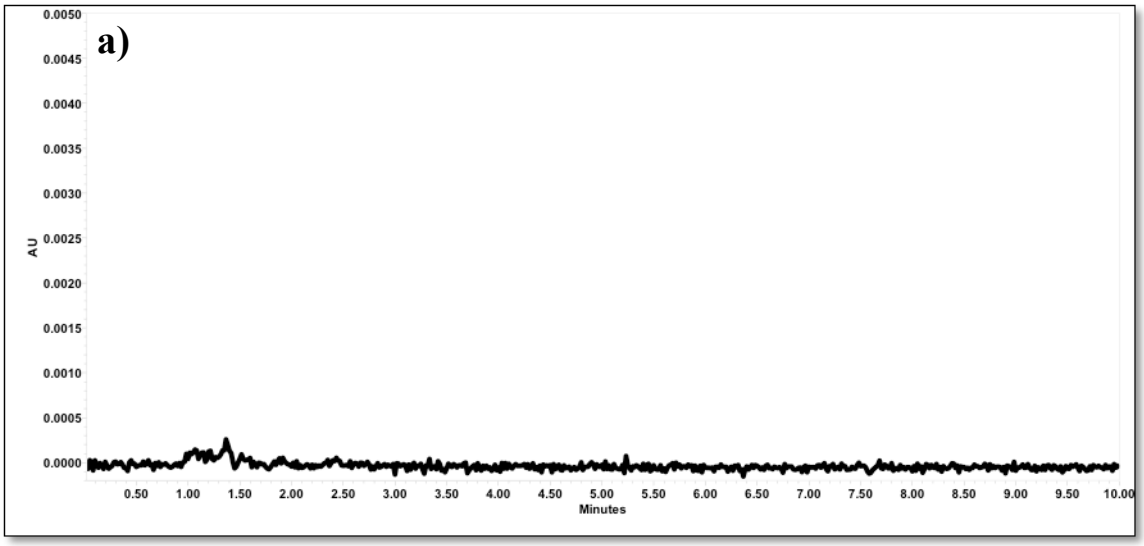

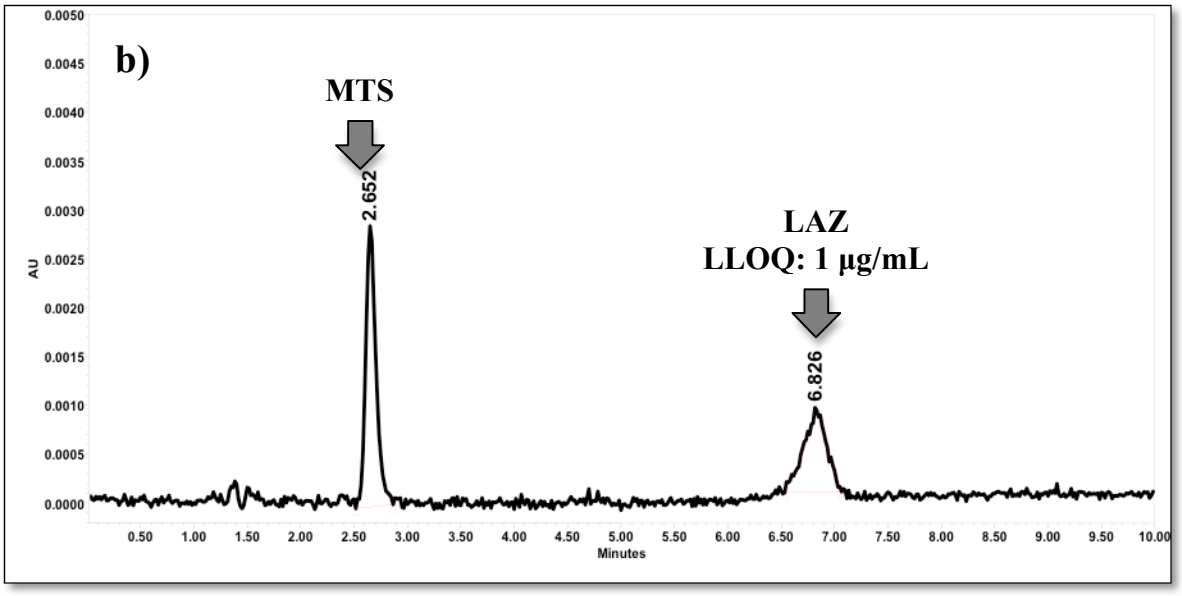

Figure 16: HPLC chromatograms of **a)** blank acetonitrile and **b)** LAZ (1 µg/mL) and methyl testosterone (IS) spiked in blank acetonitrile

Nominal Concentration (µg/mL)	Intra-day (N=9)		Inter-day (N=6)	
	%Accuracy	%Precision	%Accuracy	%Precision
4	90.61 ± 1.20	1.32	94.85 ± 10.03	10.57
40	105.86 ± 2.53	2.39	102.58 ± 5.62	5.47
80	101.08 ± 1.66	1.64	96.62 ± 6.65	6.88

Table 6: Intra-day and inter-day accuracy and precision values (mean ± SD) for LAZ in acetonitrile

4.2. Selection of Lipids

The solubility of LAZ in different liquid lipid (oils) is summarized in **Table 7.** Labrasol yielded the highest solubility for LAZ (2.26 ± 0.05 mg/mL) and was chosen as liquid lipid.

Liquid lipid (Oils)	Solubility (mg/ml)
Safflower oil	0.12 ± 0.01
Flax seed oil	Below LLOQ
Labrafac[a]	0.09 ± 0.01
Peceol[b]	1.24 ± 0.06
Oleic acid	0.60 ± 0.08
Soy bean oil	0.05 ± 0.01
Labrasol[c]	2.26 ± 0.05

Table 7: Solubility of LAZ in different liquid lipids (oils) (N=3: Mean ± SD)
a: Medium chain triglycerides, **b:** glceryl mono-oleate,
c: PEG-8 caprylic/capric glyceride

There is no direct method for determining the solubility of LAZ in solid lipids. Hence, thermal analysis and *in vitro* release of LAZ from SLNs were used to screen the suitable solid lipids. The DSC thermograms for pure LAZ and LAZ solid lipid mixtures are represented in **Figure 17**. The sharp meting endothermic peak of LAZ at 189.30°C was shifted to 176.25°C with a diffused peak for LAZ mixed with GB at the ratio (% w/w) of 1:5. However, no such peak shifts were observed with TM (187.70°C) and TS (189.25°C) at the same LAZ to lipid ratio. In addition, the percent cumulative release of LAZ loaded SLNs was determined in plasma over a period of 72 hours. LAZ loaded GB SLN (6.70 ± 2.58 %) exhibited the slowest percent cumulative release of LAZ in comparison to TM (35.17 ± 10.11 %, $p<0.05$) and TS (24.41 ± 10.47 %, $p>0.05$) SLNs.

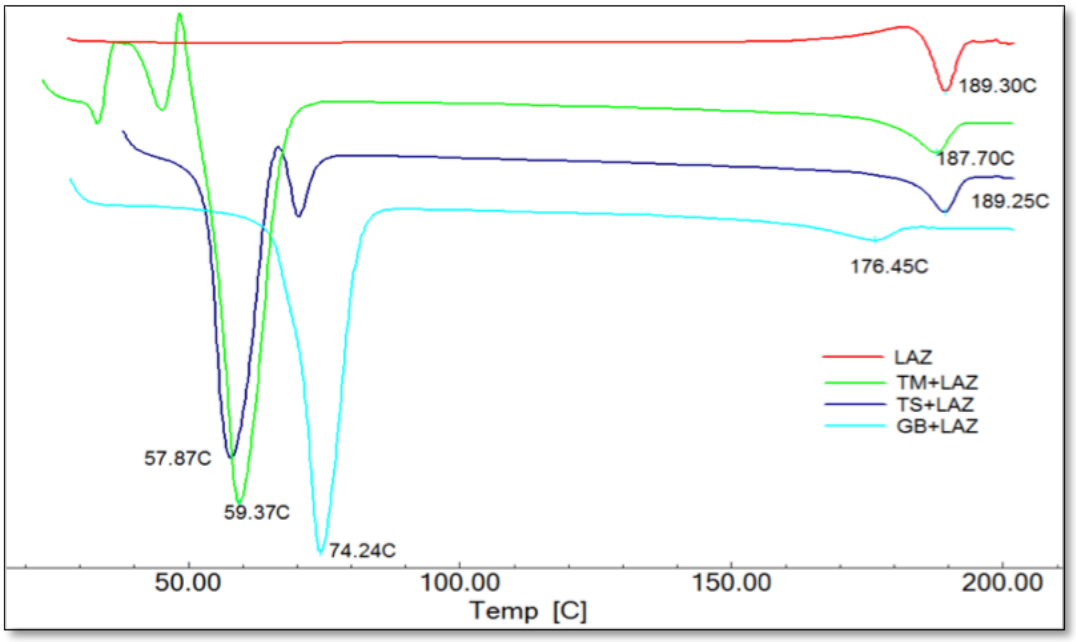

Figure 17: Differential scanning calorimetric thermograms of LAZ in different solid lipids

4.3. Development of LAZ-NLC using CCD

A two-factor five-level CCD was used to determine the optimal levels of independent variables DSPE-PEG 2k (A) and liquid lipid (B) and the composition effects on particle size, zeta potential and encapsulation efficiency (dependent response variables) using only 14 experimental runs as depicted in **Table 8**. The various NLC formulations resulting from the experimental design had particle size, zeta potential and encapsulation efficiency ranging from 99.9 to 227.0 nm, -4.52 to +25.84 mV and 54.83 to 88.92%, respectively**.**

Design	DSPE-PEG 2000 (mg)	Liquid Lipid		Solid Lipid	Particle Size (nm)	Zeta Potential (mV)	Encapsulation Efficiency (%)
		(%)[a]	(mg)	(mg)			
(0,0)	30	30	60	110	190.0± 1.04	5.36 ± 0.90	73.72 ± 2.31
(0,0)	30	30	60	110	185.7± 1.37	5.06 ± 1.06	73.13 ± 5.26
(0,0)	30	30	60	110	185.0± 7.67	5.54 ± 1.00	72.12 ± 8.36
(-1,1)	15	50	100	85	133.1± 6.36	17.33 ± 1.10	72.89 ± 2.45
(1,-1)	45	10	20	135	171.0± 8.63	(-6.67) ± 0.67	84.94 ± 3.34
(1,1)	45	50	100	55	99.9 ± 6.06	(-4.52) ± 1.81	84.26 ± 3.54
(-1,-1)	15	10	20	165	189.6± 0.97	16.91 ± 2.32	62.32 ± 6.23
(0,0)	30	30	60	110	188.2± 5.00	5.84 ± 0.41	74.07 ± 1.23
(0,0)	30	30	60	110	191.7 ± 7.08	7.31 ± 0.93	73.72 ± 6.98
(0,0)	30	30	60	110	189.4 ± 4.50	7.82 ± 2.16	75.11 ± 4.53
(-α,0)	8.79	30	60	131.21	183.1± 4.37	25.84 ± 0.89	54.83 ± 2.00
(α,0)	51.21	30	60	88.79	149.3 ± 7.17	(-6.82) ± 2.38	88.92 ± 1.47
(0,-α)	30	1.72	3.44	166.56	227.0 ± 5.37	4.45 ± 0.72	76.77 ± 9.82
(0,α)	30	58.28	116.56	53.44	106.2 ± 1.23	7.83 ± 1.40	66.71 ± 3.48

Table 8: Formulation design with coded and actual values of independent variables and measured response variables (N=3: Mean ± SD)
a: Calculated with respect to total lipid content of 200 mg;
NLC composition described in **Section 3.2.3**

The particle size and zeta potential responses best fitted a quadratic model whereas the responses for entrapment efficiency fitted a linear model. The best-fit models were selected taking into consideration low standard deviation, high multiple correlation

coefficient (R^2) and low predicted residual sum of squares. The model equations in terms of coded factors and model fit statistics are summarized in **Table 9**.

Response variables	Model equations[a]	R^2
Particle size (PS)	PS = 188.31-12.44*A-37.30*B-3.64*AB15.56*$A^2$15.35*B^2	0.9600
Zeta potential (ZP)	ZP = 6.1511.45*A+0.92*B+0.44*AB+1.16*$A^2$0.52*B^2	0.9815
Encapsulation efficiency (EE)	EE = 73.82+10.27*A-0.54*B	0.7145

Table 9: Best-fit model equations and summary statistics for particle size, zeta potential and encapsulation efficiency
a: A: DSPE-PEG, B: Liquid Lipid, AB: Interaction between DSPE-PEG and Liquid Lipid, A^2: $(DSPE\text{-}PEG)^2$, B^2: $(Liquid\ Lipid)^2$

The best-fit models for each response variable were statistically evaluated using ANOVA (significance at $p<0.05$) for quantitatively determining the effect of each independent variable alone as well as the interactions between independent variables on the response variable. The sign and value of each regression co-efficient displayed its effect on the response variables as summarized in **Table 10**. A positive value of regression co-efficient indicated a synergism, whereas a negative value of regression co-efficient indicated antagonism between the independent and dependent variables [107]. Additionally, three-dimensional response surface plots were used to visualize the effects of independent variables on the response variables.

Parameters	Particle Size		Zeta Potential		Encapsulation Efficiency	
	Coefficient	p value[b]	Coefficient	p value	Coefficient	p value
Model[a]	Quadratic	< 0.0001	Quadratic	< 0.0001	Linear	< 0.0001
Intercept	188.3		6.15		73.82	
A	-12.44	< 0.0001	-11.45	< 0.0001	10.27	< 0.0001
B	-37.30	< 0.0001	0.92	0.003	-0.54	0.6308
AB	-3.64	0.1234	0.44	0.2888		
A^2	-15.56	< 0.0001	1.16	0.0005		
B^2	-15.35	< 0.0001	-0.52	0.0895		

Table 10: Statistical analyses of coefficients for best-fit model using ANOVA for response variables, **a:** A: DSPE-PEG, B: Liquid Lipid, AB: Interaction between DSPE-PEG and Liquid Lipid, A^2: $(\text{DSPE-PEG})^2$, B^2: $(\text{Liquid Lipid})^2$,
b: p <0.01, 0.05<= p <0.10, p >=0.1

The particle size had an inverse relationship with liquid lipid (Labrasol) and DSPE-PEG **(Figure 18, a)**, indicating a decrease in particle size as the amount of liquid lipid and DSPE-PEG increased. In this case the total amount of lipids were kept constant and the proportion of solid and liquid lipids were changed. No interactions between liquid lipid and DSPE-PEG having an effect on the particle size were observed. DSPE-PEG had an antagonistic effect on zeta potential, whereas liquid lipid demonstrated a synergistic effect **(Figure 18, b)**. Only DSPE-PEG had a positive effect on encapsulation efficiency as seen from the **Figure 18, c**.

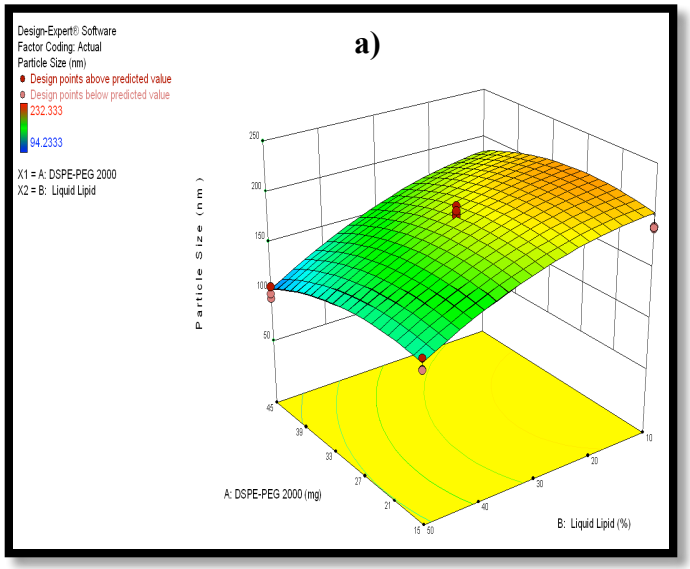

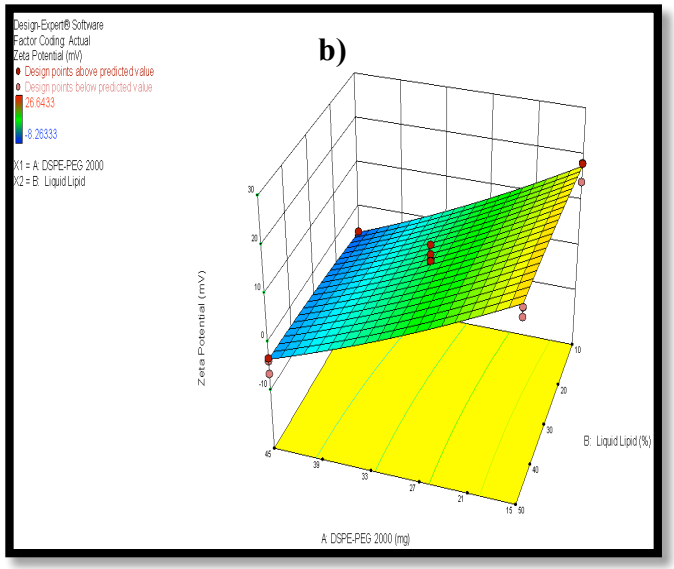

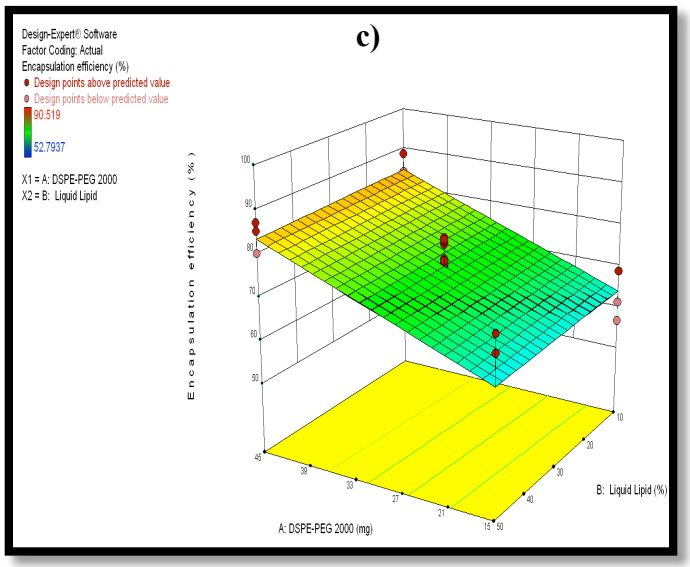

Figure 18: Three dimensional response surface plots for DSPE-PEG 2k and liquid lipid on **a)** particle size, **b)** zeta potential and **c)** encapsulation efficiency

4.4. Optimization and Validation of LAZ-NLC

The composition of optimal LAZ-NLC was obtained by using the numerical optimization feature in the Design-Expert software. The numerical optimization employs desirability function that is used for simultaneous optimization of response variables. The independent variables (DSPE-PEG 2k and liquid lipid Labrasol) are automatically contained in the 'in range' limits so that the responses are predicted within the boundaries of the experimental design. The response variables are assigned either a maximum, minimum or target value.

Optimal LAZ NLC	**Particle Size (nm)**	**Zeta Potential (mV)**	**Encapsulation Efficiency (%)**
Predicted Response	172.6	-4.67	84.28
Observed Response (N=3,Mean ± SD)	172.3 ± 3.54	-4.54 ± 0.87	85.01 ± 2.60
% Error	**-0.20**	**-2.78**	**0.86**

Table 11: Comparison of predicted and observed responses for optimal LAZ-NLC

The desired properties of optimal LAZ-NLC were particle size < 200 nm, zeta potential with a neutral surface charge and maximum encapsulation efficiency of LAZ . In order to achieve the desired response variables criterion, the software predicted the optimum composition of LAZ-NLC consisting of 45 mg DSPE-PEG 2k and 23.07 % w/w of the lipid matrix was replaced with liquid lipid Labrasol. The predicted values of particle size,

zeta potential and encapsulation efficiency at the optimum LAZ-NLC composition were 172.6 nm, -4.67 mV and 84.28 %, respectively. The validity of the model was confirmed by preparing the LAZ-NLC using the optimum composition and comparing the observed experimental values with the predicted values. The observed values for particle size, zeta potential and encapsulation efficiency were 172.3 ± 3.54 nm, -4.54 ± 0.87 mV and 85.01 ± 2.60 %, respectively, with percent bias < 3 % highlighting the predictability of the CCD model for formulation properties **(Table 11)**.

4.5. Physico-chemical Characterization of Optimal LAZ-NLC

4.5.1. TEM Analysis

Uranyl acetate and osomium tetroxide were used as negative staining agents for lipids to provide better contrast for visualization. The optimal LAZ-NLCs were spherical in shape in the TEM images.

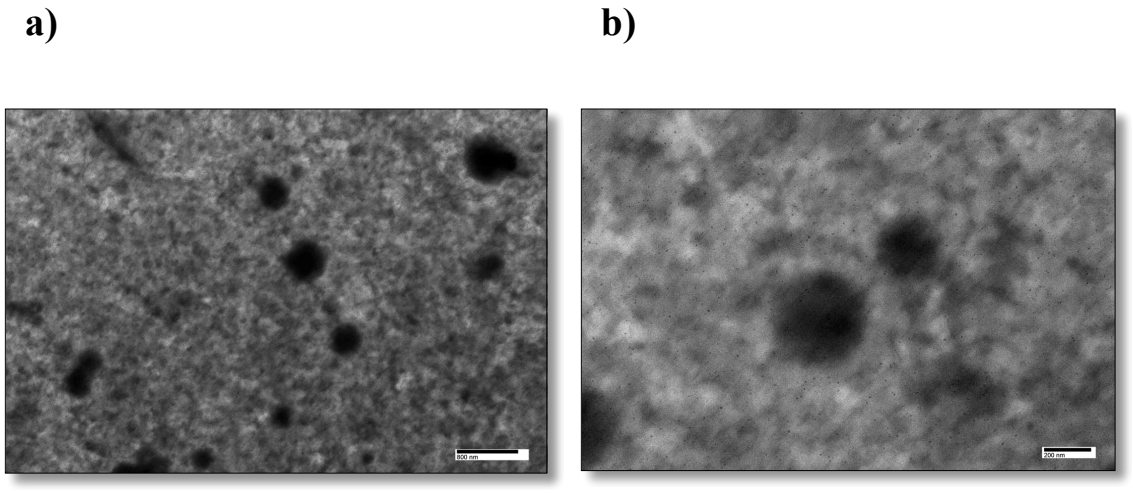

Figure 19: Transmission electron microscopy images of optimal LAZ-NLC
a) Scale: 800 nm, Magnification: 8000X, **b)** Scale: 200nm, Magnification: 25000X

The particle size and polydispersity index using DLS were 172.3 ± 3.5 nm and 0.12 ± 0.01, respectively (N=3 ± SD) with the TEM images confirming the validity of these measurements (**Figure 19, a and b**).

4.5.2. Solid-state Characterization

The DSC thermograms are represented in **Figure 20**

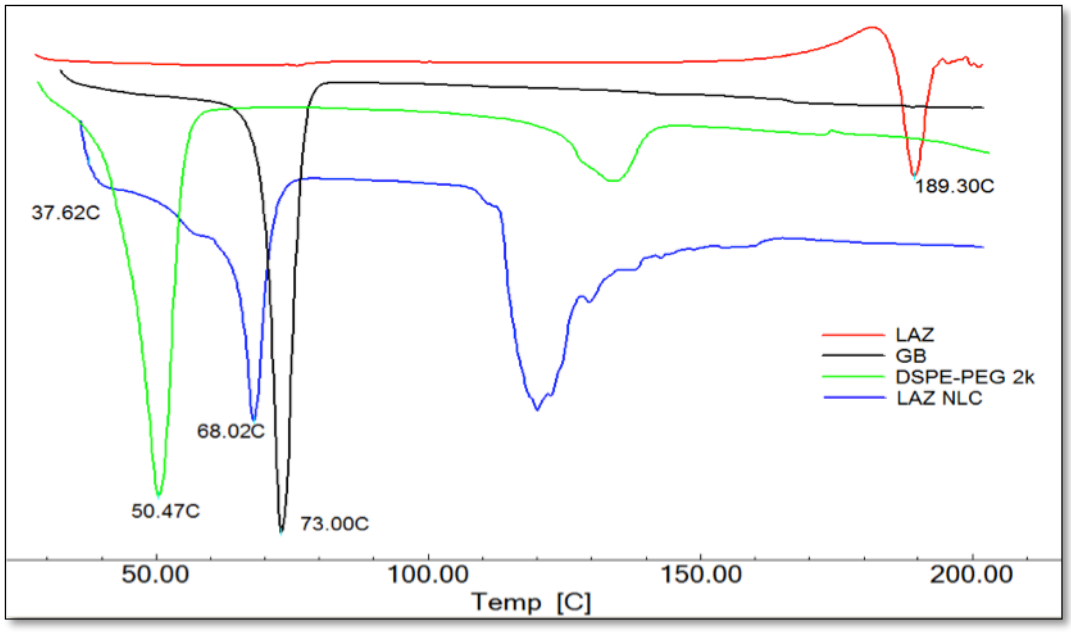

Figure 20: Differential scanning calorimetric thermograms of LAZ (red), GB (black), DSPE-PEG 2k (green) and optimal LAZ-NLC (blue)

A sharp endothermic peak for pure GB was observed at 73.00°C that shifted slightly to 68.02°C in case of LAZ-NLC, indicating a reduced crystallinity of GB in comparison to the bulk lipid. The bulk DSPE-PEG 2k showed a sharp melting endotherm at 50.47°C, while the peak became more diffused in LAZ-NLC, A sharp melting peak was observed

for LAZ at 189.30°C, which disappeared in LAZ-NLC, indicating the loss of crystalline state of LAZ and its probable conversion to an amorphous state.

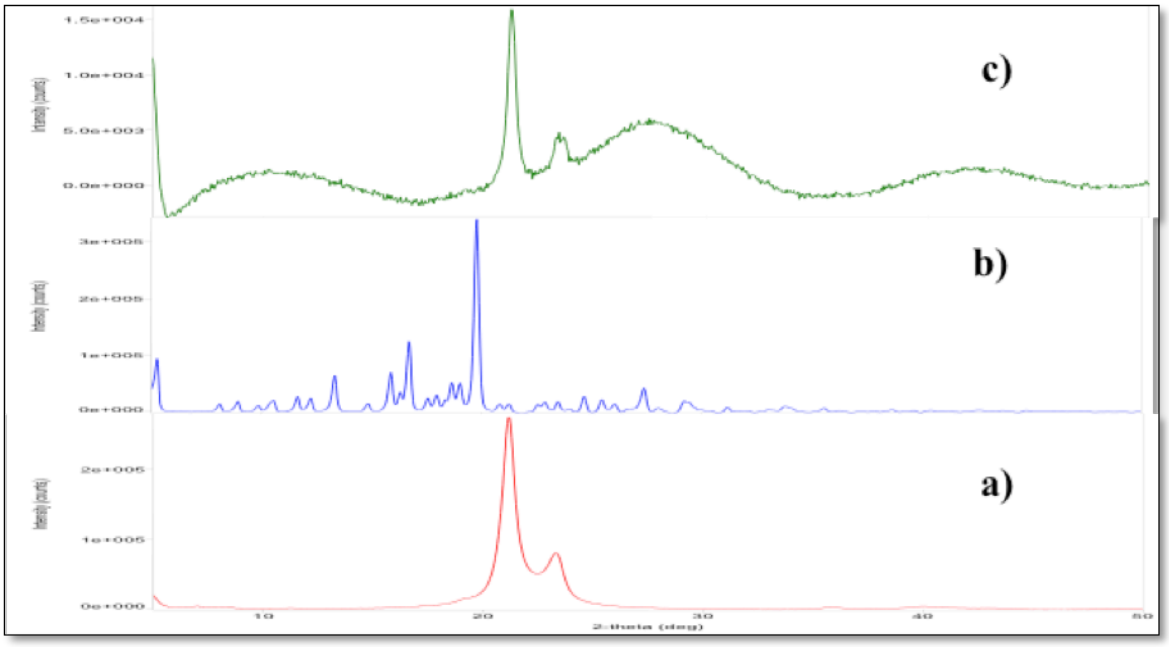

Figure 21: X-ray diffractograms for a) pure GB, b) pure LAZ and c) optimal LAZ-NLC

XRD analysis was performed in order to verify the physical state of LAZ-NLC. The findings from XRD analysis complimented the results from DSC analysis. The bulk LAZ and GB showed sharp diffraction peaks **(Figure 21,a and b)**, indicating their crystalline nature. In LAZ-NLC, the peaks for GB were retained with weakened intensity representing decreased crystallinity compared with pure GB. Also, a complete loss in intensity for LAZ peaks was observed in LAZ-NLC **(Figure 21,c)**.

4.5.3. *In-vitro* Hemolytic Potential

The hematotoxic potential of optimal LAZ-NLC was evaluated in freshly heparinzed rat blood using increasing formulation to blood ratios. The cut-off values for hemolytic potential in humans are reported to be in range of 10-25 % [108]. The formulation to blood ratio from 0.0375 to 1 demonstrated percent healthy cells in range of 85-90 %, suggesting the safety margin of the optimal LAZ-NLC on intravenous administration **(Figure 22)**. At formulation to blood ratio of 2 and higher the optimal NLC exhibited significant hemolysis ($p<0.05$) with the percent healthy cells <50%.

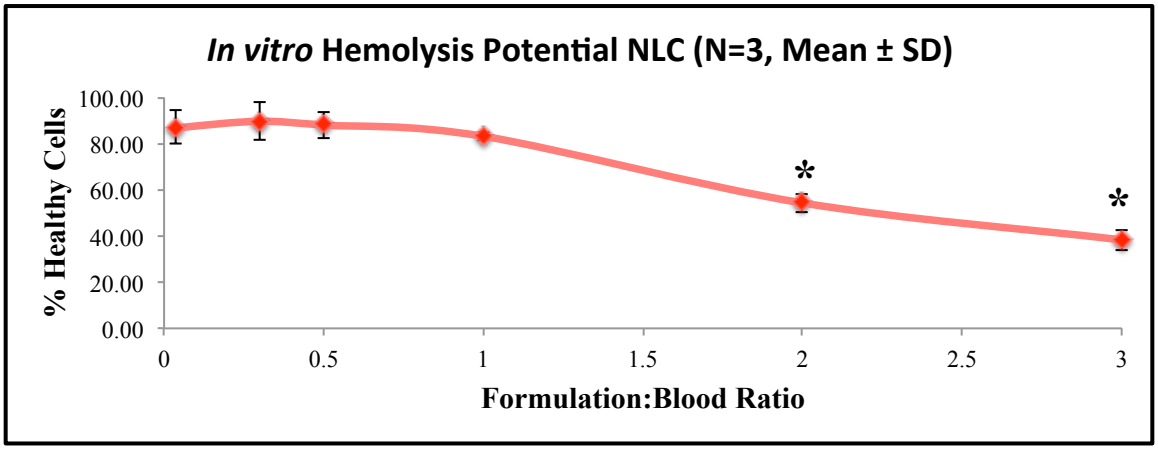

Figure 22: Hemolytic potential of optimal LAZ-NLC (N=3: Mean ± SD)
One way ANOVA with Tukey post hoc;
*Significant ($p<0.05$) when compared to F:B ratios 0.0375, 0.3, 0.5 and 1

4.5.4. Storage Stability

The storage stability of optimal LAZ-NLC at 4°C over a period of 3 months is presented in **Table 12**. The particle size of optimal LAZ-NLC exhibited a slight increase after storing at 4°C for 1 month compared to that of freshly prepared optimal LAZ-NLC (0 month), whereas the increase plateaued at 3 months. Although significant ($p<0.05$), the increase in particle size was only 1.2 times more in comparison to 0 month and still within 200 nm necessary for the enhanced brain exposure and lower exposure in liver. The encapsulation efficiency showed no significant change ($p>0.05$) in the amount of LAZ contained in the NLC over the 3 months period. The zeta potential was stable over the 1-month period whereas change in surface charge to more negative value was observed at 3 months. While LAZ-NLC displayed an optimal stability up to 3 months with slight changes in physical properties, freshly prepared optimal LAZ-NLCs were used in pharmacokinetics and bio-distribution studies.

Response variables	0 month	1 month	3 months
Particle size	155.4 ± 8.13	189.6 ± 2.35*	199.6 ± 0.40*
Zeta potential	-4.73 ± 1.35	-7.05 ± 1.02	-14.23 ± 1.27*
Encapsulation efficiency	78.96 ± 7.49	84.60 ± 4.50	77.09 ± 7.58

Table 12: Storage stability at 4°C of optimal LAZ-NLC at 0, 1 and 3 months (N=3: Mean ± SD); One way ANOVA with Tukey post hoc,
*Significant ($p<0.05$) when compared to 0 month

4.6. UPLC-MS/MS Assay of LAZ in Bio-matrices

4.6.1. Optimization of LC/MS Method

Acetonitrile and methanol were tested as organic solvents for chromatographic separation of LAZ. Acetonitrile was chosen mainly because it had better elution strength and provided sharper peaks with a better resolution for LAZ than methanol. Additionally, formic acid and trifluoroacetic acid (TFA) were tested as mobile phase additives for facilitating a better ionization of basic compounds like LAZ. Formic acid (0.1% v/v) significantly aided the ionization of LAZ whereas TFA (0.1% v/v) decreased the signal intensity of LAZ by 10 times. Therefore, formic acid was selected as the mobile phase additive. The representative chromatograms of blank rat plasma and organ homogenates and LAZ spiked rat plasma and organ homogenate samples at LLOQ (1.95 ng/mL) are depicted in **Figures 24-27**. Compound-dependent parameters like DP, EP, CE and CXP were optimized using automatic compound optimization for MS/MS analysis to get the maximum sensitivity for LAZ. The instrument-dependent parameters like curtain gas, collision gas, ionspray voltage, temperature and ion source gas were optimized manually by observing the increase or decrease in the ionization intensity of LAZ. Increasing the curtain gas and ion source gas values resulted in decreased ionization intensity of LAZ. Increasing the collision gas, ionspray voltage and temperature to optimal values increased the ionization intensity of LAZ. Any further increase in these parameters did not drastically enhance the ionization of LAZ. The MRM transition for LAZ (m/z 612 → 260) was obtained by a cleavage across the piperazine ring (**Figure 23**).

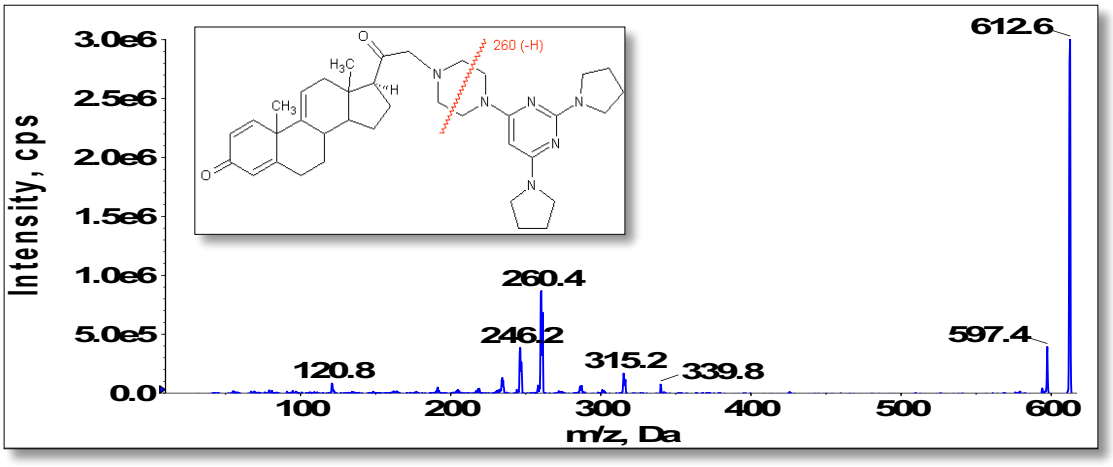

Figure 23: MRM transitions for precursor ion to specific product ion $[M+H]^+$ for LAZ (m/z 612 → 260) with structural breakdown of parent to daughter ion

Tirilazad mesylate, which is structurally related to LAZ, was not chosen as internal standard because both compounds generated the same product ion with m/z 260, which could lead to a cross-talk between LAZ and tirilazad mesylate leading to quantitation errors [109]. A stably labeled isotope of LAZ could be a potential choice for internal standard; however, due to its unavailability, DIA was chosen as the internal standard. Previously, LC-MS/MS method using atmospheric pressure chemical ionization (APCI) was developed for the quantitation of tirilazad mesylate and could be applied for the quantitative analysis of LAZ. However, APCI involved the use of high flow rates, higher amounts of volatile buffers and use of protic organic solvents such as methanol.

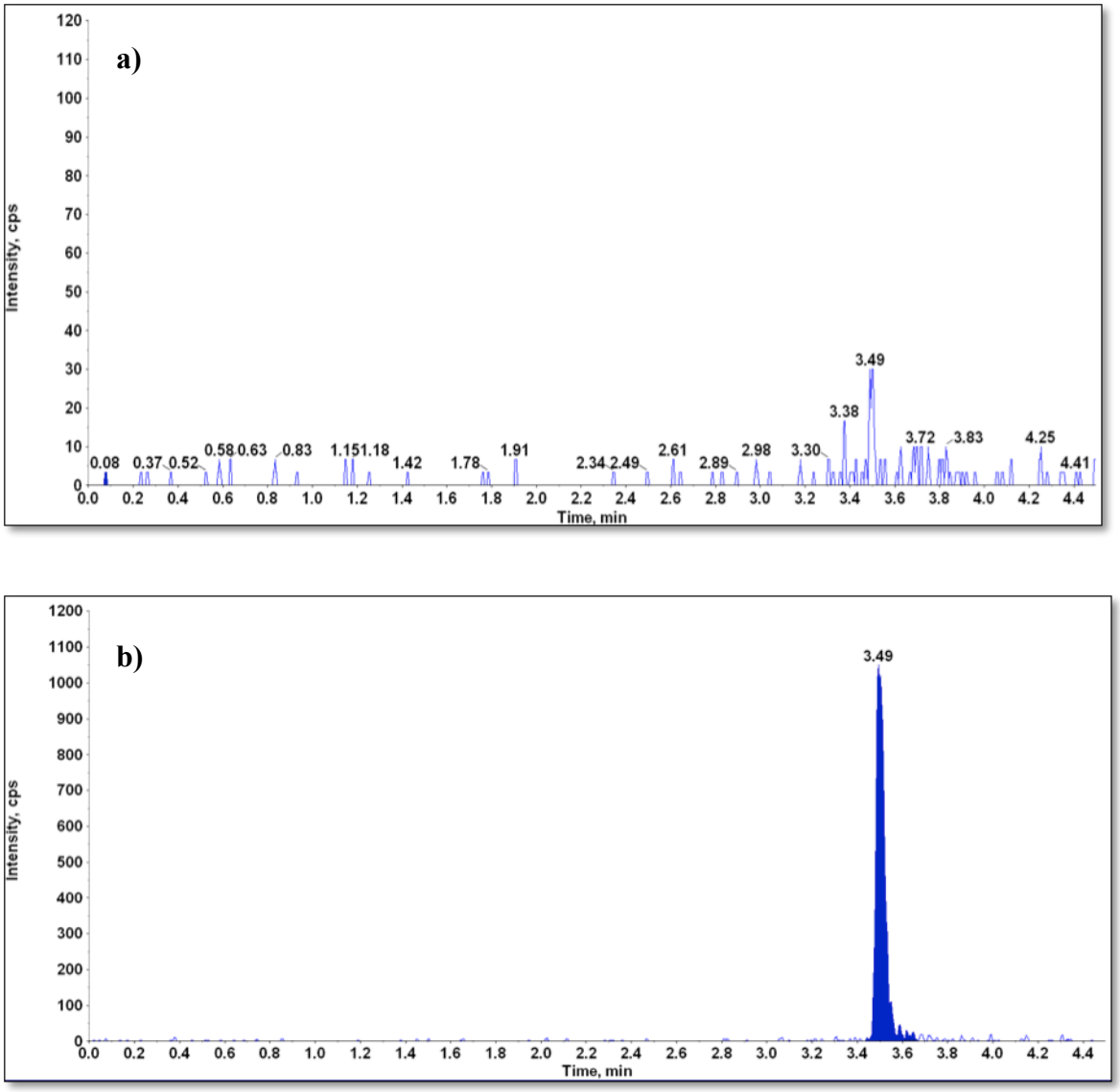

Figure 24: UPLC/MS-MS chromatograms **a)** blank rat plasma and **b)** LAZ (1.95 ng/mL) spiked in blank rat plasma

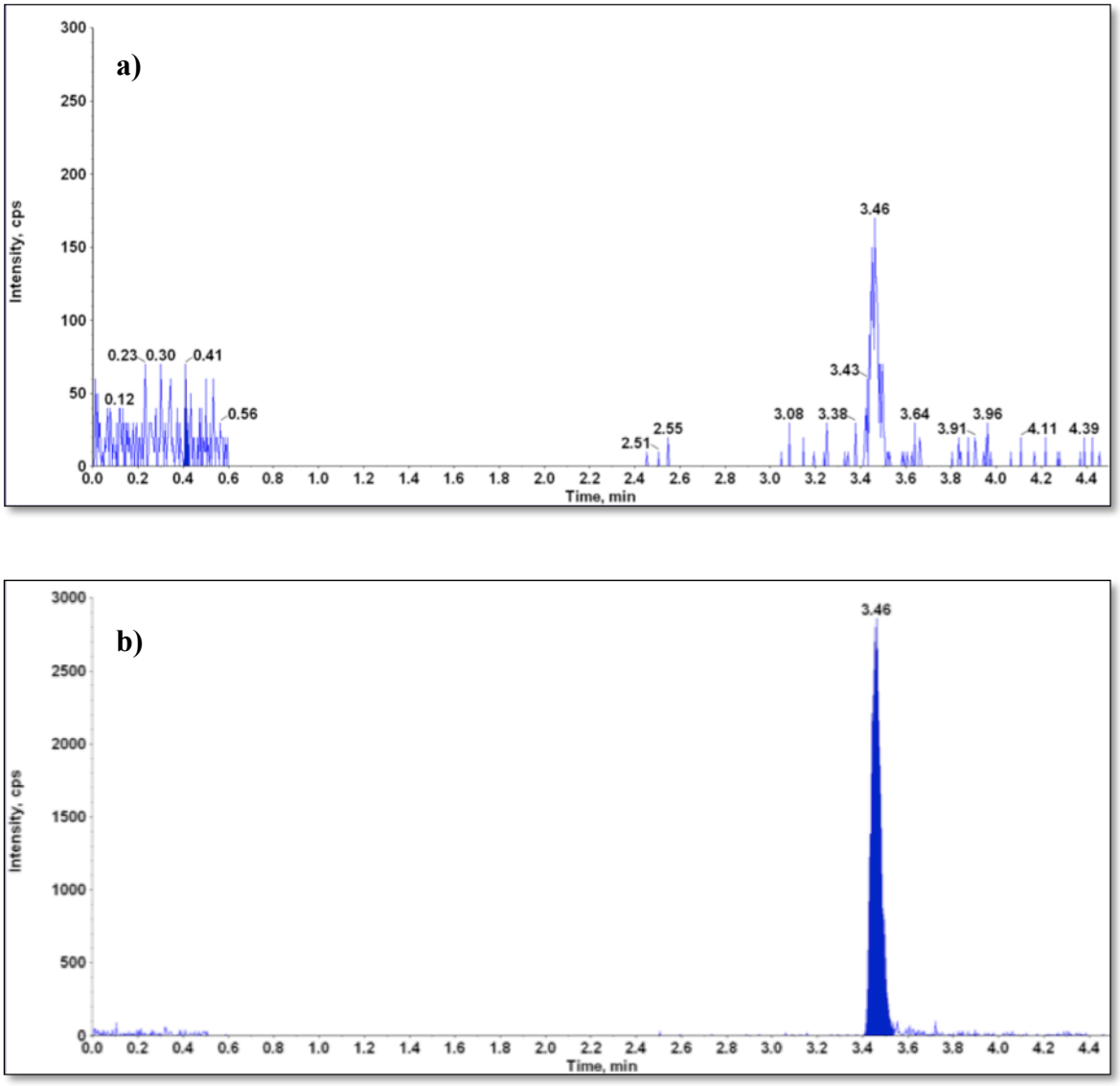

Figure 25: UPLC /MS-MS chromatograms of **a)** blank rat brain homogenate and **b)** LAZ (1.95 ng/mL) spiked in blank rat brain homogenate

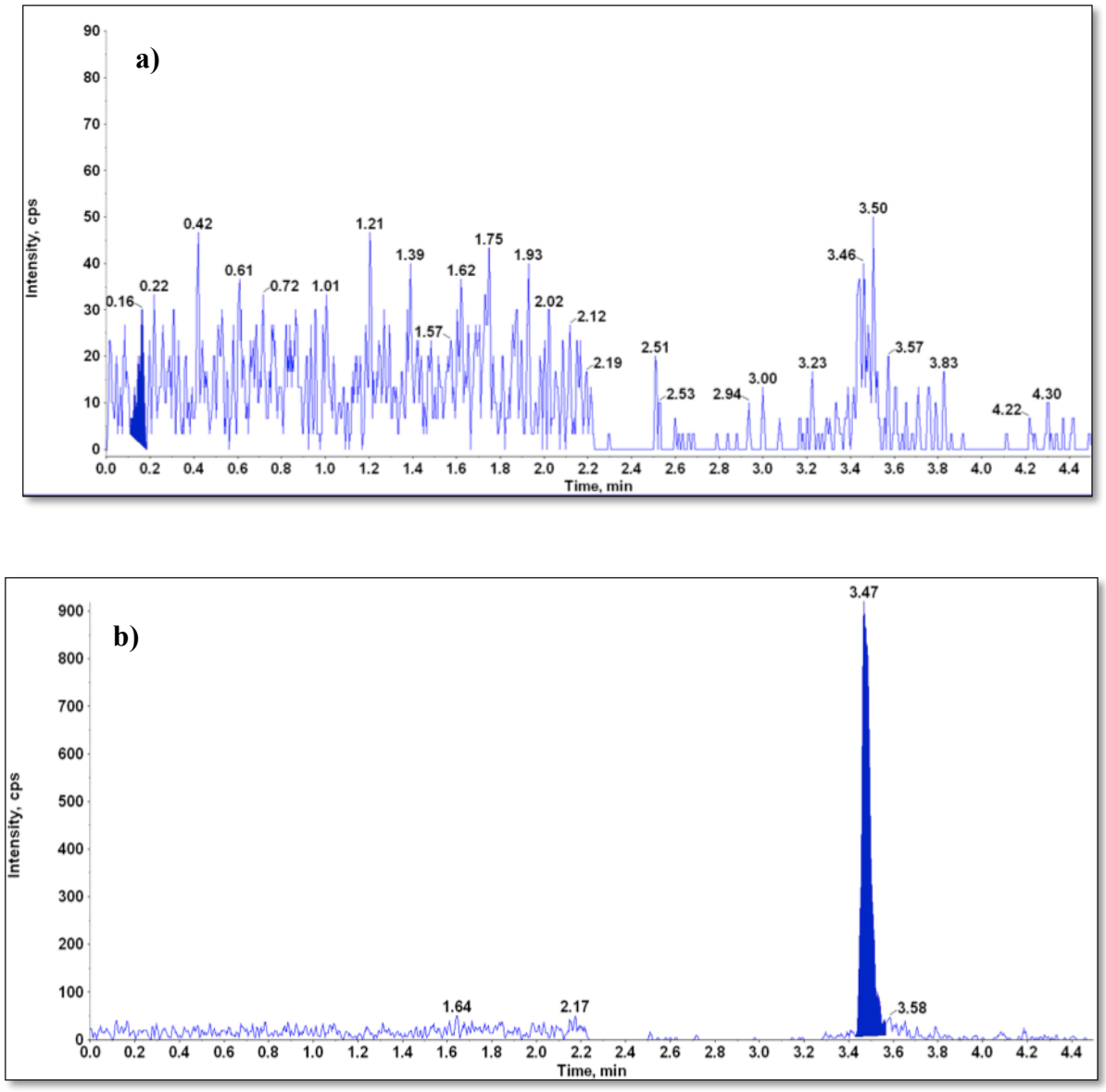

Figure 26: UPLC /MS-MS chromatograms of **a)** blank liver homogenate and **b)** LAZ (1.95 ng/mL) spiked in blank rat liver homogenate

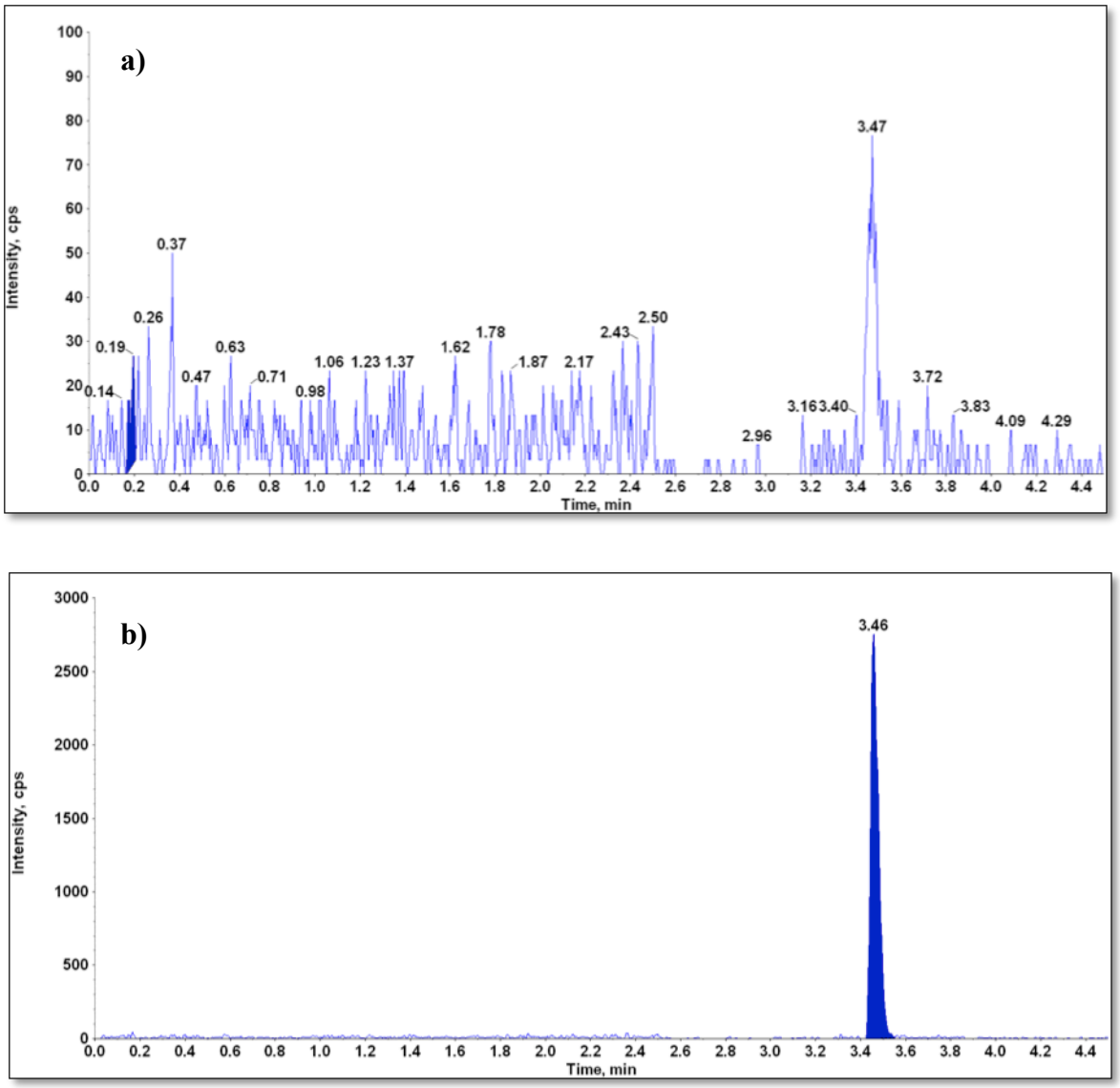

Figure 27: UPLC/MS-MS chromatograms of **a)** blank lung homogenate and **b)** LAZ (1.95 ng/mL) spiked in blank rat lung homogenate

Hence, APCI is used as an alternative to electron spray ionization (ESI), when the compound to be analyzed is not charged in solution [110]. The presently developed LC-MS/MS method successfully ionized LAZ using ESI to give product ion m/z 260, with an excellent detection intensity **(Figure 23)**. The use of ESI reduced the flow rate of the mobile phase from 1.2 mL/min (for APCI) to 0.45 mL/min. Additionally, ESI permitted the use of acetonitrile as the mobile phase, that resulted in strong signals and sharp peaks of LAZ, which are not achievable when methanol is used [110].

4.6.2. Linearity, Sensitivity and Selectivity

The linear range of calibration curve was established at 1.95-250 ng/mL. The mean coefficient of correlation (r) for inter-day calibration curve in plasma (n=5) was 0.9993 with % CV of 0.04. The mean coefficient of correlation (r) for inter-day calibration curve in brain, liver and lung homogenates (n=3) were 0.9903, 0.9972, 0.9990 with % CV of 1.03, 0.34, 0.07 respectively. The mean value for slope of inter-day calibration curve in plasma (n=5) was 0.007 with % CV of 14.37. The mean value for slope of inter-day calibration curve in brain, liver and lung homogenate (n=3) was 0.016, 0.002, 0.007 with % CV of 15.50, 6.89, 17.45 respectively. Selectivity was tested by comparing blank, zero blank and LAZ spiked samples at LLOQ concentration (1.95 ng/mL) in six individual non-pooled, analyte free, blank rat plasma samples. Due to limited availability of individual blank tissues, pooled homogenates of analyte free, blank rat brain, liver and lung tissues were used in determining the selectivity. The LAZ signal to noise ratios in all the bio-matrices was ≥ 10. The intra-day and inter-day accuracy and precision values for

LAZ LLOQ plasma sample (1.95 ng/mL) was < 12.5% and within the acceptance range of ± 20% **(Table 14)**, confirming the sensitivity of the method.

4.6.3. Recovery and Matrix Effect

The recovery and matrix effect are reported as mean ± standard deviation along with % CV in **Table 13.** The recovery and matrix effect of LAZ was calculated by comparing peak area ratios of LAZ and DIA spiked in blank rat plasma before and after extraction. The recovery of LAZ extracted from rat plasma for QC samples was in the range of 47.66 - 56.09 %, with % CV of 4.02 to 10.32 %. The percentage extraction recovery for tirilazad mesylate, from rat plasma was reported to be 66 % using a similar extraction method [48]. The percentage recovery for DIA was 89.67 ± 1.62 % (n=3, % CV= 1.81 %). The matrix effect represented as percent matrix factor of LAZ extracted from pooled rat plasma for QC samples were in the range of 85.64 - 89.35%. Furthermore, the percent matrix factor of LAZ tested in six lots of rat plasma obtained from individual rats was also in the range of 89.65 – 98.08 %, with coefficient of variation in acceptable range of ± 15 %. The percent matrix factor of DIA was 110.05 ± 4.99 % with a variability (% CV) of 4.54% (n=3).

QC standards (ng/mL)	% Recovery (% CV) (N=3)	% Matrix Factor (% CV)	
		Pooled (N=3)	Individual (N=6)
5	49.37 ± 5.09 (10.32 %)	86.12 ± 9.05 (10.50 %)	98.08 ± 4.49 (4.58 %)
50	47.66 ± 3.51 (7.36 %)	85.64 ± 5.66 (6.61 %)	91.17 ± 11.44 (12.55 %)
200	56.09 ± 2.26 (4.02 %)	89.35 ± 4.84 (5.42 %)	89.65 ± 3.21 (3.58 %)

Table 13: Percentage recovery and matrix effect (N=3-6, Mean ± SD) of LAZ from rat plasma

4.6.4. Accuracy and Precision

The intra-day and inter-day accuracy and precision values for LAZ QC plasma samples are summarized in **Table 14.**

Nominal Concentration (ng/mL)	Intra-day (N=6)		Inter-day (N=18)	
	%Accuracy	%Precision	%Accuracy	%Precision
1.95 (LLOQ)	115.60 ±13.19	11.45	110.33 ± 13.60	12.35
5	97.15 ± 4.87	5.07	98.06 ± 7.10	7.33
50	96.60 ± 9.62	10.01	101.77 ± 7.69	7.59
200	109.00 ± 7.07	6.28	103.53 ± 6.41	6.03
1000 (Very High Concentration QC)	98.17 ± 4.54	4.63	100.91 ± 6.31	6.25

Table 14: Intra-day and inter-day accuracy and precision values (Mean ± SD) for LAZ in rat plasma

The intra-day and inter-day accuracy values for QC plasma samples ranged from 96.60 – 115.60 % and 98.06 - 110.33 %, respectively. The intra-day and inter-day precision

values calculated in terms of coefficient of variation (% CV) for QC plasma samples were 5.07 to 11.41 % and 6.03 to 12.35 %, respectively. It is anticipated that the plasma concentrations in rat pharmacokinetic study can be higher than the upper limit of quantification of the calibration curve. Thus, a very high concentration QC sample (1,000 ng/mL) was prepared in blank rat plasma and was further diluted 10 times with blank rat plasma to give a final concentration of 100 ng/mL. The intra-day and inter-day accuracy and precision values for the very high concentration QC plasma sample were between 98.17 – 100.91 % and < 6.3 %, respectively. The intra-day and inter-day accuracy and precision, calculated in terms of coefficient of variation (% CV) for QC samples, ranged from 100.5 to 110.6% and 7.11 to 12.03% in brain tissue, 91.3 to 115.7% and 1.4 to 10.6% in liver tissue and 101.5 to 109.3% and 6.92 to 12.50% in lung tissue **(Table 15).** The intra-day and inter-day accuracy and precision values for QC samples in blank rat plasma and tissue homogenates were within the acceptance range of ± 15%.

Tissue	**Nominal Concentration (ng/mL)**	**Intra-day (N=3)**		**Inter-day (N=6)**	
		%Accuracy	**%Precision**	**%Accuracy**	**%Precision**
Brain	5	104.67 ± 7.23	7.11	100.53 ± 8.95	9.02
	200	106.27 ± 13.12	12.03	110.63 ± 9.84	8.76
Liver	5	91.33± 9.64	10.56	95.98± 9.18	9.56
	200	115.67± 1.53	1.39	112.83± 5.91	4.96
Lung	5	109.33 ± 13.58	12.50	101.51 ± 12.38	12.28
	200	103.87 ± 9.77	9.60	102.22 ± 6.94	6.92

Table 15: Intra-day and inter-day accuracy and precision values (Mean ± SD) for LAZ in rat brain, liver and lung tissue homogenates

4.6.5. Stability

The results of stability study are reported in **Table 16**. The measurements for the stability study were expressed as remaining percentages of nominal concentrations. LAZ plasma samples were stable on bench-top at 25°C for 1 hour with values within 15% of nominal concentrations. However, 20-30% of LAZ was degraded at 25°C by 3 hours. Additionally, to increase the bench-top stability of LAZ in plasma, we tested the stability of LAZ on ice bath at 25°C for 1 and 3 hours. LAZ QC samples stored on ice-bath were stable even at 3 hours within acceptable range of nominal concentration. LAZ plasma samples stored at -80°C for one month were stable with values within 15 % of nominal concentration (95.74 - 98.11 %). The freeze-thaw stability was tested after one and three cycles of freezing at -80°C and thawing to room temperature. The stability of LAZ in plasma after one and three freeze thaw cycles was within 15 % of nominal concentrations. The processed sample stability indicated that the processed samples were stable with values between 93.37 - 99.91 % of nominal concentrations, when placed in the auto-sampler at 10°C for 24 hours of analysis.

QC standard (ng/mL)	Short-term Stability (25°C)				Freeze Thaw Stability		Processed Sample Stability in Auto-sampler (24 hours at 10°C)	Long-term Stability (1month at -80°C)
	1 hour		3 hours					
	Normal	Ice-bath	Normal	Ice-bath	1 Cycle	3 Cycles		
5	95.43 (±12.64)	97.84 (±5.53)	81.63 (±1.68)	102.24 (±7.40)	88.55 (±1.78)	103.99 (±4.98)	99.91 (± 6.93)	98.11 (±5.04)
200	88.92 (±1.77)	94.00 (±4.88)	71.07 (±1.96)	87.88 (±4.38)	99.17 (±8.17)	90.90 (±6.40)	93.37 (± 3.29)	95.74 (±1.88)

Table 16: Stability of LAZ in rat plasma under different storage conditions expressed as percentages of nominal concentrations (N=3: Mean ± SD)

4.7. Pharmacokinetics and Bio-distribution Studies

The time frame for treatment initiation had a significant effect on the outcome of two-phase III clinical trials of tirilazad mesylate (structural analog of LAZ), while accessing its neuroprotective effect in stroke. Patients treated within 4 hours of the onset of stroke had a significant improvement in neurological function, compared to patients who were treated at 6 hours or later [33]. Furthermore, previous *in vivo* studies have reported the optimal dose of LAZ to exert radio-protective effect to be 15 mg/kg in rats [36]. These observations where included in our study design wherein the brain exposure of LAZ was monitored specifically between 4 to 8 hours after dosing LAZ at a therapeutic dose of 15 mg/kg. The solubility of LAZ citrate solution (2 mg/mL) limited the dose to 5 mg/kg,

while the optimal LAZ-NLC (5 mg/mL) and LAZ co-solvent (8.5 mg/ml) could be administered at 15 mg/kg due to its high drug payload. The plasma pharmacokinetic profiles of LAZ citrate, co-solvent and optimal NLC groups fitted a two-compartment IV bolus model **(Figure 28)** and plasma pharmacokinetic parameters were derived **(Figure 29 and Table 17)**.

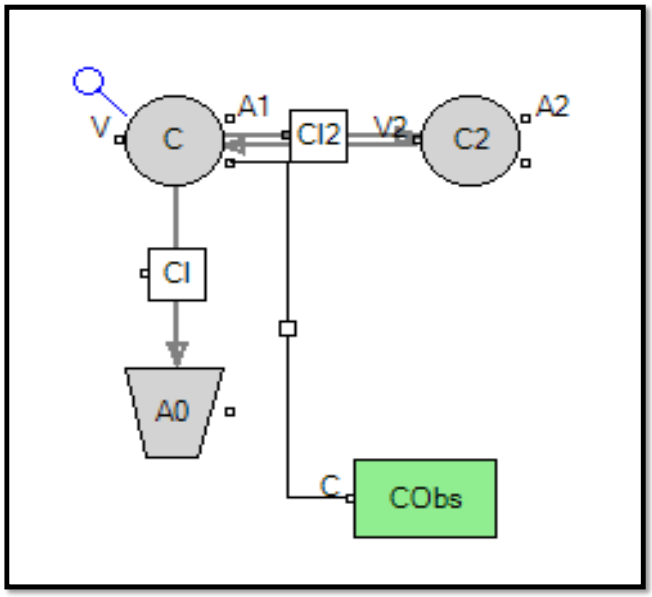

Phoneix NLME 2 compartment model
C: Central compartment
C2: Peripheral compartment
Cl2: Inter-compartmental clearance
Cl: Clearance from central compartment
V: Volume of distribution for central compartment
V2: Volume of distribution for peripheral compartment

Figure 28: 2-compartment IV bolus model

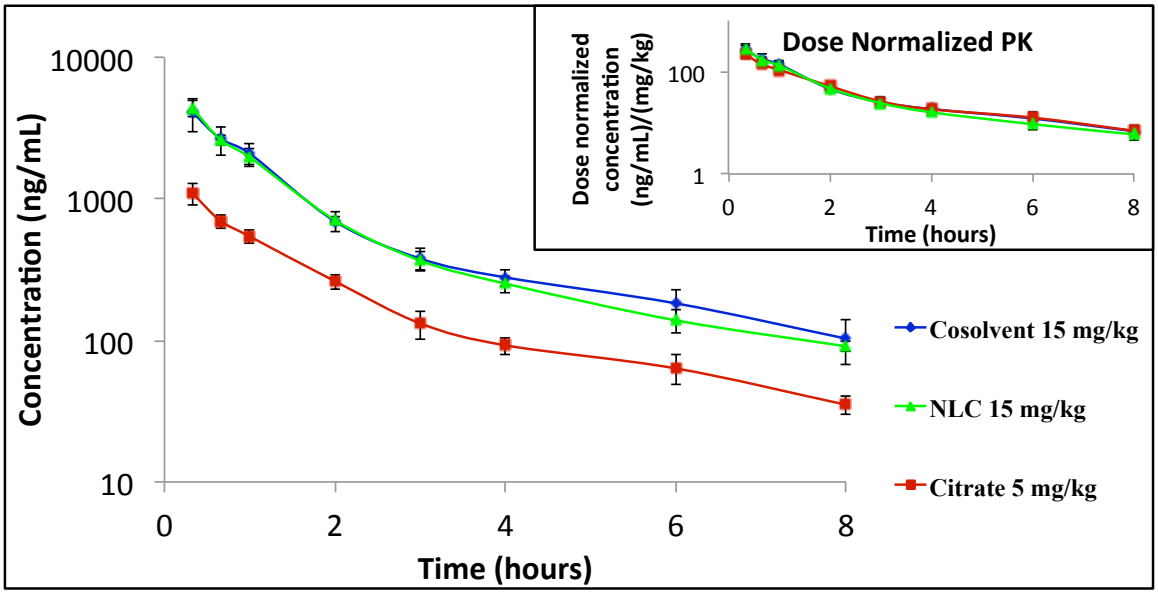

Figure 29: Plasma pharamcokinetic profile of LAZ citrate solution (5 mg/kg), LAZ co-solvent and optimal LAZ-NLC (15 mg/kg) in rats after single dose IV adminsatrtion (N=3-4: Mean ± SD);
Inset: Dose normalized plasma pharamcokinetic profile

The LAZ-NLC and LAZ co-solvent groups had significantly higher ($p<0.05$) $AUC_{0\text{-}8hr}$ (6698.98 ± 320.62 and 6905.97 ± 1391.98 vs 1833.26 ± 413.87 hr*ng/mL) and C_{max} (6508.23 ± 813.73 and 6516.98 ± 1860.77 vs 1577.28 ± 281.49 ng/mL) values in comparison to LAZ citrate group. On dose normalization, the $AUC_{0\text{-}8hr}$ (446.60 ± 21.37 and 460.40 ± 92.80 vs 366.65 ± 82.77 {hr*ng/ml}/mg/kg) and C_{max} (433.88 ± 54.25 and 434.47 ± 124.05 vs 315.46 ± 56.30 {ng/mL}/mg/kg) values although non-significant ($p>0.05$) were slightly higher for LAZ-NLC and LAZ co-solvent groups compared to LAZ citrate group. The slight increase in systemic exposure did not translate into lower clearance and longer $t_{1/2}$ values for LAZ-NLC and LAZ co-solvent groups compared to

LAZ citrate group. Interestingly, the LAZ-NLC group (797.98 ± 33.53 {mL/hr}/kg) showed a significantly lower inter-compartmental or distribution clearance (Cl2) between central and peripheral compartment in comparison to LAZ citrate (1476.77 ± 429.24 {mL/hr}/kg) groups. The inter-compartmental clearance for LAZ-NLC group was non-significant but indicated a lower trend compared to the LAZ co-solvent group (950.44 ± 256.59 {mL/hr}/kg). The inter-compartmental or distributional clearance indicates the rate of transfer between central and peripheral compartment. The lower Cl2 value (LAZ-NLC group) suggested slower distribution and redistribution whereas higher Cl2 values (LAZ citrate and LAZ co-solvent groups) indicated a rapid distribution and redistribution between the compartments. Additionally, slightly higher ratios V2/V with NLC group (1.26) compared to co-solvent and citrate (1.17 and 0.96) groups, implied the presence of a large fraction of LAZ from NLC present in the peripheral compartment [111].

Parameters, Units	Citrate 5 mg/kg	Co-solvent 15 mg/kg	NLC 15 mg/kg
AUC, hr*ng/mL	1833.26 ± 413.87	6905.97 ± 1391.98*	6698.98 ± 320.62*
Cmax, ng/mL	1577.28 ± 281.49	6516.98 ± 1860.77*	6508.23 ± 813.73*
AUC/dose, hr*ng/mL*mg	366.65 ± 82.77	460.40 ± 92.80	446.60 ± 21.37
Cmax/dose, ng/mL*mg	315.46 ± 56.30	434.47 ± 124.05	433.88 ± 54.25
AUMC, hr*hr*ng/mL	4155.39 ± 980.70	16585.56 ± 6137.58	14875.68 ± 3047.34
tvCl, mL/(kg*hr)	2837.56 ± 732.59	2235.80 ± 477.15	2243.19 ± 112.66
tvCl2, mL/(kg*hr)	1476.77 ± 429.24	950.44 ± 256.59	797.98 ± 33.53*
tvV, mL/(kg)	3246.68 ± 644.59	2427.08 ± 667.03	2368.59 ± 383.93
tvV2, mL/(kg)	3160.79 ± 932.15	2863.04 ± 1363.25	3070.81 ± 1373.63
VSS, mL/(kg)	6407.46 ± 1569.58	5290.12 ± 1617.20	5439.40 ± 1753.66
Ke, 1/hr	0.87 ± 0.05	0.93 ± 0.09	0.97 ± 0.08
K12, 1/hr	0.45 ± 0.10	0.40 ± 0.09	0.35 ± 0.04
K21, 1/hr	0.47 ± 0.08	0.35 ± 0.07	0.33 ± 0.11
Ke_hl, hr	0.80± 0.04	0.75 ± 0.07	0.72 ± 0.06
Alpha_hl, hr	0.46 ± 0.05	0.48 ± 0.04	0.49 ± 0.06
Beta_hl, hr	2.61 ± 0.15	3.21 ± 0.97	3.42 ± 1.42
MRT, hr	2.26 ± 0.07	2.39 ± 0.73	2.24 ± 0.58

Table 17: Plasma pharamacokinetic parameters for LAZ citrate solution (5 mg/kg), LAZ co-solvent (15 mg/kg) and optimal LAZ-NLC (15 mg/kg) after single dose IV adminstration (N=3-4: Mean ± SD);
$p < 0.05$ One-way ANOVA with Tukey's post hoc;
*Significant when compared to Citarte 5mg/kg

The optimal LAZ-NLC (43.07 ± 20.59 ng/gm) exhibited significantly ($p<0.05$) higher levels of LAZ in brain compared to LAZ citrate group (6.32 ± 1.33 ng/gm) at 4 hours **(Figure 30, a)**. The LAZ co-solvent group (37.47 ± 7.06 ng/gm) similarly had higher but non-significant LAZ levels in brain compared to LAZ citrate group. Furthermore, NLC (4.40 ± 0.47 ng/gm) and co-solvent (4.13 ± 0.61 ng/gm) groups delivered LAZ across the BBB and were retained in the brain up to 8 hours, compared to LAZ citrate solution that exhibited unquantifiable LAZ levels in brain beyond 4 hours. Even on dose normalization at 4 hours, LAZ-NLC (2.87 ± 1.37 {ng/gm}/{mg/kg}) and LAZ co-solvent (2.50 ± 0.47 {ng/gm}/{mg/kg}) groups were able to deliver two-fold higher amounts of LAZ in the brain compared to citrate group (1.26 ± 0.27 {ng/gm}/{mg/kg}) **(Figure 30, d)**.

Although, the LAZ co-solvent and LAZ-NLC groups exhibited comparable LAZ brain exposure levels, the liver distribution of LAZ from these formulations showed a significant difference. The LAZ-NLC (164.17 ± 44.88 and 41.87 ± 7.39 ng/gm) group exhibited significantly lower ($p<0.05$) exposure to liver at 4 and 8 hours compared to LAZ co-solvent (360.00 ± 141.12 and 94.89 ± 30.02 ng/gm) group. Moreover, the LAZ co-solvent group had significant higher ($p<0.05$) levels in liver compared to LAZ citrate (88.67 ± 39.18 and 30.87 ± 7.88 ng/gm) group at 4 and 8 hours **(Figure 30, b)**. Even on dose normalization, the LAZ-NLC (10.94 ± 2.99 and 2.79 ± 0.49 {ng/gm}/{mg/kg}) had significantly lower ($p<0.05$) levels in liver compared to LAZ co-solvent (24.00 ± 9.41 and 6.33 ± 2.00 {ng/gm}/{mg/kg}) group at 4 and 8 hours and significantly lower

($p<0.05$) levels compared to LAZ citrate (6.18 ± 1.58 {ng/gm}/{mg/kg}) group at 8 hours **(Figure 30, e)**.

The optimal LAZ-NLC and LAZ co-solvent enhanced LAZ brain exposure by almost twice the amount compared to LAZ from citrate solution. However, the optimal LAZ-NLC had an added advantage of lower hepatic exposure decreasing the amount delivered to the liver by half, a less off-target delivery than LAZ citrate and co-solvent groups. The higher brain and lower liver uptake of the optimal LAZ-NLC in comparison to LAZ citrate and co-solvent groups could be attributed to the particle size and the surface properties of the NLC with similar observation noted by other researchers for lipid nanoparticles [72, 73].

LAZ co-solvent group (906.93 ± 312.02 and 432.78 ± 130.17 ng/gm) had significantly higher levels in lung tissue compared to LAZ citrate group (300.76 ± 10.37 and 105.40 ± 12.22 ng/gm) between 4 and 8 hours, whereas LAZ-NLC (368.23 ± 82.30 ng/gm) demonstrated a significantly higher ($p<0.05$) level at 8 hours compared to LAZ citrate group. However, at the same dose basis, no significantly higher levels in lung tissue were observed with LAZ formulations compared to citrate solution. Nevertheless, the NLC group showed a sustained LAZ release at 6 and 8 hours, which could be validated by the higher elimination half-life compared to citrate group **(Figures 30, c and f)**.

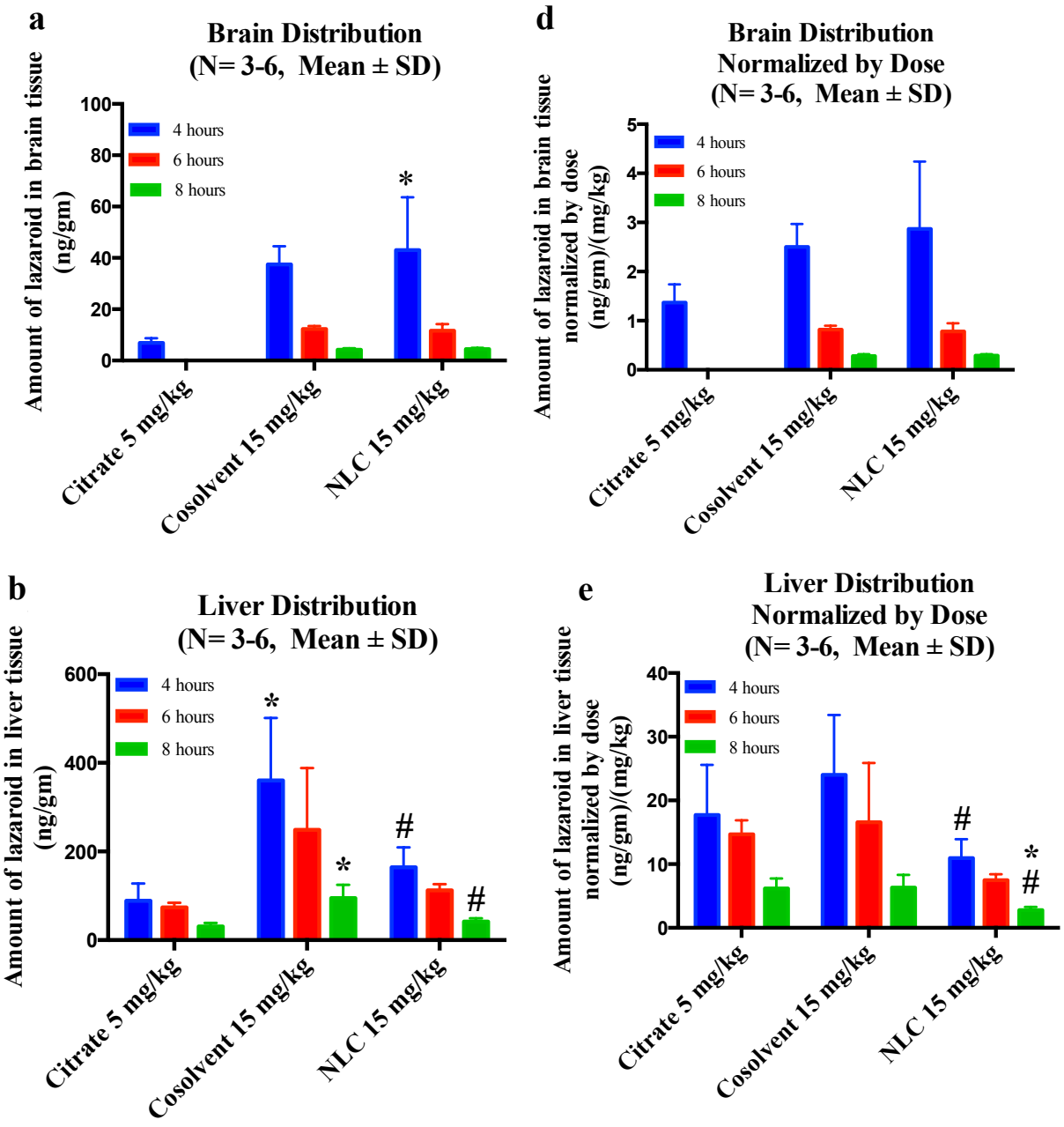
a
Brain Distribution
(N= 3-6, Mean ± SD)
Amount of lazaroid in brain tissue (ng/gm)
4 hours
6 hours
8 hours
Citrate 5 mg/kg
Cosolvent 15 mg/kg
NLC 15 mg/kg
d
Brain Distribution
Normalized by Dose
(N= 3-6, Mean ± SD)
Amount of lazaroid in brain tissue normalized by dose (ng/gm)/(mg/kg)
b
Liver Distribution
(N= 3-6, Mean ± SD)
Amount of lazaroid in liver tissue (ng/gm)
e
Liver Distribution
Normalized by Dose
(N= 3-6, Mean ± SD)
Amount of lazaroid in liver tissue normalized by dose (ng/gm)/(mg/kg)

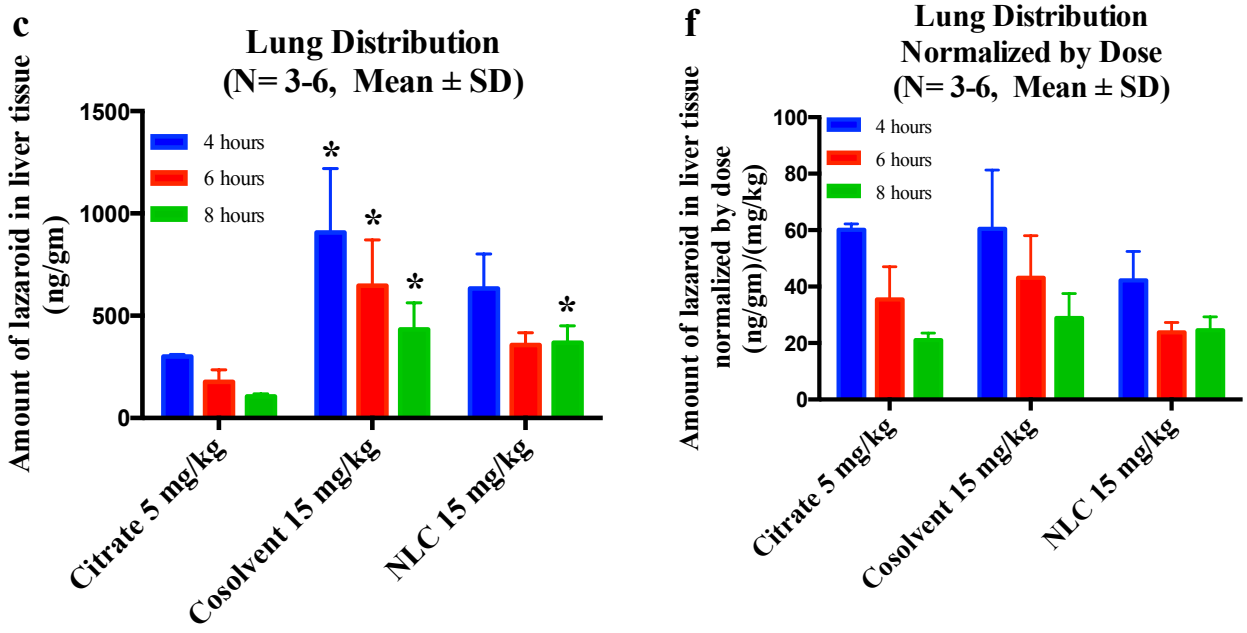

Figure 30: Tisue distribution of LAZ citrate solution (5 mg/kg), LAZ co-solvent (15mg/kg) and optimal LAZ-NLC (15 mg/kg) in a) brain, b) liver, c) lungs, d) brain dose normalized, e) liver dose normalized and f) lung dose normalized (N=3-6: Mean ± SD); $p < 0.05$ One-way ANOVA with Tukey's post hoc;
*Significant difference when compared with citrate group, # Significant difference between NLC and cosolvent group.

Since the tissue profiles of the citrate, co-solvent and NLC groups were truncated, the slopes of terminal phase were used to estimate the terminal half-life ($t_{1/2}$) of LAZ in the brain, liver and lung tissues. Log-linear trapezoidal rule was used to calculate the AUC for the truncated LAZ plasma and tissue profile **(Table 18).**

Although the optimal LAZ-NLC and LAZ citrate solution had similar plasma terminal half-lives, the $t_{1/2}$ in brain for LAZ-NLC (1.21 hr) was almost 1.5 times higher than LAZ citrate solution (0.84 hr) indicating the increased retention of LAZ in brain. The increased brain half-life of LAZ using the NLC system was corroborated by 2.75-fold increase in

the brain to plasma ratio ($AUC_{brain\ 4\text{-}8h}/AUC_{plasma\ 4\text{-}8h}$) for LAZ-NLC group (0.11) in comparison to LAZ citrate solution group (0.04) indicating enhanced permeation and exposure of LAZ in the brain. The $t_{1/2}$ for LAZ-NLC (2.04 hr) in liver was 1.2 times less than LAZ citrate solution (2.63 hr), which was verified by the lower liver to plasma ratio ($AUC_{liver\ 4\text{-}8h}/AUC_{plasma\ 4\text{-}8h}$) for LAZ-NLC compared to LAZ citrate solution (0.56 vs 0.92). The $t_{1/2}$ in lungs for LAZ-NLC (5.33 hr) was 2 times higher than LAZ citrate solution (2.67 hr) indicating increased residence time in lung tissue. No statistical analyses were carried for tissue terminal half-lives and tissue to plasma ratios since the parameter values were derived from the mean profile constructed from sparse sampling design.

Parameters (Units)	Citrate 5 mg/kg	NLC 15 mg/kg
$t_{1/2}$ plasma (hr)	0.80	0.72
$t_{1/2}$ brain (hr)	0.84	1.21
Brain/Plasma Ratio	0.04	0.11
$t_{1/2}$ liver (hr)	2.63	2.04
Liver/Plasma Ratio	0.92	0.56
$t_{1/2}$ lung (hr)	2.67	5.33
Lung/Plasma Ratio	3.12	3.08

Table 18: Brain, liver and lung tissue pharamacokinetic parameters for LAZ citrate solution (5 mg/kg) and optimal LAZ-NLC (15 mg/kg) after single dose IV administration

4.8. Dose Linearity Studies

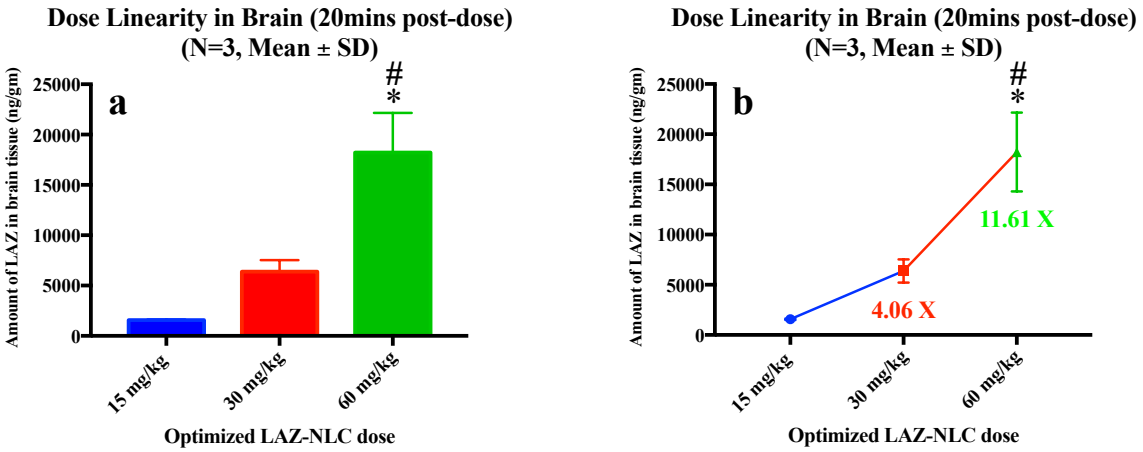

Figure 31: Brain distribution of optimal LAZ-NLC 20 minutes post-dose at 15, 30 and 60 mg/kg (N=3: Mean ± SD);
$p < 0.05$ One-way ANOVA with Tukey's post hoc;
* Significant difference compared with 15 mg/kg group, # Significant difference when compared with 30 mg/kg group

The amount of LAZ in brain tissue 20 minutes after administration of optimal LAZ-NLC at 15, 30 and 60 mg/kg is depicted in **Figures 31, a and b**. The amount of LAZ in brain tissue at 60 mg/kg (18220.59 ± 3926.67 ng/gm) dose is significantly ($p<0.05$) higher compared to the amount measured at 30 mg/kg (6377.84 ± 1159.91 ng/gm) and 15 mg/kg (1569.47 ± 71.53 ng/gm) doses. The amount of LAZ in brain tissue at 60 mg/kg is 11.61 times higher compared to the amount post 15 mg/kg dose. Although non-significant ($p>0.05$, $p=0.0529$), the amount of LAZ in brain tissue at 30 mg/kg is 4.06 times higher than15 mg/kg dose.

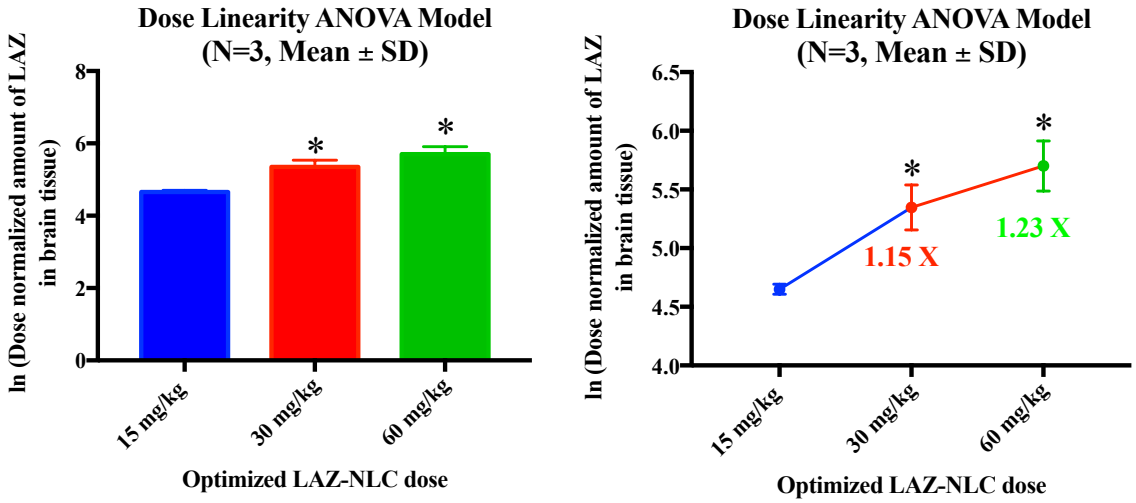

Figure 32: Dose normalized natural log-transformed brain distribution of optimal LAZ-NLC 20 minutes post-dose at 15, 30 and 60 mg/kg (N=3: Mean ± SD);
$p < 0.05$ One-way ANOVA with Tukey's post hoc;
* Significant difference compared with 15 mg/kg group

The ANOVA model and the power model are used to assess the dose linearity of the optimal LAZ-NLC in brain. The PK parameters have lognormal distribution leading to residuals that do not show normal distribution. In order to satisfy the assumption of ANOVA, which indicate normal distributions of residuals, the PK parameters are natural log-transformed [112]. The dose-normalized natural log-transformed amount of LAZ in brain tissue at 20 minutes after administration of optimal LAZ-NLC at 15, 30 and 60 mg/kg is depicted in **Figures 32, a and b.**

The dose normalized amounts of LAZ in brain tissues at 20 minutes after administering 60 mg/kg and 30 mg/kg doses are significantly higher ($p<0.05$) than the dose normalized amount of LAZ in brain obtained after dosing 15 mg/kg. Even after dose normalization,

the amount of LAZ in brain tissue at 60 and 30 mg/kg is 1.23 and 1.15 times higher compared to the amount post 15 mg/kg dose. Thus the ANOVA model indicates a non-linear increase in amount of LAZ in brain tissue after linear increase in doses of optimal LAZ-NLC.

The power model utilizes weighted linear regression analysis to determine the slope and its corresponding 90 % confidence interval for natural log-transformed PK parameter and dose. The slope (β_1) is determined to 1.77 and the 90 % confidence interval is computed to be **0.84, 1.16.** The user-defined critical region ($1+\frac{\ln(\theta_l)}{\ln(r)}$, $1+\frac{\ln(\theta_h)}{\ln(r)}$) is calculated by using values for θ_l and θ_h as 0.8 and 1.25, and r (ratio of highest dose 60 mg/kg to lowest dose 15 mg/kg) as 4. The range for the user-defined critical region is computed to be **1.59, 1.97**. The dose proportionality is established when the confidence interval of slope (β_1) falls within the user-defined critical region. The, 90 % confidence interval for β_1 0.84, 1.16 does not fall within the user-defined critical region 1.59, 1.97. Thus, the power model reiterated findings of the ANOVA model, indicating a non-linear increase in amount of LAZ in brain tissues as dose of optimal LAZ-NLC linearly increased.

Chapter 5: Discussion

5.1. HPLC assay of LAZ

The aqueous calibration curve of LAZ was linear in range of 1-100 μg/mL with LLOQ established at 1 μg/mL sufficient for quantifying the solubility of LAZ in oil and determining the encapsulation efficiency of LAZ-SLNs and NLCs. The signal to noise ratio of ≥ 10 indicated no endogenous substances interfered with the quantification of LAZ. The intra-day and inter-day accuracy and precision values were within ±15 % indicating that the developed HPLC assay was accurate, precise and reproducible for quantification of LAZ.

5.2. Selection of Lipids

It is critical to select optimal lipid blends for manufacturing NLC with desired physico-chemical properties. The ideal lipid matrix should have high drug solubility in order to have sufficient drug loading in the NLC, which would directly influence the particle size, encapsulation efficiency and storage stability [67, 69].

Labrasol is obtained by esterification of medium-chain triglycerides (caprylic C8:0 and capric C10:0 glycerides) from coconut oil and PEG 400. It is mainly used as a solubilizer for increasing the solubility of lipophilic compounds in lipid based formulations [113]. Additionally, Labrasol is less susceptible to oxidation owing to presence of saturated lipids compared to unsaturated lipids such as Pecol (glycerol mono-oleate) and oleic acid [80]. Thus, higher solubility of LAZ and reported reduced oxidation potential justified the selection of Labrasol as liquid lipid.

Lipid-drug solubility, *in vitro* release rates and storage stability can strongly influence the selection of solid lipids. GB consists of diacylglycerols of behenic acid (C22:0) together with variable quantities of mono- and tri-acylglycerols. TM and TS are triglycerides prepared from myristic acid (C14:0) and stearic acid (C18:0) respectively. Mixture of mono-, di- and tri- glycerides display higher drug solubility compared to pure triglycerides [90]. The shift in the endothermic peak of LAZ mixed with GB indicated the miscibility of LAZ in GB and the partial loss in crystal structure of LAZ. The absence of LAZ peak shift with TM and TS reflected less solubilizing potential of LAZ by TM and TS. Manjunath et.al., reported SLNs prepared with longer-chain triglycerides exhibited slower *in vitro* drug release which translated as increased *in vivo* systemic exposure with enhanced brain delivery [75]. Moreover, longer-chain triglycerides have displayed higher storage stability due to slower polymorphic transitions compared to shorter-chain triglycerides [78]. Thus, GB was selected as the solid lipid mainly due its miscibility with LAZ as supported by thermal analysis coupled with sustained *in vitro* release of LAZ form GB SLN.

5.3. Development, Optimization and Validation of LAZ-NLC using CCD

The three-dimensional contour plots were used to analyze the effect of LAZ-NLC composition on the response variables. The increase in amount of liquid lipid Labrasol decreased the particle size of LAZ-NLC and this finding was ascribed to the viscosity of the melted lipid matrix. The viscosity of GB and caprylic:capric triglyceride mixtures decreased at 73°C (the melting point of GB) as compared with that of GB alone [114].

Thus, increasing the amount of liquid lipid (Labrasol) in NLC resulted in decreased viscosity, which reduced surface tension conducive for the reduction in particle size. Researchers have previously observed a similar trend of decreasing particle size on increasing the proportion of liquid lipid in formulations of NLC [115, 116]. Increasing the proportion of DSPE-PEG 2k also affects the particle size of NLC in a contrariwise fashion with an initial slight increase followed by a decrease resulting in an umbrella shaped curve. A similar phenomenon was reported in DSPE-PEG grafted liposomes. An increase in particle size was observed with the increase in DSPE-PEG from 4 to 8 mol%, which was attributed to the transition of PEG moiety from mushroom to brush configuration, resulting in extension of PEG moiety away from the surface. This was followed by a decrease in particle size with DSPE-PEG above 8 mol% due to the increased PEG-PEG resulting in a structural transition from liposomes to micelles [117].

In general, nano-dispersions possessing surface charge greater than ±30 mV are considered stable [118]. However, the adsorption of opsonins on surface of lipid nanoparticles is related to its surface charge and surface hydrophobicity. The primary reason for the addition of DSPE-PEG is to prevent opsonization and subsequent clearance of LAZ-NLCs via RES organs, such as liver. The hydrophilic residues of PEG align towards the aqueous phase while insoluble hydrophobic residues are oriented towards the lipid matrix of NLC [68]. Thus, increasing the amount of DSPE-PEG 2k displayed a decrease in zeta potential from +25.84 to -4.52 mV due to the formation of shell around the lipid matrix of NLC shielding the surface charge and hydrophobicity.

The amount of LAZ encapsulated in NLC increased with increasing DSPE-PEG 2k, possibly due to the molecular interaction between an piperazine nitrogen of LAZ and phosphate group in DSPE moiety resulting in an enhanced solubilization of LAZ in lipid matrix [44, 119].

After analyzing the effect of independent variables on the response variables, the criterion for particle size, zeta potential and encapsulation efficiency was selected based on the objective of enhancing the brain exposure of LAZ with LAZ-NLC. It has been previously reported that lipid nanoparticles measuring less than 200 nm bypass the clearance mechanisms of RES resulting in a longer contact time with the BBB for passive diffusion or active uptake of the nanoparticles [55, 120]. Thus, the particle size of LAZ-NLC was selected to be in the range of 150 to 200 nm. The surface charge and opsonization are directly correlated, with neutrally charged nanoparticles undergoing less clearance than charged nanoparticles [121, 122]. Additionally, neutral or negatively charged nanoparticles have demonstrated enhanced permeability across the brain without compromising the integrity of BBB and have less immunogenic potential than positively charged particles [123, 124]. Accordingly, zeta potential that measures the surface charge density was selected to be in range of 0 to -6 mV. Since LAZ possesses poor aqueous solubility and is susceptible to metabolism, a high proportion of LAZ needs to be encapsulated in a protective lipid matrix of NLC. Thus, it is critical to have a maximum encapsulation efficiency of LAZ in NLC to ensure maximum delivery of LAZ payload.

The optimal composition of LAZ-NLC was determined using the above desired response variable criterion. The developed CCD matrix was able to accurately predict (< 3 % error) the particle size (172.3 nm), zeta potential (-4.54 mV) and encapsulation efficiency (85.01 %) of the optimal LAZ-NLC for the purpose of enhanced brain delivery of LAZ.

5.4. Physico-chemical Characterization of Optimal LAZ-NLC

TEM is a microscopic technique used in determining the particle morphology, surface characteristic and size, and also for validating the results obtained from the particle size analyzing techniques. The particle size of the optimal LAZ-NLC were <200nm verifying the measurements from DLS analysis. The polydispersity index as reported by DLS was less than 0.3, considered as a monodispersed nanoparticles dispersion [88] and the homogeneous and uniform size distribution of the optimal LAZ-NLC were visually confirmed by the TEM images.

DSC and XRD are widely used in conjunction to characterize crystal structure and polymorphic state of drug loaded lipid nanoparticles. The nano-size of LAZ-NLC with high surface area and presence of surfactant could result in the melting point depression of GB in the optimal LAZ-NLC. Additionally, the shift in the endothermic peak of GB in LAZ-NLC could be attributed to the presence of liquid lipid Labrasol and its interaction with the GB. In a previously reported study, lipid nanoparticles prepared from solid and liquid lipid mixtures demonstrated a linear trend in lowering the melting point of solid lipid (GB) with increasing concentration of liquid lipid (Miglyol; medium chain triglyceride) in lipid nanoparticles [114]. The crystallinity of GB was not completely lost

in LAZ-NLC and was confirmed by the overlapping diffraction patterns of LAZ-NLC with pure GB. The shift in DSPE-PEG 2k melting peak could be attributed to the interaction of DSPE-PEG 2k with components of NLC, especially LAZ and GB [44]. Similar complex multiple interactions between lipid, surfactant and PEGylating agent affecting the physical state of the lipid nanoparticles were earlier reported [125]. The DSC endothermic peak for LAZ disappeared in LAZ-NLC and was corroborated with the loss of sharp diffraction pattern corresponding to LAZ in the XRD analysis. This suggested the probable solubilization and incorporation of LAZ in the lipid matrix of NLC and the conversion of LAZ to amorphous state. The aqueous solubility of lazaroids at physiological pH 7.4 is very low (< 65 ng/mL) [126]. Amorphous drugs have demonstrated better solubility than their crystalline equivalents and thus the amorphous nature of LAZ in NLC would aid in its better solubilization in systemic circulation and reduce the risk of precipitation in physiological conditions.

The particle size, nature of surfactant and incorporation of drug in the lipid matrix could influence the crystallinity of lipid matrix [77, 127]. Muhlen et.al., previously reported the presence of β and β' form of GB in SLNs prepared with Compritol (GB) [128]. Similarly, GB in the optimal LAZ-NLC could possess some degree of crystallinity (β and β' form). However the presence of surfactant (Polysorbate 80) having no effect on the lipid crystalline structure, the nano-size of NLC and interactions between LAZ, GB, DSPE-PEG 2k and Labrasol could stabilize the crystal structure of GB and prevent its possible polymorphic transition from β' to more stable β form. In the absence of lipid

polymorphic transitions, the drug expulsion from lipid matrix is prevented resulting in extended storage stability. This is highlighted by unchanged encapsulation efficiency of optimal LAZ-NLC over 3-month storage period.

In case of formulations intended for intravenous administration, hemolysis may occur causing pain and series of adverse effects such as vascular irritation, phlebitis and death in some cases. These reactions are mainly attributed to the release of hemoglobin from erythrocytes into the plasma. The percent hemolysis for optimal LAZ-NLC with concentration of 5 mg/mL and formulation to blood ratio from 0.0375 to 1 was within accepted limit of 15 %. The corresponding formulation to blood ratios at 15, 30 and 60 mg/kg doses were 0.0375, 0.075 and 0.15 respectively and within the established hematocompatible range for the optimal LAZ-NLC. Thus, the optimal LAZ-NLC can be dosed intravenously even at a high dose of 60 mg/kg without any danger of red blood cell lysis. The hematocompatibility of optimal LAZ-NLC could be attributed to negative surface charge [122] and use of GRAS (Generally Recognized As Safe) excipients. The presence of increased surfactant (Polysorbate 80) at higher formulation to blood ratio may be responsible to the increased hemolytic potential.

5.5. Development and Validation of UPLC/MS-MS Assay for LAZ in Bio-matrices

There is no single method reported for quantitative analysis of LAZ in plasma and organ homogenates. There are HPLC and HPLC-MS/MS methods reported for bio-analytical quantification of tirilazad mesylate (U-74006F), with the most recent assay being developed in 1999. In the past 16 years, no validated analytical method has been reported

for the quantification of lazaroids (a literature search was performed in PubMed). Furthermore, the previously reported assays have long run times (18 minutes), using complex sample processing procedures with requirements of high plasma volumes and use of alternative detection system such as atmospheric pressure chemical ionization (APCI) [129, 130]. Therefore, it was imperative to develop a simple and sensitive bio-analytical method and validate it specifically for the quantification of LAZ in biological matrices that would aid in studying the pharmacokinetics and bio-distribution of this compound.

The UPLC/MS-MS for quantification of LAZ in bio-matrices was validated as per US-FDA guidelines for bio-analytical validation. A full validation was performed for LAZ in blank rat plasma. Since, the availability of blank rat bio-matrices is limited, a partial validation was performed for LAZ in brain, liver and lung homogenates. The partial validation included testing of selectivity, intra-day and inter-day accuracy and precision. The calibration curve of LAZ in plasma and tissue homogenates was linear in range of 1.95-250 ng/mL with LLOQ concentration established at 1.95 ng/mL. In previously reported pharmacokinetics studies in rats, tirilazad mesylate solution dosed intravenously at 10 mg/kg was not detectable in plasma and tissues after 8 hours post dose leading to an insufficient characterization of the plasma pharmacokinetics and poor understanding of tissue distribution. These drawbacks were attributed to the insufficient sensitivity of HPLC assay with the LLOQ of 100 ng/mL [48]. The LLOQ (1.95 ng/mL) of the presently developed assay was 100 times greater than the LLOQ of previously reported

assay. Moreover, in the pharmacokinetic study using LAZ citrate group dosed at 5 mg/kg (2 times lower dose than tirilzad mesylate study 10 mg/kg) the average plasma, liver and lung concentrations of LAZ at 8 hours were 28.60, 9.27 and 29.51 ng/mL, 5 to 15 times higher than the LLOQ (1.95 ng/mL) of the presently developed assay. Although the average brain concentration at 8 hours (0.35 ng/mL) was lower than the LLOQ, it was still detectable and could be estimated. Thus, the developed and validated UPLC-MS/MS was sensitive to quantify the low concentrations of LAZ beyond 8 hours post dose, enabling the accurate characterization of pharmacokinetics and in particular, tissue distribution of LAZ. Moreover, the analytical quantification method for tirilazad mesylate involved the use of high volumes of plasma samples (500 μL) and complex extraction procedure using combination of protein precipitation and solid phase extraction [129, 131]. In the present developed method, only 100 μL of plasma or tissue homogenates were needed to extract LAZ using a simple protein precipitation method with acetonitrile. It was crucial for the developed method to be selective specifically for quantifying LAZ. The selectivity of LAZ was determined by comparing the ratio of LAZ signal to signal generated by inherent endogenous substances present in the bio-matrices. The signal to noise ratio >10 indicated that no endogenous substances interfered with the quantification of LAZ. The modest recovery of LAZ from plasma was initially speculated to the ion suppression of LAZ by plasma matrix and the instability of LAZ in plasma. However, it was later determined that the matrix effect was concentration-independent and there was no significant ion suppression of LAZ. In addition, the stability studies indicated that

LAZ was stable under different storage and processing conditions. Another probable explanation for the low recovery could be due to the high plasma protein binding of LAZ. The plasma protein binding of lazaroids is in range of 75-99% in rat and human plasma [132]. Therefore, the moderate recovery of LAZ could be partially attributed to the high plasma protein binding resulting in loss of LAZ during protein precipitation. Although, recovery and matrix effect of LAZ from brain, liver and lung tissue homogenates was not evaluated, the accuracy and precision of QC samples in the blank tissue homogenates were within the acceptable limits demonstrating that the key validation parameters were not compromised.

The intra-day and inter-day accuracy and precision values were within ±15 % indicating that the developed assay was accurate, precise and reproducible for quantification of LAZ in bio-matrices. The stability study was designed to cover expected sample handling and storage conditions during the course of study. It was advisable to process LAZ plasma samples within one hour at an ambient temperature and should be processed on ice-bath especially when large numbers of samples requires processing time of about 3 hours. The long-term storage stability of LAZ in plasma indicated that pharmacokinetic samples could be stored at -80°C for up to one month before analysis without compromising the integrity of the sample. The aforementioned conditions were taken into consideration while processing and storing LAZ brain, liver and lung tissue samples.

5.6. Pharmacokinetics and Bio-distribution of LAZ Formulations

The plasma pharmacokinetic parameters for LAZ citrate, co-solvent, and NLC groups were comparable except for the inter-compartmental clearance. This disparity in inter-compartmental clearance between the three groups could possibly be due to the differential distribution of LAZ from NLC in tissues such as the brain and liver, which was apparent from our bio-distribution studies. The enhanced brain exposure and reduced accumulation in the liver could be attributed to the physico-chemical properties of the optimal LAZ-NLC.

The LAZ from buffered citrate solution and co-solvent system form unstable suspensions on precipitating at physiological pH and are phagocytized and cleared by the macrophages in the liver and spleen [94, 126]. The particle size of < 200 nm and presence of PEG coating lowered the possible adsorption of opsonins on the surface of NLC resulting in reduced accumulation in the liver compared to the unprotected LAZ citrate solution and LAZ co-solvent [55].

The transport of the optimal LAZ-NLC across the BBB could be ascribed to the following transport mechanisms.

- **Passive diffusion**:

  LAZ is highly lipophilic with log P value of 8 [45]. Thus, free unbound LAZ can be transported across the BBB by passive diffusion in healthy animals with intact BBB. The comparable levels of LAZ in the brain tissue between LAZ co-solvent and LAZ-NLC group could be attributed to the diffusion of free LAZ through the

BBB. The intact optimal LAZ-NLC can also cross the BBB as supported by Nance et.al., in an *ex vivo* study in human and rodent brain tissues. This study demonstrated successfully penetration of the nanoparticles possessing similar properties as LAZ-NLC with particle size < 200 nm and a neutral surface charge penetrating across the brain extracellular space [133]. Another study by Brigger et.al., reported the transport of PEG coated nanospheres across the intact BBB and its higher affinity with enhanced accumulation in 9L gliosarcoma in rats compared to non-PEG coated nanospheres [134]. The aforementioned studies validated our hypothesis of passive transport of intact LAZ-NLC across the BBB mainly due to the presence of PEG coating on NLC surface along with optimal size and surface charge.

- **Active endocytic uptake:**

  The presence of DSPE-PEG 2k and polysorbate 80 in LAZ-NLC composition could possibly prolong the residence time of LAZ in brain. Studies have reported active endocytic uptake via specific receptors in the brain such as LDL (low density lipoprotein), especially for nanoparticles coated with PEG moiety and in presence of polysorbate 80. This receptor-mediated uptake in the brain could possibly be due to the specific adsorption of apolipoprotein B and E on the surface of nanoparticle, resulting in their internalization by LDL receptors [135, 136].

- **Inhibition of P-gp efflux transporters:**

LAZ is a potential substrate of P-gp efflux transporters present on BBB resulting in poor brain exposure of LAZ. The presence of surface modifiers (PEG derivatives) and surfactants (polysorbate 80) have demonstrated inhibitory effects on P-gp efflux transporter [137], thus enabling increased retention of passively diffused LAZ in the brain tissue.

A medley of passive diffusion, inhibition of P-gp efflux transporters and/or active endocytic uptake could be credited for transport of optimal LAZ-NLCs across the intact and healthy BBB leading to enhanced LAZ brain exposure. In glioblastoma, a loss in expression of tight junction proteins has been reported causing disruption of BBB and increase in transport permeability [53]. Thus along with aforementioned transport mechanisms, the LAZ-NLCs can extravasate from the systemic circulation to the glioma tissues through the disrupted BBB resulting in passive targeting of NLCs. This passive targeting is called as Enhanced Permeability and Retention (EPR) effect, a characteristic feature of tumor tissues marked with extensive angiogenesis, defective vasculature with fenestrations, inefficient lymphatic drainage and venous return resulting in increased retention in tumor tissues. The leaky tumor vasculature and lack of lymphatic clearance could play an important role in retention of the NLCs in the glioma tissues [138, 139].

Apart from its neuro-protective action, LAZ has shown efficacy in lung ischemia and reperfusion injury and hence the bio-distribution of LAZ in the lung was also evaluated [140]. The lung is a highly perfused organ receiving about half of total cardiac output during each systole and the pulmonary vasculature comprises of about one third of the

total vascular network in the body. A large proportion of intravenously administered drugs are available for absorption by the lung owing to the large surface area, rich blood supply, low thickness of epithelial membrane and absence of first pass metabolism [141, 142]. The LAZ formulated in citrate buffered solution has poor solubility at physiological pH resulting in precipitation of LAZ as micron-sized particles lodging in the arterioles and rapid phagocytized by the lung surface macrophages [143]. The nano-size of optimal LAZ-NLC (< 200 nm) can be delivered into the deep alveolar region and could be internalized by alveolar type I epithelial cells via clathrin and caveolin-mediated endocytic pathways, validating the longer retention of LAZ loaded in optimal NLC in the lungs. Moreover, alveolar type II epithelial cells release surfactants rich in phospholipids that help to reduce the surface tension at air-liquid interface and promote adsorption by alveolar type I epithelial cells via pinocytosis. The presence of DSPE-PEG 2k and surfactant Polysorbate 80 could potentially enhance the pinocytosis of LAZ-NLC by alveolar type I epithelial cells [144, 145].

Thus, the optimal LAZ-NLC specifically enhanced delivery of LAZ to the brain with decreased off-targeting potential to liver and could be used as a prospective platform for delivering therapeutic agents to the brain possessing a hepato-toxic potential. Additionally, the optimal LAZ-NLC sustained the LAZ levels in the lung tissue and could also be possibly used for delivering therapeutics intended for pulmonary delivery.

5.7. Dose Linearity of Optimal LAZ-NLC

In linear pharmacokinetics AUC, half-life, clearance and volume of distribution are dependent on dose, whereas these parameters become dose independent as the dose increases and pharmacokinetics become non-linear. Dose dependent changes in plasma pharmacokinetics and tissue distribution of drugs could be due to alteration in plasma protein binding, capacity limited metabolism or excretion and/or saturable carrier mediated transport [146].

The non-proportional increase in LAZ brain levels after increasing the dose of optimal LAZ-NLC could be attributed to the interplay between passive diffusion, saturable carrier-mediated transport and inhibition of efflux transport. As proposed in **Section 5.6**, the optimal LAZ-NLC could be transported across the BBB via three mechanisms; passive diffusion, active endocyctic uptake and/or inhibition of Pgp efflux transport. The active endocytic uptake by receptors such as LDL could cause the initial linear increase in amount of LAZ in brain tissue after increasing the dose of optimal LAZ-NLC from 15 to 30 mg/kg. A further increase in the dose of optimal LAZ-NLC to 60 mg/kg, could result in saturation of the LDL receptor sites leading to plateauing of the linear increase in amount of LAZ in brain tissue. However, a non-linear increase in amount of LAZ in brain tissue was observed at 60 mg/kg of optimal LAZ-NLC, indicating a supplementary mechanism causing transport of LAZ across the BBB. The nano-sized optimal LAZ-NLC as well as free LAZ released from the NLC can cross the BBB by passive diffusion. Being substrate of Pgp transporters, free unbound LAZ can be effluxed out from the

brain. However, the presence of DSPE-PEG 2k and Polysorbate 80 could inhibit the Pgp efflux transporters and thus contribute in the non-proportional increase in amount of LAZ in brain tissues with increasing dose. Similar mechanisms involving passive diffusion, along with active saturable influx and active efflux were observed for transport of morphine across the BBB [147] Moreover, higher doses of optimal LAZ-NLC could result in increased systemic exposure of LAZ resulting in saturation of plasma protein binding and limiting the capacity of metabolic enzymes.

Chapter 6: Summary

6.1. Development, Optimization and Validation of LAZ-NLC using CCD

The primary reason of selecting NLC over other conventional nano-carrier system was its high drug loading capacity and improved storage and physiological stability, in addition to its nano-size, controlled drug release, ease of surface modification and manufacture. Our study successfully demonstrated the logical selection of formulation compositions (GB, Labrasol, DSPE-PEG 2k, Tween 80) and the use of systematic DoE approach for a rational optimization of LAZ-NLC with physico-chemical properties suited for enhanced brain exposure. The development and optimization of LAZ-NLC was divided into three phases. Phase 1 involved selection of suitable liquid and solid lipid, which exhibited the maximum drug solubility and loading capacity. The liquid lipid Labrasol was chosen since it demonstrated the highest solubility for LAZ. The solid lipid GB was chosen taking into consideration its high degree of miscibility with LAZ and the ability of GB to sustain LAZ release over a period of time. Phase 2 involved the use of logical CCD methodology that helped generate maximum information about influence of formulation components such as DSPE-PEG 2k and liquid lipid Labrasol on formulation properties such as particle size, zeta potential and encapsulation efficiency using minimal experimental runs. The DSPE-PEG 2k had a negative effect on particle size and zeta potential while having a synergistic effect on the encapsulation efficiency of the LAZ-NLC. The liquid lipid Labrasol had an antagonistic effect on particle size, synergistic effect on zeta potential while having no effect on encapsulation efficiency.

The LAZ-NLC was manufactured using a simple ultra-sonication technique, mainly due to the ease of preparation, economical and readily available apparatus, less time intensive procedure and reproducibility in achieving consistent formulation properties over several batches. The criterion for selecting the optimal composition of LAZ-NLC was based on increasing the brain exposure of LAZ while reducing its liver accumulation. The composition of LAZ-NLC was chosen to yield the particle size < 200 nm with neutral surface charge and high encapsulation efficiency. The developed CCD model was used in predicting the optimal LAZ-NLC composition and properties with minimal error (<3 %).

6.2. Physico-chemical Characterization of Optimal LAZ-NLC

The average particle size and polydispersity index of optimal LAZ-NLC measured was 172.3 nm and 0.12 respectively, with neutral surface charge of -4.54 mV and encapsulation efficiency of 85.01 %. The TEM images confirmed the spherical shape of optimal LAZ-NLCs, and validated the observations of particle size analyzing techniques (DLS) with particle size of < 200 nm and uniform and homogeneous size distribution. The use of GRAS components in formulation of LAZ as NLC resulted in minimal (<15 %) hemolytic potential on intravenous administration and the increased drug payload enabled the administration of high LAZ doses as bolus injection eliminating the possibility of painful infusions. The solid lipid GB partially retained its crystallinity while there was complete loss of LAZ crystal structure with probable transformation into amorphous state. The retention of lipid crystallinity, resulted in the LAZ-NLCs to be

stable on storage over 3-months period at 4°C with minimal change in particle size and zeta potential and no change in the encapsulation efficiency.

6.3. Development and Validation of UPLC/MS-MS Assay for LAZ in Bio-matrices

An UPLC-MS/MS method was successfully developed and validated for the quantification of LAZ in rat plasma and brain, liver and lung tissue homogenates. In comparison to the previously reported HPLC analytical methods, the current assay was fast, involving simple sample preparation procedure and utilization of minimal sample volume (100 μL versus 500 μL) to obtain sensitive responses. A full validation in rat plasma and a partial validation in rat brain, liver and lung tissues were performed for quantification of LAZ. The assay method is selective, sensitive, accurate, precise and reproducible with a linear range of 1.95 – 250 ng/mL in rat plasma and tissue homogenates with the LLOQ of 1.95 ng/mL. The assay is capable of quantifying samples with concentrations higher than 250 ng/mL by dilution, maintaining the accuracy and precision. This assay for the first time reports the stability of LAZ in plasma at different storage and handling conditions, with LAZ being within the acceptable limits on exposures to these conditions. The developed UPLC-MS/MS method was employed to establish the pharmacokinetic and bio-distribution profile of LAZ formulations in rats after an intravenous administration.

6.4. Pharmacokinetics and Bio-distribution of LAZ Formulations

This study dispelled a common notion about the extrapolation of plasma pharmacokinetics data to organ bio-distribution patterns. Even though there was no

difference in plasma pharmacokinetic profiles of LAZ citrate, LAZ co-solvent and optimal LAZ-NLC groups, a stark disparity was observed in the brain and liver distribution profiles for the three groups. The optimal surface properties of LAZ-NLC namely particle size < 200 nm, neutral surface charge and presence of DSPE-PEG 2k and Polysorbate 80 increased the brain permeability and residence time of LAZ by two times while limiting the amount of LAZ distributed in the liver by half compared to citrate solution. A combination of transport mechanisms such as passive diffusion, inhibition of P-gp efflux transport and active endocytic uptake were proposed for passage of free unbound LAZ as well as intact LAZ loaded NLC across the BBB.

6.5. Dose Linearity of Optimal LAZ-NLC

A non-proportional increase in LAZ brain level was achieved as the dose of LAZ-NLC increased linearly from 15 to 60 mg/kg. Though an initial dose increase could cause the saturation of endocytic receptors at the BBB, an alternative auxiliary mechanism involving inhibition of P-gp efflux transport accounted for the non-linearity in LAZ in the brain tissues. The contribution of this finding is note-worthy since optimal LAZ-NLC would help achieve maximum therapeutic LAZ levels in brain (12 times higher) within a safe dose range (4 times higher dose) without the potential risk of toxicity.

The impact of our overall study is significant since it laid the foundation for the pre-clinical efficacy testing of LAZ-NLC for its dual role as radio-protectant and anti-proliferative agent in treatment of glioblastoma and its potential translation to clinical setting.

Finally, our research provides two key universal messages pertinent in study of delivery systems in a pre-clinical setting.

1) A systematic and rational CCD model utilizing minimal number of experiments in generating maximal information regarding the effects of composition on formulation properties while predicting the optimal formulation composition with accurate predictability.
2) The plasma pharmacokinetic profiles and parameters are not predictive of the organ bio-distribution and needs to be well characterized in a pre-clinical setting, to ensure accurate extrapolation to the clinical data.

References

[1] Q.T. Ostrom, H. Gittleman, J. Fulop, M. Liu, R. Blanda, C. Kromer, Y. Wolinsky, C. Kruchko, J.S. Barnholtz-Sloan, CBTRUS Statistical Report: Primary Brain and Central Nervous System Tumors Diagnosed in the United States in 2008-2012, Neuro-oncology, 17 (2015) iv1-iv62.

[2] H. Zong, The cellular origin for malignant glioma and prospects for clinical advancements, 12 (2012) 383-394.

[3] F.A. Siebzehnrubl, B.A. Reynolds, A. Vescovi, D.A. Steindler, L.P. Deleyrolle, The origins of glioma: E Pluribus Unum?, Glia, 59 (2011) 1135-1147.

[4] K. Aldape, G. Zadeh, S. Mansouri, G. Reifenberger, A. Deimling, Glioblastoma: pathology, molecular mechanisms and markers, Acta Neuropathologica, 129 (2015) 829-848.

[5] D.N. Louis, H. Ohgaki, O.D. Wiestler, W.K. Cavenee, P.C. Burger, A. Jouvet, B.W. Scheithauer, P. Kleihues, The 2007 WHO Classification of Tumours of the Central Nervous System, Acta Neuropathol, 114 (2007) 97-109.

[6] R. Stupp , W.P. Mason , M.J. van den Bent , M. Weller , B. Fisher , M.J.B. Taphoorn , K. Belanger , A.A. Brandes , C. Marosi , U. Bogdahn , J. Curschmann , R.C. Janzer , S.K. Ludwin , T. Gorlia , A. Allgeier , D. Lacombe , J.G. Cairncross , E. Eisenhauer , R.O. Mirimanoff Radiotherapy plus Concomitant and Adjuvant Temozolomide for Glioblastoma, New England Journal of Medicine, 352 (2005) 987-996.

[7] D.J. Brat, T.B. Mapstone, Malignant glioma physiology: cellular response to hypoxia and its role in tumor progression, Ann Intern Med, 138 (2003) 659-668.

[8] P.Y. Wen , S. Kesari Malignant Gliomas in Adults, New England Journal of Medicine, 359 (2008) 492-507.

[9] S. Agarwal, R. Sane, R. Oberoi, J.R. Ohlfest, W.F. Elmquist, Delivery of molecularly targeted therapy to malignant glioma, a disease of the whole brain, Expert reviews in molecular medicine, 13 (2011) e17.

[10] M. M., N. H., Principles & Practice of Neuro-Oncology: A Multidisciplinary Approach, Springer Publishing Company, 2010.

[11] M.M. Mrugala, Advances and challenges in the treatment of glioblastoma: a clinician's perspective, Discovery medicine, 15 (2013) 221-230.

[12] P.J. Tofilon, J.R. Fike, The radioresponse of the central nervous system: a dynamic process, Radiat Res, 153 (2000) 357-370.

[13] C. Sen, L. Packer, O. Hänninen, Handbook of Oxidants and Antioxidants in Exercise, Elsevier Science, 2000.

[14] A. Ayala, M.F. Munoz, S. Arguelles, Lipid peroxidation: production, metabolism, and signaling mechanisms of malondialdehyde and 4-hydroxy-2-nonenal, Oxid Med Cell Longev, 2014 (2014) 360438.

[15] D.E. Coricovac, C.A. Dehelean, Pathological Aspects with Global Impact Induced by Toxicants at Cellular Level, 2015.

[16] H.A.H.M.A. El-Aal, Lipid Peroxidation End-Products as a Key of Oxidative Stress: Effect of Antioxidant on Their Production and Transfer of Free Radicals, 2012.

[17] J.G. Kiang, Lipid Peroxidation After Ionizing Irradiation Leads to Apoptosis and Autophagy, InTech, 2012.

[18] A. Siu, J.J. Wind, J.B. Iorgulescu, T.A. Chan, Y. Yamada, J.H. Sherman, Radiation necrosis following treatment of high grade glioma--a review of the literature and current understanding, Acta Neurochir (Wien), 154 (2012) 191-201; discussion 201.

[19] D. Greene-Schloesser, M.E. Robbins, A.M. Peiffer, E.G. Shaw, K.T. Wheeler, M.D. Chan, Radiation-induced brain injury: A review, Frontiers in Oncology, 2 (2012) 73.

[20] C.I. Sze, W.P. Su, M.F. Chiang, C.Y. Lu, Y.A. Chen, N.S. Chang, Assessing current therapeutic approaches to decode potential resistance mechanisms in glioblastomas, Frontiers in Oncology, 3 (2013) 59.

[21] M.E. Hegi, A.C. Diserens, S. Godard, P.Y. Dietrich, L. Regli, S. Ostermann, P. Otten, G. Van Melle, N. de Tribolet, R. Stupp, Clinical trial substantiates the predictive value of O-6-methylguanine-DNA methyltransferase promoter methylation in glioblastoma patients treated with temozolomide, Clin Cancer Res, 10 (2004) 1871-1874.

[22] Y.P. Ramirez, J.L. Weatherbee, R.T. Wheelhouse, A.H. Ross, Glioblastoma Multiforme Therapy and Mechanisms of Resistance, Pharmaceuticals, 6 (2013) 1475-1506.

[23] E.D. Hall, Neuroprotective actions of glucocorticoid and nonglucocorticoid steroids in acute neuronal injury, Cell Mol Neurobiol, 13 (1993) 415-432.

[24] R. Schmid-Elsaesser, S. Zausinger, E. Hungerhuber, N. Plesnila, A. Baethmann, H.-J. Reulen, Superior Neuroprotective Efficacy of a Novel Antioxidant (U-101033E) With Improved Blood-Brain Barrier Permeability in Focal Cerebral Ischemia, Stroke, 28 (1997) 2018-2024.

[25] J.M. Braughler, J.F. Pregenzer, R.L. Chase, L.A. Duncan, E.J. Jacobsen, J.M. McCall, Novel 21-amino steroids as potent inhibitors of iron-dependent lipid peroxidation, J Biol Chem, 262 (1987) 10438-10440.

[26] Sarah L. Smith, Heidi M. Scherch, Edward D. Hall, Protective effects of tirilazad mesylate and metabolite U-89678 against blood-brain barrier damage after subarachnoid hemorrhage and lipid peroxidative neuronal injury, Journal of Neurosurgery, 84 (1996) 229-233.

[27] E.D. Hall, K.E. Pazara, J.M. Braughler, 21-Aminosteroid lipid peroxidation inhibitor U74006F protects against cerebral ischemia in gerbils, Stroke, 19 (1988) 997-1002.

[28] K. Kanamaru, B.K. Weir, J.M. Findlay, M. Grace, R.L. Macdonald, A dosage study of the effect of the 21-aminosteroid U74006F on chronic cerebral vasospasm in a primate model, Neurosurgery, 27 (1990) 29-38.

[29] Douglas K. Anderson, J. Mark Braughler, Edward D. Hall, Thomas R. Waters, John M. McCall, Eugene D. Means, Effects of treatment with U-74006F on neurological outcome following experimental spinal cord injury, Journal of Neurosurgery, 69 (1988) 562-567.

[30] E.D. Hall, J.M. Braughler, P.A. Yonkers, S.L. Smith, K.L. Linseman, E. Means, H. Scherch, P. Von Voigtlander, R. Lahti, E.J. Jacobsen, U-78517F: a potent inhibitor of lipid peroxidation with activity in experimental brain injury and ischemia, Journal of Pharmacology and Experimental Therapeutics, 258 (1991) 688-694.

[31] D.E. Steinke, B.K. Weir, J.M. Findlay, T. Tanabe, M. Grace, B.W. Krushelnycky, A trial of the 21-aminosteroid U74006F in a primate model of chronic cerebral vasospasm, Neurosurgery, 24 (1989) 179-186.

[32] W.M. Clark, J.S. Hazel, B.M. Coull, Lazaroids. CNS pharmacology and current research, Drugs, 50 (1995) 971-983.

[33] K.M. Woodbury-Harris, B.M. Coull, Clinical Trials in the Neurosciences, Karger, 2009.

[34] J.M. Buatti, W.A. Friedman, D.P. Theele, F.J. Bova, W.M. Mendenhall, The lazaroid U74389G protects normal brain from stereotactic radiosurgery-induced radiation injury, Int J Radiat Oncol Biol Phys, 34 (1996) 591-597.

[35] D. Kondziolka, S. Somaza, A.J. Martinez, J. Jacobsohn, A. Maitz, L.D. Lunsford, J.C. Flickinger, Radioprotective effects of the 21-aminosteroid U-74389G for stereotactic radiosurgery, Neurosurgery, 41 (1997) 203-208.

[36] D. Kondziolka, Y. Mori, A.J. Martinez, M.R. McLaughlin, J.C. Flickinger, L.D. Lunsford, Beneficial effects of the radioprotectant 21-aminosteroid U-74389G in a radiosurgery rat malignant glioma model, Int J Radiat Oncol Biol Phys, 44 (1999) 179-184.

[37] R. Durmaz, S. Deliorman, S. Isiksoy, R. Uyar, K. Erol, E. Tel, Antiproliferative properties of the lazaroids U-83836E and U-74389G on glioma cells in vitro, Pathology oncology research : POR, 5 (1999) 223-228.

[38] P. Arora, Y.S. Lee, T.C. Origitano, R.D. Wurster, Lazaroids inhibit proliferation of cultured human astrocytoma cells, J Neurooncol, 29 (1996) 143-148.

[39] V. Bonatsos, I. Kappas, K. Birbas, D. Vlachodimitropoulos, K. Toutouzas, E. Karampela, N. Syrmos, G. Bonatsos, A.E. Papalois, Effects of U-74389G (21-Lazaroid) and Ascorbic Acid on Liver Recovery After Acute Ischemia and Reperfusion in Rats, In Vivo, 29 (2015) 585-594.

[40] I. Flessas, I. Bramis, E. Menenakos, K. Toutouzas, G. Agrogiannis, E. Patsouris, A. Nonni, D. Chrysikos, M. Korontzi, A. Gioxari, G. Zografos, A. Papalois, Effects of lazaroid U-74389G on intestinal ischemia and reperfusion injury in porcine experimental model, Int J Surg, 13 (2015) 42-48.

[41] D.T. Chrysikos, T.N. Sergentanis, F. Zagouri, T. Psaltopoulou, G. Theodoropoulos, I. Flessas, G. Agrogiannis, N. Alexakis, M. Lymperi, A.I. Katsarou, E.S. Patsouris, C.G. Zografos, A.E. Papalois, Lazaroid U-74389G Administration in Pancreatic Ischemia-Reperfusion Injury: A Swine Model Encompassing Ischemic Preconditioning, JOP, 16 (2015) 176-184.

[42] A. Bimpis, A. Papalois, K. Voumvourakis, O. Olah, L. Tiszlavicz, C. Liapi, Neuronal tumour necrosis factor-alpha and interleukin-1beta expression in a porcine

model of intracerebral haemorrhage: Modulation by U-74389G, Brain Res, 1615 (2015) 98-105.

[43] E. Alhan, S. Turkyilmaz, C. Ercin, B.V. Kural, Effects of lazaroid U-74389G on acute necrotizing pancreatitis in rats, European surgical research. Europaische chirurgische Forschung. Recherches chirurgicales europeennes, 38 (2006) 70-75.

[44] R. Kavanagh, P. Kam, Lazaroids: efficacy and mechanism of action of the 21-aminosteroids in neuroprotection, British Journal of Anaesthesia, 86 (2001) 110-119.

[45] E.D. Hall, J.M. McCall, E.D. Means, Therapeutic potential of the lazaroids (21-aminosteroids) in acute central nervous system trauma, ischemia and subarachnoid hemorrhage, Adv Pharmacol, 28 (1994) 221-268.

[46] E.C. Haley, O.b.o.t.R.I. Investigators, High-Dose Tirilazad for Acute Stroke (RANTTAS II), Stroke, 29 (1998) 1256a-1257.

[47] T.R. Investigators, A Randomized Trial of Tirilazad Mesylate in Patients With Acute Stroke (RANTTAS), Stroke, 27 (1996) 1453-1458.

[48] S.C. Laizure, L.K. Franklin, D.G. Kaiser, C.L. Williams, R.C. Stevens, P.L. Sanders, M. Miller, Disposition of tirilazad (U74006F), a 21-aminosteroid, in the plasma, heart, brain, and liver of the rat, Drug Metab. Dispos., 21 (1993) 951-954.

[49] L.C. Wienkers, R.C. Steenwyk, S.A. Mizsak, P.G. Pearson, In vitro metabolism of tirilazad mesylate in male and female rats. Contribution of cytochrome P4502C11 and delta 4-5 alpha-reductase, Drug metabolism and disposition: the biological fate of chemicals, 23 (1995) 383-392.

[50] U. Microfilms, U.M. International, Dissertation Abstracts International: The sciences and engineering, University Microfilms, 2008.

[51] Y. Persidsky, S.H. Ramirez, J. Haorah, G.D. Kanmogne, Blood–brain Barrier: Structural Components and Function Under Physiologic and Pathologic Conditions, Journal of Neuroimmune Pharmacology, 1 (2006) 223-236.

[52] Y. Chen, L. Liu, Modern methods for delivery of drugs across the blood–brain barrier, Advanced Drug Delivery Reviews, 64 (2012) 640-665.

[53] N. Weiss, F. Miller, S. Cazaubon, P.-O. Couraud, The blood-brain barrier in brain homeostasis and neurological diseases, Biochimica et Biophysica Acta (BBA) - Biomembranes, 1788 (2009) 842-857.

[54] W.M. Pardridge, CNS drug design based on principles of blood-brain barrier transport, J Neurochem, 70 (1998) 1781-1792.

[55] I.P. Kaur, R. Bhandari, S. Bhandari, V. Kakkar, Potential of solid lipid nanoparticles in brain targeting, J Control Release, 127 (2008) 97-109.

[56] H. Pajouhesh, G.R. Lenz, Medicinal Chemical Properties of Successful Central Nervous System Drugs, NeuroRx, 2 (2005) 541-553.

[57] J.M. Koziara, P.R. Lockman, D.D. Allen, R.J. Mumper, The blood-brain barrier and brain drug delivery, J Nanosci Nanotechnol, 6 (2006) 2712-2735.

[58] N.J. Abbott, L. Ronnback, E. Hansson, Astrocyte-endothelial interactions at the blood-brain barrier, Nat Rev Neurosci, 7 (2006) 41-53.

[59] Y.E. Koo, G.R. Reddy, M. Bhojani, R. Schneider, M.A. Philbert, A. Rehemtulla, B.D. Ross, R. Kopelman, Brain cancer diagnosis and therapy with nanoplatforms, Adv Drug Deliv Rev, 58 (2006) 1556-1577.

[60] R. Gabathuler, Approaches to transport therapeutic drugs across the blood-brain barrier to treat brain diseases, Neurobiol Dis, 37 (2010) 48-57.

[61] A. Misra, S. Ganesh, A. Shahiwala, S.P. Shah, Drug delivery to the central nervous system: a review, J Pharm Pharm Sci, 6 (2003) 252-273.

[62] P.R. Lockman, R.J. Mumper, M.A. Khan, D.D. Allen, Nanoparticle technology for drug delivery across the blood-brain barrier, Drug Dev Ind Pharm, 28 (2002) 1-13.

[63] A. Beduneau, P. Saulnier, J.P. Benoit, Active targeting of brain tumors using nanocarriers, Biomaterials, 28 (2007) 4947-4967.

[64] H.L. Wong, X.Y. Wu, R. Bendayan, Nanotechnological advances for the delivery of CNS therapeutics, Adv Drug Deliv Rev, 64 (2012) 686-700.

[65] M.D. Joshi, R.H. Muller, Lipid nanoparticles for parenteral delivery of actives, European journal of pharmaceutics and biopharmaceutics : official journal of Arbeitsgemeinschaft fur Pharmazeutische Verfahrenstechnik e.V, 71 (2009) 161-172.

[66] J. Pardeike, A. Hommoss, R.H. Müller, Lipid nanoparticles (SLN, NLC) in cosmetic and pharmaceutical dermal products, International Journal of Pharmaceutics, 366 (2009) 170-184.

[67] R.H. Müller, K. Mäder, S. Gohla, Solid lipid nanoparticles (SLN) for controlled drug delivery – a review of the state of the art, European Journal of Pharmaceutics and Biopharmaceutics, 50 (2000) 161-177.

[68] M. Üner, G. Yener, Importance of solid lipid nanoparticles (SLN) in various administration routes and future perspectives, International journal of nanomedicine, 2 (2007) 289-300.

[69] S.A. Wissing, O. Kayser, R.H. Muller, Solid lipid nanoparticles for parenteral drug delivery, Adv Drug Deliv Rev, 56 (2004) 1257-1272.

[70] A. Fundaro, R. Cavalli, A. Bargoni, D. Vighetto, G.P. Zara, M.R. Gasco, Non-stealth and stealth solid lipid nanoparticles (SLN) carrying doxorubicin: pharmacokinetics and tissue distribution after i.v. administration to rats, Pharmacol Res, 42 (2000) 337-343.

[71] S.C. Yang, L.F. Lu, Y. Cai, J.B. Zhu, B.W. Liang, C.Z. Yang, Body distribution in mice of intravenously injected camptothecin solid lipid nanoparticles and targeting effect on brain, J Control Release, 59 (1999) 299-307.

[72] G.P. Zara, R. Cavalli, A. Bargoni, A. Fundaro, D. Vighetto, M.R. Gasco, Intravenous administration to rabbits of non-stealth and stealth doxorubicin-loaded solid lipid nanoparticles at increasing concentrations of stealth agent: pharmacokinetics and distribution of doxorubicin in brain and other tissues, J Drug Target, 10 (2002) 327-335.

[73] J. Madan, R.S. Pandey, V. Jain, O.P. Katare, R. Chandra, A. Katyal, Poly (ethylene)-glycol conjugated solid lipid nanoparticles of noscapine improve biological half-life, brain delivery and efficacy in glioblastoma cells, Nanomedicine, 9 (2013) 492-503.

[74] S. Dhawan, R. Kapil, B. Singh, Formulation development and systematic optimization of solid lipid nanoparticles of quercetin for improved brain delivery, The Journal of pharmacy and pharmacology, 63 (2011) 342-351.

[75] K. Manjunath, V. Venkateswarlu, Pharmacokinetics, tissue distribution and bioavailability of clozapine solid lipid nanoparticles after intravenous and intraduodenal administration, J Control Release, 107 (2005) 215-228.

[76] W. Mehnert, K. Mader, Solid lipid nanoparticles: production, characterization and applications, Adv Drug Deliv Rev, 47 (2001) 165-196.

[77] M. Uner, Preparation, characterization and physico-chemical properties of solid lipid nanoparticles (SLN) and nanostructured lipid carriers (NLC): their benefits as colloidal drug carrier systems, Die Pharmazie, 61 (2006) 375-386.

[78] H. Bunjes, K. Westesen, M.H.J. Koch, Crystallization tendency and polymorphic transitions in triglyceride nanoparticles, International Journal of Pharmaceutics, 129 (1996) 159-173.

[79] J. Weiss, E.A. Decker, D.J. McClements, K. Kristbergsson, T. Helgason, T. Awad, Solid Lipid Nanoparticles as Delivery Systems for Bioactive Food Components, Food Biophysics, 3 (2008) 146-154.

[80] F. Tamjidi, M. Shahedi, J. Varshosaz, A. Nasirpour, Nanostructured lipid carriers (NLC): A potential delivery system for bioactive food molecules, Innovative Food Science & Emerging Technologies, 19 (2013) 29-43.

[81] R.H. Müller, M. Radtke, S.A. Wissing, Solid lipid nanoparticles (SLN) and nanostructured lipid carriers (NLC) in cosmetic and dermatological preparations, Advanced Drug Delivery Reviews, 54, Supplement (2002) S131-S155.

[82] R.H. Müller, M. Radtke, S.A. Wissing, Nanostructured lipid matrices for improved microencapsulation of drugs, International Journal of Pharmaceutics, 242 (2002) 121-128.

[83] X. Liu, Z. Zhang, Y. Jiang, Y. Hu, Z. Wang, J. Liu, R. Feng, J. Zhang, G. Huang, Novel PEG-grafted nanostructured lipid carrier for systematic delivery of a poorly soluble anti-leukemia agent Tamibarotene: characterization and evaluation, Drug delivery, 22 (2015) 223-229.

[84] S.H. Hsu, C.J. Wen, S.A. Al-Suwayeh, H.W. Chang, T.C. Yen, J.Y. Fang, Physicochemical characterization and in vivo bioluminescence imaging of nanostructured lipid carriers for targeting the brain: apomorphine as a model drug, Nanotechnology, 21 (2010) 405101.

[85] F. Li, Y. Weng, L. Wang, H. He, J. Yang, X. Tang, The efficacy and safety of bufadienolides-loaded nanostructured lipid carriers, International Journal of Pharmaceutics, 393 (2010) 204-212.

[86] W.M. Lim, P.S. Rajinikanth, C. Mallikarjun, Y.B. Kang, Formulation and delivery of itraconazole to the brain using a nanolipid carrier system, International Journal of Nanomedicine, 9 (2014) 2117-2126.

[87] M.-J. Tsai, P.-C. Wu, Y.-B. Huang, J.-S. Chang, C.-L. Lin, Y.-H. Tsai, J.-Y. Fang, Baicalein loaded in tocol nanostructured lipid carriers (tocol NLCs) for enhanced stability and brain targeting, International Journal of Pharmaceutics, 423 (2012) 461-470.

[88] S. Das, A. Chaudhury, Recent advances in lipid nanoparticle formulations with solid matrix for oral drug delivery, AAPS PharmSciTech, 12 (2011) 62-76.

[89] A. Beloqui, M.A. Solinis, A. Rodriguez-Gascon, A.J. Almeida, V. Preat, Nanostructured lipid carriers: Promising drug delivery systems for future clinics, Nanomedicine, 12 (2016) 143-161.

[90] P. Severino, T. Andreani, A.S. Macedo, J.F. Fangueiro, M.H. Santana, A.M. Silva, E.B. Souto, Current State-of-Art and New Trends on Lipid Nanoparticles (SLN and NLC) for Oral Drug Delivery, J Drug Deliv, 2012 (2012) 750891.

[91] ICH, Q8(R2) Pharmaceutical Development 2009,http://www.fda.gov/downloads/Drugs/.../Guidances/ucm073507.pdf.

[92] M.G. Shivhare M, Practical Considerations for DoE Implementation in Quality By Design, BioProcess International, 8 (2010) 22-30.

[93] R.H. Myers, D.C. Montgomery, C.M. Anderson-Cook, Response Surface Methodology: Process and Product Optimization Using Designed Experiments, Wiley, 2016.

[94] Y. Wang, G.-M. Mesfin, C.A. Rodríguez, J.G. Slatter, M.R. Schuette, A.L. Cory, M.J. Higgins, Venous Irritation, Pharmacokinetics, and Tissue Distribution of Tirilazad in Rats Following Intravenous Administration of a Novel Supersaturated Submicron Lipid Emulsion, Pharmaceutical Research, 16 (1999) 930-938.

[95] M. Ciuffi, G. Gentilini, S. Franchi-Micheli, L. Zilletti, Effect of 21-aminosteroid U74500A (pregna-1,4,9(11)-triene-3,20-dione, 21-(4-(5,6-bis(diethylamino)-2-pyridinyl)-1-piperazinyl)-16-methyl-, HCl (16 alpha)) on rat brain cortex lipid peroxidation induced "in vivo" by iron-carbohydrate, Biochemical pharmacology, 47 (1994) 2181-2186.

[96] A. Hejri, A. Khosravi, K. Gharanjig, M. Hejazi, Optimisation of the formulation of β-carotene loaded nanostructured lipid carriers prepared by solvent diffusion method, Food Chemistry, 141 (2013) 117-123.

[97] W. Zhang, X. Li, T. Ye, F. Chen, X. Sun, J. Kong, X. Yang, W. Pan, S. Li, Design, characterization, and in vitro cellular inhibition and uptake of optimized genistein-loaded NLC for the prevention of posterior capsular opacification using response surface methodology, International Journal of Pharmaceutics, 454 (2013) 354-366.

[98] B. Gupta, B.K. Poudel, T.H. Tran, R. Pradhan, H.-J. Cho, J.-H. Jeong, B.S. Shin, H.-G. Choi, C.S. Yong, J.O. Kim, Modulation of Pharmacokinetic and Cytotoxicity Profile of Imatinib Base by Employing Optimized Nanostructured Lipid Carriers, Pharmaceutical Research, 32 (2015) 2912-2927.

[99] Z. Liu, C.I. Okeke, L. Zhang, H. Zhao, J. Li, M.O. Aggrey, N. Li, X. Guo, X. Pang, L. Fan, L. Guo, Mixed polyethylene glycol-modified breviscapine-loaded solid lipid nanoparticles for improved brain bioavailability: preparation, characterization, and in vivo cerebral microdialysis evaluation in adult Sprague Dawley rats, AAPS PharmSciTech, 15 (2014) 483-496.

[100] V. Venkateswarlu, K. Manjunath, Preparation, characterization and in vitro release kinetics of clozapine solid lipid nanoparticles, J Control Release, 95 (2004) 627-638.

[101] A.O. Nornoo, D.W. Osborne, D.S. Chow, Cremophor-free intravenous microemulsions for paclitaxel I: formulation, cytotoxicity and hemolysis, Int J Pharm, 349 (2008) 108-116.

[102] Guidance for Industry Bioanalytical Method Validation, U.S. Department of Health and Human Services Food and Drug Administration Center for Drug Evaluation and Research (CDER), Center for Veterinary Medicine (CVM) 2013,http://www.fda.gov/downloads/drugs/guidancecomplianceregulatoryinformation/guidances/ucm368107.pdf.

[103] C.T. Viswanathan, S. Bansal, B. Booth, A.J. DeStefano, M.J. Rose, J. Sailstad, V.P. Shah, J.P. Skelly, P.G. Swann, R. Weiner, Quantitative bioanalytical methods validation and implementation: best practices for chromatographic and ligand binding assays, Pharm Res, 24 (2007) 1962-1973.

[104] J. Gabrielsson, D. Weiner, Non-compartmental analysis, Methods Mol Biol, 929 (2012) 377-389.

[105] J. Hummel, S. McKendrick, C. Brindley, R. French, Exploratory assessment of dose proportionality: review of current approaches and proposal for a practical criterion, Pharm Stat, 8 (2009) 38-49.

[106] B.P. Smith, F.R. Vandenhende, K.A. DeSante, N.A. Farid, P.A. Welch, J.T. Callaghan, S.T. Forgue, Confidence interval criteria for assessment of dose proportionality, Pharm Res, 17 (2000) 1278-1283.

[107] J. Hao, F. Wang, X. Wang, D. Zhang, Y. Bi, Y. Gao, X. Zhao, Q. Zhang, Development and optimization of baicalin-loaded solid lipid nanoparticles prepared by coacervation method using central composite design, European Journal of Pharmaceutical Sciences, 47 (2012) 497-505.

[108] K. Amin, R.M. Dannenfelser, In vitro hemolysis: guidance for the pharmaceutical scientist, J Pharm Sci, 95 (2006) 1173-1176.

[109] D.T. Rossi, M. Sinz, Mass Spectrometry in Drug Discovery, CRC Press, 2001.

[110] E. Naegele, Making your LC Method Compatible with Mass Spectrometry, © Agilent Technologies, Inc, 2011,https://www.agilent.com/cs/library/technicaloverviews/public/5990--7413EN.pdf.

[111] S.E. Rosenbaum, Basic Pharmacokinetics and Pharmacodynamics: An Integrated Textbook and Computer Simulations, Wiley, 2012.

[112] P.L. Bonate, D.R. Howard, Pharmacokinetics in Drug Development: Clinical Study Design and Analysis, American Assoc. of Pharm. Scientists, 2005.

[113] R.G. Strickley, Solubilizing excipients in oral and injectable formulations, Pharm Res, 21 (2004) 201-230.

[114] V. Jenning, A.F. Thunemann, S.H. Gohla, Characterisation of a novel solid lipid nanoparticle carrier system based on binary mixtures of liquid and solid lipids, Int J Pharm, 199 (2000) 167-177.

[115] X. Lin, X. Li, L. Zheng, L. Yu, Q. Zhang, W. Liu, Preparation and characterization of monocaprate nanostructured lipid carriers, Colloids and Surfaces A: Physicochemical and Engineering Aspects, 311 (2007) 106-111.

[116] R.A. Sanad, N.S. Abdelmalak, T.S. Elbayoomy, A.A. Badawi, Formulation of a novel oxybenzone-loaded nanostructured lipid carriers (NLCs), AAPS PharmSciTech, 11 (2010) 1684-1694.

[117] O. Garbuzenko, Y. Barenholz, A. Priev, Effect of grafted PEG on liposome size and on compressibility and packing of lipid bilayer, Chemistry and Physics of Lipids, 135 (2005) 117-129.

[118] R.H. Müller, C. Jacobs, O. Kayser, Nanosuspensions as particulate drug formulations in therapy: Rationale for development and what we can expect for the future, Advanced Drug Delivery Reviews, 47 (2001) 3-19.

[119] K. Moribe, K. Maruyama, M. Iwatsuru, Encapsulation characteristics of nystatin in liposomes: effects of cholesterol and polyethylene glycol derivatives, International Journal of Pharmaceutics, 188 (1999) 193-202.

[120] S. Wohlfart, S. Gelperina, J. Kreuter, Transport of drugs across the blood-brain barrier by nanoparticles, J Control Release, 161 (2012) 264-273.

[121] D.E. Owens, 3rd, N.A. Peppas, Opsonization, biodistribution, and pharmacokinetics of polymeric nanoparticles, Int J Pharm, 307 (2006) 93-102.

[122] K. Xiao, Y. Li, J. Luo, J.S. Lee, W. Xiao, A.M. Gonik, R. Agarwal, K.S. Lam, The effect of surface charge on in vivo biodistribution of PEG-oligocholic acid based micellar nanoparticles, Biomaterials, 32 (2011) 3435-3446.

[123] R. Kedmi, N. Ben-Arie, D. Peer, The systemic toxicity of positively charged lipid nanoparticles and the role of Toll-like receptor 4 in immune activation, Biomaterials, 31 (2010) 6867-6875.

[124] P.R. Lockman, J.M. Koziara, R.J. Mumper, D.D. Allen, Nanoparticle surface charges alter blood-brain barrier integrity and permeability, J Drug Target, 12 (2004) 635-641.

[125] M.D. Howard, X. Lu, J.J. Rinehart, M. Jay, T.D. Dziubla, Physicochemical characterization of nanotemplate engineered solid lipid nanoparticles, Langmuir, 27 (2011) 1964-1971.

[126] J.W. Cox, G.P. Sage, M.A. Wynalda, R.G. Ulrich, P.G. Larson, C.C. Su, Plasma compatibility of injectables: comparison of intravenous U-74006F, a 21-aminosteroid antioxidant, with Dilantin brand of parenteral phenytoin, J Pharm Sci, 80 (1991) 371-375.

[127] C. Olbrich, O. Kayser, R.H. Müller, Lipase degradation of Dynasan 114 and 116 solid lipid nanoparticles (SLN)—effect of surfactants, storage time and crystallinity, International Journal of Pharmaceutics, 237 (2002) 119-128.

[128] A. zur Mühlen, C. Schwarz, W. Mehnert, Solid lipid nanoparticles (SLN) for controlled drug delivery – Drug release and release mechanism, European Journal of Pharmaceutics and Biopharmaceutics, 45 (1998) 149-155.

[129] J.W. Cox, R.H. Pullen, High-performance liquid chromatographic determination of a 21-aminosteroid antioxidant in plasma, J Chromatogr, 424 (1988) 293-302.

[130] J.C. Fleishaker, P.G. Pearson, L.C. Wienkers, L.K. Pearson, T.A. Moore, G.R. Peters, Biotransformation of tirilazad in human: 4. effect of finasteride on tirilazad clearance and reduced metabolite formation, J Pharmacol Exp Ther, 287 (1998) 591-597.

[131] J.C. Fleishaker, R.N. Straw, C.J. Cross, Pharmacokinetics of tirilazad and U-89678, an active, reduced metabolite, following acute head trauma in adults, J Pharm Sci, 86 (1997) 434-437.

[132] P.A. Bombardt, J.E. Brewer, M.G. Johnson, Protein binding of tirilazad (U-74006) in human, Sprague-Dawley rat, beagle dog and cynomolgus monkey serum, J Pharmacol Exp Ther, 269 (1994) 145-150.

[133] E.A. Nance, G.F. Woodworth, K.A. Sailor, T.Y. Shih, Q. Xu, G. Swaminathan, D. Xiang, C. Eberhart, J. Hanes, A Dense Poly(ethylene glycol) Coating Improves Penetration of Large Polymeric Nanoparticles within Brain Tissue, Science translational medicine, 4 (2012) 149ra119.

[134] I. Brigger, J. Morizet, G. Aubert, H. Chacun, M.-J. Terrier-Lacombe, P. Couvreur, G. Vassal, Poly(ethylene glycol)-Coated Hexadecylcyanoacrylate Nanospheres Display a Combined Effect for Brain Tumor Targeting, Journal of Pharmacology and Experimental Therapeutics, 303 (2002) 928-936.

[135] J. Kreuter, D. Shamenkov, V. Petrov, P. Ramge, K. Cychutek, C. Koch-Brandt, R. Alyautdin, Apolipoprotein-mediated transport of nanoparticle-bound drugs across the blood-brain barrier, J Drug Target, 10 (2002) 317-325.

[136] H.R. Kim, K. Andrieux, S. Gil, M. Taverna, H. Chacun, D. Desmaële, F. Taran, D. Georgin, P. Couvreur, Translocation of Poly(ethylene glycol-co-hexadecyl)cyanoacrylate Nanoparticles into Rat Brain Endothelial Cells: Role of Apolipoproteins in Receptor-Mediated Endocytosis, Biomacromolecules, 8 (2007) 793-799.

[137] S.W. Wang, J. Monagle, C. McNulty, D. Putnam, H. Chen, Determination of P-glycoprotein inhibition by excipients and their combinations using an integrated high-throughput process, J Pharm Sci, 93 (2004) 2755-2767.

[138] F. Danhier, O. Feron, V. Préat, To exploit the tumor microenvironment: Passive and active tumor targeting of nanocarriers for anti-cancer drug delivery, Journal of Controlled Release, 148 (2010) 135-146.

[139] Y. Matsumura, H. Maeda, A New Concept for Macromolecular Therapeutics in Cancer Chemotherapy: Mechanism of Tumoritropic Accumulation of Proteins and the Antitumor Agent Smancs, Cancer Research, 46 (1986) 6387-6392.

[140] K. Kuwaki, K. Komatsu, H. Sohma, T. Abe, The effect of various doses of lazaroid U74389G on lung ischemia reperfusion injury, The Thoracic and cardiovascular surgeon, 47 (1999) 67-72.

[141] V.P. Torchilin, Nanoparticulates as Drug Carriers, Imperial College Press, 2006.

[142] Y. Wei, L. Zhao, Passive lung-targeted drug delivery systems via intravenous administration, Pharmaceutical Development And Technology, 19 (2014) 129-136.

[143] J. Todoroff, R. Vanbever, Fate of nanomedicines in the lungs, Current Opinion in Colloid & Interface Science, 16 (2011) 246-254.

[144] A.J. Thorley, P. Ruenraroengsak, T.E. Potter, T.D. Tetley, Critical Determinants of Uptake and Translocation of Nanoparticles by the Human Pulmonary Alveolar Epithelium, ACS Nano, 8 (2014) 11778-11789.

[145] X. Zhang, Y. Gan, L. Gan, S. Nie, W. Pan, PEGylated nanostructured lipid carriers loaded with 10-hydroxycamptothecin: an efficient carrier with enhanced anti-tumour effects against lung cancer, The Journal of pharmacy and pharmacology, 60 (2008) 1077-1087.

[146] H. Marquardt, S.G. Schäfer, R.O. McClellan, F. Welsch, Toxicology, Elsevier Science, 1999.

[147] D. Groenendaal, J. Freijer, D. de Mik, M.R. Bouw, M. Danhof, E.C.M. de Lange, Population pharmacokinetic modelling of non-linear brain distribution of morphine: influence of active saturable influx and P-glycoprotein mediated efflux, British Journal of Pharmacology, 151 (2007) 701-712.

Appendix

Appendix 1.1: Procedure for *in vitro* release of LAZ from SLN

LAZ-SLNs corresponding to 1 mg LAZ were placed in dialysis bags (Spectra/Por Dialysis membrane MWCO: 6000-8000) containing 1 mL of pooled human plasma. The dialysis bags were submerged in 50 mL plastic tubes containing 20 ml of medium (PBS with 0.2% Tween 80). The tubes were placed in a temperature controlled water bath at 37°C and were shaken at 50 rpm. At 12, 24, 36, 48 and 72 hours a 1 mL of the medium was drawn and immediately replenished with fresh medium. After every 24 hours, the entire medium was replaced with a fresh medium. The samples taken at each time point were analyzed by HPLC to determine the amount of LAZ released.

Appendix 1.2: *In vitro* release profile of LAZ-SLN in plasma at 37°C

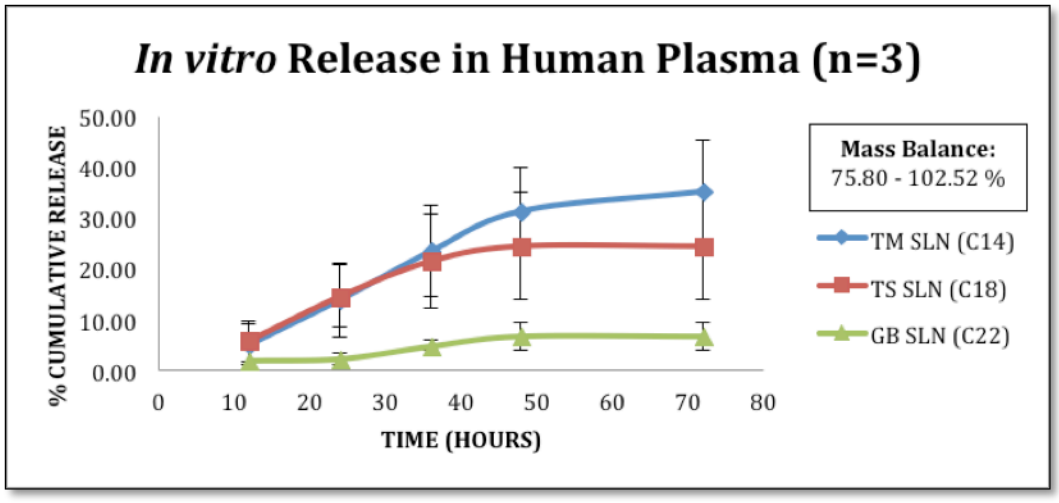

Appendix 1.3: Percent cumulative LAZ release from SLN at 37°C

Time (Hours)	% Cumulative Release (N=3: Mean ± SD)		
	TM-SLN	**TS-SLN**	**GB-SLN**
12	5.07 ± 3.92	5.73 ± 3.94	1.97 (N=1)
24	13.85 ± 7.17	14.52 ± 6.07	2.25 ± 1.14
36	23.39 ± 8.96	21.44 ± 9.24	4.73 ± 0.98
48	31.32 ± 8.56	24.41 ± 10.47	6.71 ± 2.58
72	35.17 ± 10.11	24.41 ± 10.47	6.71 ± 2.58

Appendix 1.4: Physico-chemical properties of LAZ-SLNs

Parameters	**TM-SLN**	**TS-SLN**	**GB-SLN**
Particle Size (nm)	106.3 ± 1.3	135.4 ± 4.3	200.1 ± 5.3
Polydispersity Index (PDI)	0.280 ± 0.01	0.282 ± 0.02	0.298 ± 0.01
Zeta Potential (nm)	36.97 ± 0.85	37.75 ± 0.92	26.82 ± 1.74
Encapsulation Efficiency (%)	80.87 ± 4.27	68.93 ± 2.65	85.44 ± 7.02

Appendix 2: Percent healthy RBC's for formulation (LAZ-NLC) to blood ratios

Formulation: Blood ratio (F:B)	**% Healthy RBC's N=3, (Mean ± SD)**
0.0375	87.05 ± 7.07
0.3	89.61 ± 8.02
0.5	87.99 ± 5.78
1	83.12 ± 1.82
2	54.27 ± 4.01
3	38.30 ± 4.42

Appendix 3.1: Plasma concentrations of LAZ formulations in rats

Time (Hours)	**Plasma Concentration (ng/mL)**		
	Citrate (5 mg/kg)	**Co-solvent (15 mg/kg)**	**NLC (15 mg/kg)**
0.33	1094.00 ± 185.17	4070.67 ± 1075.82	4402.00 ± 573.94
0.66	699.00 ± 79.08	2653.33 ± 610.68	2610.00 ± 186.55
1	544.33 ± 59.14	2100.00 ± 343.95	1975.00 ± 271.97
2	262.33 ± 31.66	696.33 ± 108.03	709.00 ± 45.57
3	132.13 ± 30.04	379.33 ± 68.81	367.50 ± 54.02
4	92.43 ± 12.85	279.33 ± 36.02	252.50 ± 34.76
6	63.47 ± 15.16	183.00 ± 44.93	138.75 ± 26.68
8	35.10 ± 5.31	103.03 ± 35.99	90.93 ± 6.79

Appendix 3.2: Dose normalized plasma concentrations of LAZ formulations in rats

Time (Hours)	Dose normalized plasma concentration (ng/mL)/(mg/kg)		
	Citrate (5 mg/kg)	**Co-solvent (15 mg/kg)**	**NLC (15 mg/kg)**
0.33	218.80 ± 37.03	271.38 ± 71.72	293.47 ± 38.26
0.66	139.80 ± 15.82	176.89 ± 40.71	174.00 ± 12.44
1	108.87 ± 11.83	140.00 ± 22.93	131.67 ± 18.13
2	52.47 ± 6.33	46.42 ± 7.20	47.27 ± 3.04
3	26.43 ± 6.01	25.29 ± 4.59	24.50 ± 3.60
4	18.49 ± 2.57	18.62 ± 2.40	16.83 ± 2.32
6	12.69 ± 3.03	12.20 ± 3.00	9.25 ± 1.78
8	7.02 ± 1.06	6.87 ± 2.40	6.06 ± 0.45

Appendix 4: Brain concentrations of LAZ formulations in rats

Time (Hours)	Dose non-normalized brain concentration (ng/gm)		
	Citrate (5 mg/kg)	**Co-solvent (15 mg/kg)**	**NLC (15 mg/kg)**
4	6.84 ± 1.87	37.47 ± 7.06	43.07 ± 20.59
6	1.31 ± 0.14 (Below LLOQ)	12.26 ± 1.18	11.66 ± 2.57
8	0.49 ± 0.10 (Below LLOQ)	4.13 ± 0.61	4.40 ± 0.47
Time (Hours)	**Dose normalized brain concentration (ng/gm)/(mg/kg)**		
	Citrate (5 mg/kg)	**Co-solvent (15 mg/kg)**	**NLC (15 mg/kg)**
4	1.37 ± 0.37	2.50 ± 0.47	2.87 ± 1.37
6	0.26 ± 0.03[1]	0.82 ± 0.08	0.78 ± 0.17
8	0.10 ± 0.02[1]	0.28 ± 0.04	0.29 ± 0.03

1: Estimated from below LLOQ values

Appendix 5: Liver concentrations of LAZ formulations in rats

Time (Hours)	**Dose non-normalized liver concentration (ng/gm)**		
	Citrate (5 mg/kg)	**Co-solvent (15 mg/kg)**	**NLC (15 mg/kg)**
4	88.67 ± 39.18	360.00 ± 141.12	164.17 ± 44.85
6	73.52 ± 10.84	248.56 ± 139.89	112.31 ± 13.74
8	30.89 ± 7.88	94.89 ± 30.02	41.87 ± 7.39
Time (Hours)	**Dose normalized liver concentration (ng/gm)/(mg/kg)**		
	Citrate (5 mg/kg)	**Co-solvent (15 mg/kg)**	**NLC (15 mg/kg)**
4	17.73 ± 7.84	24.00 ± 9.41	10.94 ± 2.99
6	14.70 ± 2.17	16.57 ± 9.33	7.49 ± 0.92
8	6.18 ± 1.58	6.33 ± 2.00	2.79 ± 0.49

Appendix 6: Lung concentrations of LAZ formulations in rats

Time (Hours)	**Dose non-normalized lung concentration (ng/gm)**		
	Citrate (5 mg/kg)	**Co-solvent (15 mg/kg)**	**NLC (15 mg/kg)**
4	300.76 ± 10.37	906.93 ± 312.02	633.61 ± 167.99
6	177.26 ± 57.85	646.63 ± 223.45	356.43 ± 60.78
8	105.40 ± 12.22	432.78 ± 130.17	368.23 ± 82.30
Time (Hours)	**Dose normalized lung concentration (ng/gm)/(mg/kg)**		
	Citrate (5 mg/kg)	**Co-solvent (15 mg/kg)**	**NLC (15 mg/kg)**
4	60.15 ± 2.07	60.46 ± 20.80	42.24 ± 10.22
6	35.45 ± 11.57	43.11 ± 14.90	23.76 ± 3.51
8	21.08 ± 2.44	28.85 ± 8.68	24.55 ± 4.75

Appendix 7: Brain concentrations of LAZ with increasing doses of LAZ-NLC in rats

Amount of LAZ in brain at 20 minutes	**Doses (mg/kg)**		
	15	**30**	**60**
Dose non-normalized (ng/gm)	1569.47 ± 71.53	6377.84 ± 1159.91	18220.59 ± 3926.67
Dose normalized (ng/gm)/(mg/kg)	104.63 ± 4.77	212.59 ± 38.66	303.68 ± 65.44

Appendix 8: Dose linearity models for optimal LAZ-NLC in rats

LN (dose normalized LAZ concentration in brain at 20 minutes)	**Doses (mg/kg)**		
	15	**30**	**60**
ANOVA Model	4.65 ± 0.05	5.35 ± 0.19	5.70 ± 0.21
LN (LAZ concentration in brain at 20 minutes)	**LN (Doses)**		
	2.71	**3.40**	**4.09**
Power Model	7.36 ± 0.05	8.75 ± 0.19	9.80 ± 0.21